ELECTRODEPOSITION OF METALS FROM DILUTE SOLUTIONS OF THEIR IONS

by

C.L. LOPEZ-CACICEDO

Thesis submitted for the Degree of Doctor of Philosophy in the Faculty of Applied Science of the University of Newcastle upon Tyne.

Department of Chemical Engineering

University of Newcastle upon Tyne.

May 1973.

SUMMARY

The possibility of recovering metals from dilute solutions of their ions is examined using the deposition of copper from acidic cupric sulphate solutions as the test reaction and the fluidised bed electrode as the electrochemical reactor.

Practical design aspects, together with an explanation of the behaviour of fluidised bed electrodes are sought. Thus, reactor and distributor design, current efficiencies and electrode potentials are examined under diverse experimental conditions of bed expansion, copper concentration, particle size and diaphragm current density.

A mathematical model is used to interpret theoretically the electrode potentials and in its light several facts emerge.

It is concluded that fluidised beds are suitable for metal deposition from dilute solutions, high current efficiencies are obtained and their cost compare favourably with plate electrodes. The limitations are also emphasised, particularly electrode thickness and relatively low bed expansions.

On the theoretical side, it is shown that the fluidised bed system is essentially dynamic and its explanation in fundamental terms require a different approach from the ones used so far. Very elementary experiments are described and the results show the way in which further work should be carried out.

I hereby declare that the thesis submitted by me is a record of experiments carried out by me, that it is my own composition and that it has not previously been presented in application for a higher Degree in this or any other University.

ACKNOWLEDGEMENTS

The author wishes to acknowledge

DR. R.E. PLIMLEY for his continuous help and encouragement.

PROF. J.M. COULSON in whose laboratories the experiments were carried out.

MR. C.A. CURRIE and his Technical Staff.

THE SPANISH GOVERNMENT for their economic support.

CONTENTS

CHAPTER 1. INTRODUCTION

The work described is concerned with the application of fluidised bed electrodes to the recovery of metals from dilute solutions of their ions, and in particular, with the recovery of copper.

The fluidised electrode comprises a bed of electrically conducting particles maintained in a fluidised state by the passage of electrolyte. Electrical contact with the bed is made by a submerged metal rod, plate or gauze connected to an external power supply, the second terminal of which is connected to a counter electrode to complete the electrical circuit.

Fluidised electrodes offer a large surface area of electrode per unit volume of cell, the ratio being typically 70 cm^{-1} compared with values of 2 cm^{-1} or less for conventional filter press cells or plate electrodes in a cell tank. This characteristic makes the fluidised electrode especially attractive for processes which take place at low current densities, and not surprisingly, therefore, its commercial prospects have been largely linked to the electrosynthesis of organic chemicals where low current density operation is the rule rather than the exception. There are, however, other fields in which this type of electrode may prove effective, notably in the electrodeposition of metals from dilute solutions of their ions where high current density operation is precluded by diffusion control. Such solutions are encountered in industrial effluents (c.f. Appendix A) and in this area the fluidised electrode holds out the possibility of offsetting the cost of treatment by economic recovery of the metal content. The present research study

was designed to explore the feasibility of this method in the context of copper recovery.

The research was carried out in three stages, the first of which was devoted to the determination of cathodic polarisation data for copper in concentrations ranging from 0.001 M to 0.1 M. These limits were broadly dictated by the range of concentrations encountered in typical effluents which vary from a few tens of p.p.m. to a few grams per litre. In view of the fact that most copper-containing effluents are acidic in nature, both these and subsequent observations were carried out in the presence of 0.1 M sulphuric acid.

The second stage of the work was designed to confirm[41] that copper deposition proceeded satisfactorily on a fluidised electrode and to define, in broad terms, the dependence of overall electrode performance on some of the more important process variables, e.g. bed expansion, copper ion concentration, diaphragm current density, etc.

In the third stage, conditions within the bed were studied by determining potential profiles in both the continuous and dispersed phases. From these measurements the distribution of electrode activity in the bed was established and K_m values were calculated according to the mathematical model proposed by GOODRIDGE et al[25].

Finally, some preliminary thought was given to the mode of operation of a fluidised electrode for copper recovery from dilute solution, which together with the experimental data has provided the basis of a comparative costing against conventional plate electrodes. In view of the lack of scale-up data, however, the conclusions reached must be

regarded with caution. The wider view of electrolytic versus chemical treatment has not at this stage been considered.

CHAPTER 2. SURVEY OF FLUIDISED BED ELECTRODES

2.1. Introduction

The fluidised electrode is one of a group of electrodes commonly termed "three-dimensional" or "volumetric", to distinguish them from the conventional plate or plane electrodes. Their purpose is to provide large active specific surface areas so that compact cell design can be achieved to handle low current density operations.

The adaptation of the concept of fluidisation to electrode design was first reported by BACKHURST et al[14] and forms the subject matter of British Patent No. 1194181/70. After establishing that a bed of electrically conducting particles fluidised by an electrolyte would perform the function of an electrode, BACKHURST et al[15] undertook a preliminary investigation of the fluidised electrode with reference to its salient variables.

The cell designs they employed are shown schematically in Figure 2.1 a, b and c. In all three cases the conducting beads rest on a porous distributor through which electrolyte passes and acts as the fluidising agent. Current is fed to or collected from the bed by means of a continuous conductor, taking the form of a rod, gauze, or spiral, which passes out of the cell to make contact with an external circuit. Figures 2.1 a and b depict a combination of fluidised and plane electrodes mounted in undivided and divided cells respectively, and Figure 2.1 c depicts two fluidised electrodes contained in a cell which, although undivided in the example shown, could easily be modified to give a divided one. These designs have persisted, in principle,

FIG. 2.1

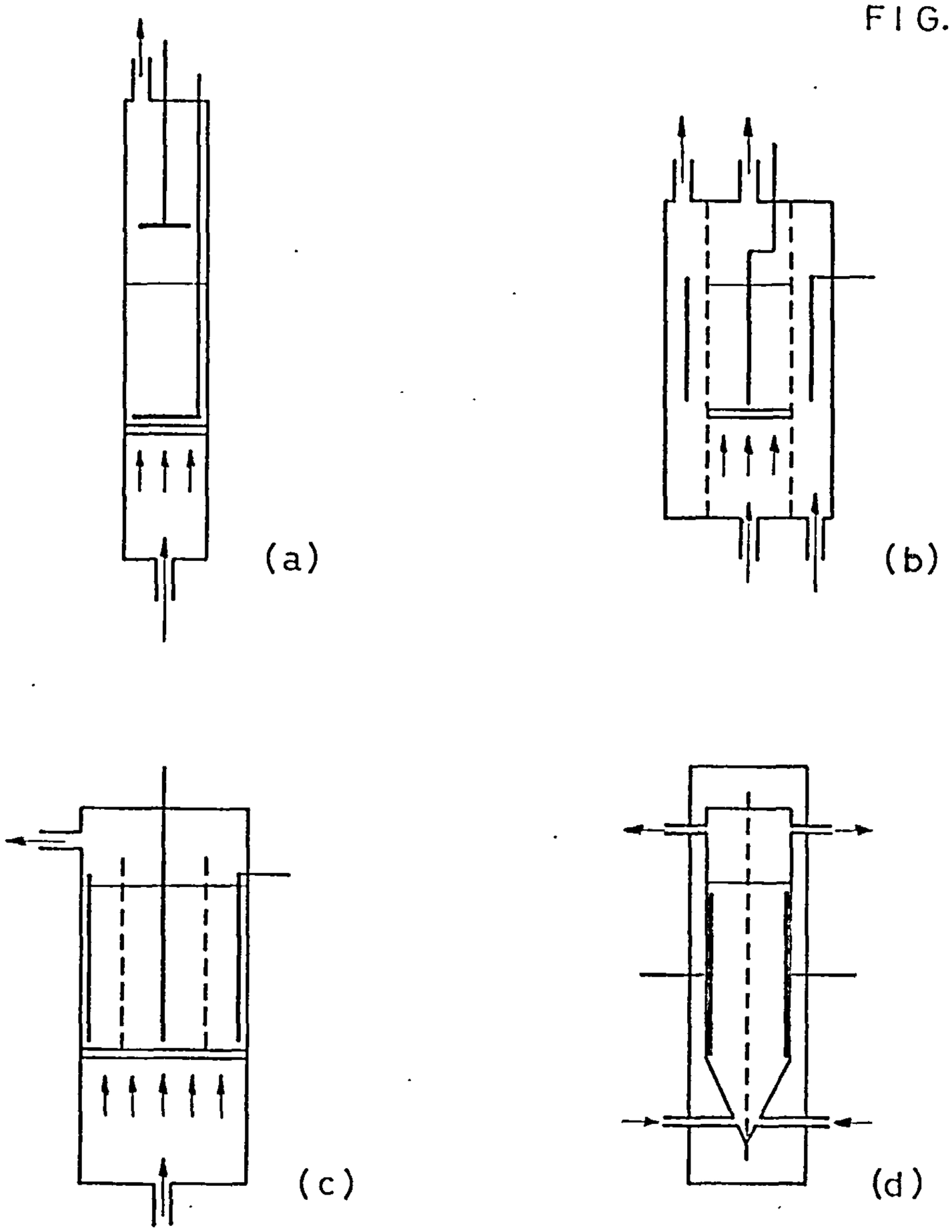
(a)
(b)
(c)
(d)

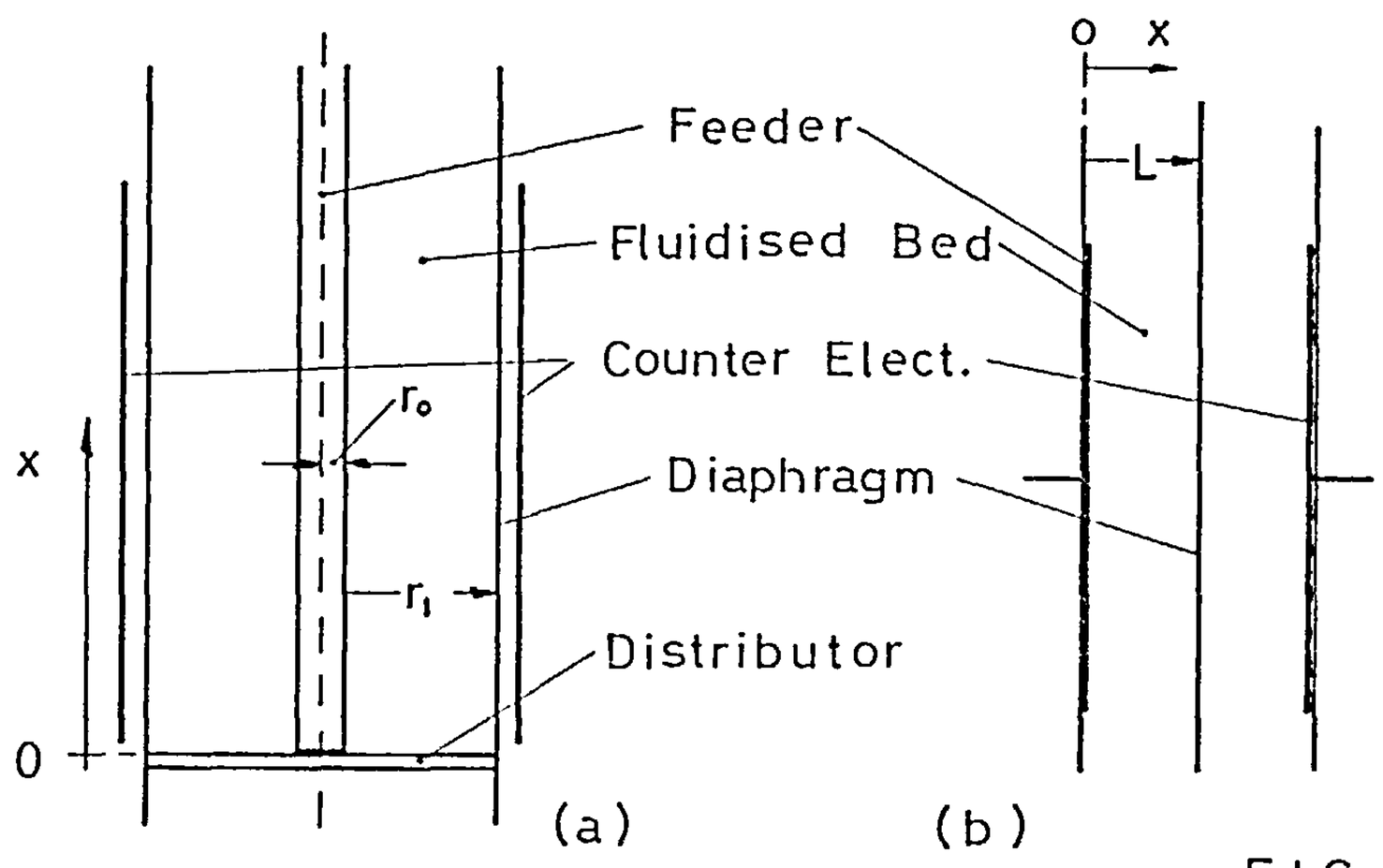
Feeder
Fluidised Bed
Counter Elect.
Diaphragm
Distributor
x
0
r_0
r_1
O x
L
(a)
(b)

FIG. 2.2

in nearly all subsequent small scale work, except for the introduction of the so-called rectangular or planar cell, which is best exemplified by the Chemical Electronics Cell[48], available commercially and shown in Figure 2.1 d. In this design the flow section is rectangular in contrast to the circular and annular sections of the cells previously described. It is noted too that the porous distributor has here given way to a slot for ease of manufacture and assembly, and more will be said on this point in a later chapter.

BACKHURST et al observed the behaviour of the fluidised electrode in a cathodic mode, and employed the reduction of m-nitrobenzene sulphonic acid to metanilic acid in the presence of sulphuric acid as their test reaction. The beds comprised either copper-coated-glass or solid copper spheres of various size ranges. Their results indicated that the optimum performance, in terms of current supported for a given feeder potential, was attained for bed expansions in the region of 5 - 25%. Within this region a bed of copper coated glass beads approximately 500 microns in diameter sustained a specific current some 20 or more times greater than that of a typical plate cell, for a reaction proceeding with a current density of about 70 A m^{-2}. Specific current in this context was defined as the current supported by unit volume of the cathode chamber. With increase in current density the improvement falls off, but even at 400 A m^{-2} it still shows a gain of 7. It was pointed out by the authors that the use of terminology such as "current density" is not altogether meaningful in the context of a three dimensional system where almost inevitably there will be a distribution of electrode potential rather than a unique value. For

purposes of comparison, therefore, they identified the operating conditions of the bed with those of the feeder.

Before leaving the initial studies of BACKHURST et al, two more observations are worthy of note. Firstly, they found that in scaling up a fluidised electrode in a direction perpendicular to current flow, a linear increase in cell capacity was achieved, but in a direction parallel to current flow the increase was well short of linear, and size in this direction appeared to be limited to about 2 - 3 cm. Secondly, they found that the performance of the bed near the distributor was atypical and superior to the rest of the bed. They attributed this to a hydrodynamic entrance effect.

Progress on fluidised electrodes subsequent to the work of BACKHURST et al is conveniently described under two separate headings, reflecting the different but complementary approaches which have emerged. The first deals with the theoretical treatment of fluidised electrodes and the second with their industrial application.

2.2. Theory

It has been proposed by both FLEISCHMANN and OLDFIELD[21] and GOODRIDGE et al[25], that the dispersal of electric charge in the fluidised electrode is the result of charge transfer during particle collisions.

Regarding the dispersed and continuous phases as coincident continua and neglecting second and higher order terms, GOODRIDGE et al showed that this postulate leads to the relationship,

$$I_m = - K_m A \left(\frac{d \phi_m}{d n}\right) \qquad \ldots\ldots\ldots(1)$$

where I_m is the flow of current in the dispersed phase across a plane of area A; $d \phi_m / d n$ is the potential gradient in the dispersed phase normal to the plane, and K_m is a constant of proportionality termed the charge transfer coefficient.

A similar relationship holds for the electrolyte, namely

$$I_s = - K_s A \left(\frac{d \phi_s}{d n}\right) \qquad \ldots\ldots\ldots(2)$$

where the symbols have the same significance as in Equation (1), except that they now refer to conditions in the electrolyte phase. The constant of proportionality K_s is an effective conductivity and is related to the true conductivity of the electrolyte by some function of the voidage.

The relationship defined by Equation (1) is mathematically identical to that arising from the NEWMAN and TOBIAS model[16] for porous electrodes. In phenomenological terms, however, there is an important difference. The constant of proportionality in the Newman-Tobias equation, termed the effective specific conductivity, is almost entirely determined by the electrical properties of the matrix material and the porosity, whereas K_m, which has the dimensions of conductivity, will have a strong and additional dependency on the hydrodynamics of the system and the nature of the electrolyte. On these grounds, GOODRIDGE et al felt that K_m had more in common with a transfer coefficient, and accordingly referred to it in those terms.

Application of their model to a bed of cylindrical geometry, depicted in Figure 2.2.a to identify the nomenclature, gave rise to the following equations:

For the dispersed phase,

$$\frac{d}{dr}\left(K_m\, r\, \frac{d\,\phi_m}{dr}\right) = A_p\, r\, F\,(\phi_m - \phi_s) \qquad \ldots\ldots\ldots(3)$$

For the electrolyte phase,

$$-\frac{d}{dr}\left(K_s\, r\, \frac{d\,\phi_s}{dr}\right) = A_p\, r\, F\,(\phi_m - \phi_s) \qquad \ldots\ldots\ldots(4)$$

Here A_p denotes the superficial surface area of the particles per unit volume of the fluidised bed, and $F\,(\phi_m - \phi_s)$ is the equation of the polarisation curve appropriate to the reaction occurring at the electrode.

Designating the local values of electrode potential, $\phi_m - \phi_s$, by ϕ, and assuming K_m and K_s to be constant, the above equations were combined to give

$$K_m\, K_s\, \frac{d}{dr}\left(r\, \frac{d\phi}{dr}\right) = (K_m + K_s)\, A_p\, r\, F(\phi) \qquad \ldots\ldots\ldots(5)$$

If the feeder is situated centrally, as in Figure 2.2.a, the following boundary conditions were shown to apply

$$\text{At } r = r_1\,, \qquad \frac{d\,\phi_m}{dr} = 0 \qquad \ldots\ldots\ldots(6)$$

$$\text{At } r = r_o\,, \qquad \frac{d\,\phi_s}{dr} = 0 \qquad \ldots\ldots\ldots(7)$$

$$\phi_s = \phi_s{}^{o} \qquad \ldots\ldots\ldots(8)$$

$$\phi_m = 0 \qquad \ldots\ldots\ldots(9)$$

The last two conditions merely arose from the arbitrary choice of feeder potential as a datum, and electrolyte potential adjacent to the feeder as descriptive of the electrode operating condition.

Application of the model to an electrode of planar symmetry as shown in Figure 2.2.b, produced a similar family of equations:

For the dispersed phase,

$$\frac{d}{dx}\left(K_m \frac{d\,\phi_m}{dx}\right) = A_p\, F\,(\phi) \qquad \ldots\ldots\ldots(10)$$

For the electrolyte,

$$-\frac{d}{dx}\left(K_s \frac{d\,\phi_s}{dx}\right) = A_p\, F\,(\phi) \qquad \ldots\ldots\ldots(11)$$

These can again be combined assuming K_m and K_s constant, to give

$$K_m\, K_s \frac{d^2\,\phi}{dx^2} = (K_m + K_s)\, A_p\, F\,(\phi) \qquad \ldots\ldots\ldots(12)$$

For a feeder located at x = 0, the following boundary conditions apply:

$$\text{At } x = L, \quad \frac{d\,\phi_m}{dx} = 0 \qquad \ldots\ldots\ldots(13)$$

$$\text{At } x = 0, \quad \frac{d\,\phi_s}{dx} = 0 \qquad \ldots\ldots\ldots(14)$$

$$\phi_s = \phi_s^{\,o} \qquad \ldots\ldots\ldots(15)$$

$$\phi_m = 0 \qquad \ldots\ldots\ldots(16)$$

Integration of the above sets of equations, i.e. (3) and (4) or (10) and (11), leads to expressions for potential distribution in both the dispersed and electrolyte phases.

GOODRIDGE et al have pointed out that if voidage and hydrodynamic conditions vary from point to point in the bed, a similar variation in K_m and K_s should be expected. Unless this variation is known, and can be expressed in terms of the relevant spatial co-ordinates, an analytical solution of the equations is not possible. On the assumption that such variation can be neglected, however, FLEISCHMANN and OLDFIELD[21] have solved Equation (12) for two different feeder locations, and in each case have derived expressions for cell current and potential distribution.

According to GOODRIDGE et al[26] their assumption would appear to be quite valid for regions outside the hydrodynamic entrance region, which extends upwards from the distributor for a distance of about 5 cm. Nevertheless the Fleischmann-Oldfield equations are still not generally applicable since they were derived for electrolysis carried out either close to or well removed from reversible equilibrium, or under conditions of diffusion control. For other cases GOODRIDGE et al have shown that a solution by the hybrid-analogue computer is feasible, provided experimental polarisation data are available. ISMAIL[51] has suggested that not all the surface area of the electrode (A_p) may be active and accordingly introduced an effective area coefficient (α) to account for it.

By comparison of theory with experimental data, both FLEISCHMANN and OLDFIELD[22] and GOODRIDGE et al[25] have been able to

determine values of K_m, some of which are given in Table 2.1.

TABLE 2.1. Typical Values of K_m

Particle Size microns	Bed Material	Chemical System	K_m $\Omega^{-1}cm^{-1}$	Source
452 - 520	Silver coated glass beads	Reduction of oxygen	0.01	(23)
450 - 520	Solid copper and copper coated glass	Electrodeposition of copper	0.015	(24)
500	Copper coated glass beads	Reduction of m-nitrobenzene sulphonic acid	0.4	(25)

It is to be noted that the values in Table 2.1 are appropriate to regions of the electrode where the flow is fully developed. In the hydrodynamic entrance region much higher values can be achieved[26].

FLEISCHMANN and OLDFIELD[22] have also derived a theoretical relationship for K_m, based on the following postulates:

"(i) Charge transfer in a fluidised bed electrode occurs by complete or partial charge sharing during collision; the ratio of the collision time to the RC-time constant for charge sharing determines the extent of the charge sharing.

(ii) Collisions between particles are elastic.

(iii) The motion of a single particle can be satisfactorily mapped by assuming that the remaining particles form a stationary matrix (as in the simple kinetic theory of gases)."

The expression they derived for conditions usually encountered in fluidised electrodes takes the form:

$$K_m = \frac{3.6\ \rho^{\frac{1}{3}}\ v_p^{\frac{1}{3}}}{\epsilon^{\frac{1}{3}}\ (\epsilon^{\frac{1}{3}} - 1)\ \gamma^{\frac{1}{3}}\ \rho_s} \qquad \ldots\ldots\ldots(17)$$

ϵ = ratio of fluidised height to the stationary height

ρ = particle density (g/cm^3)

v_p = mean particle velocity (cm/sec)

γ = Young's modulus for the material of the particles ($dyne/cm^2$)

ρ_s = effective specific resistivity of the electrolyte phase ($\Omega.cm$)

GOODRIDGE et al[25] have suggested a semi-empirical relationship for K_m, namely,

$$K_m = \text{constant}\ \frac{v_p}{\epsilon^{\frac{1}{3}} - 1} \qquad \ldots\ldots\ldots(18)$$

The most noticeable difference between Equations (17) and (18) is the absence in the later of the term $\epsilon^{\frac{1}{3}}$. This is not surprising since in the range of expansions encountered, namely $1 < \epsilon < 1.5$, this term would be relatively insensitive, and not readily revealed by experimental results which at best are indicative and certainly far from definitive.

FLEISCHMANN and OLDFIELD[22] conclude that surface tension effects at the particle-electrolyte interface are of minor importance and single particle collisions are dominant.

2.3. Industrial Application

Possible applications of the fluidised electrode to commercial processes have been explored in both academic and industrial research

laboratories. Of the latter, CJB (Projects) Ltd. have mounted by far the largest effort,but for commercial reasons much of their work has not yet reached the stage of publication.

The underlying theme has been the observation of current efficiency and conversion attainable in the fluidised electrode in respect of electrode reactions which are commercially attractive but proceed at low current density.

The state of the art is classified below according to the branch of industry to which the work is relevant. To be completely general the last section should include the hydrometallurgy of metals other than copper. The reason for not doing so is twofold. Firstly, very little has been published outside the field of copper, and secondly, the present study is wholly confined to the copper system.

2.3.1. Inorganic and Organic Chemicals

Although a great deal of interest has been and is being shown in the application of fluidised bed electrodes to the production of chemicals, information is as yet shrouded in commercial secrecy. In such a climate it is frequently the case that the failures come to press more quickly. Thus ISMAIL[51] reports that the use of dispersed electrodes in the production of chlorine gave no advantage.

2.3.2. Batteries and Fuel Cells

BACKHURST et al[17] have reported the possibility of using a fluidised zinc electrode in the development of a high energy density secondary battery based on the Zinc/Air system.

Electrode structures previously employed have suffered from the formation of dendrites during the charging period, with consequent shorting of the cell. It is thought that in the fluidised system, which offers good mass transfer and high specific electrode area, conditions may favour the suppression of dendrites by allowing deposition to take place short of diffusion control. This work has been taken up by the National Research Development Council in conjunction with Electric Power Storage Ltd.

The possibility of using fluidised anodes and cathodes in fuel cells has also received attention. BERENT, MASON and FELLS[18] found great difficulty, however, in using gaseous reactants in fluidised electrodes and concentrated on the use of soluble ones. From their results they concluded that fluidised anodes were relatively unsatisfactory, but that fluidised cathodes showed sufficient promise in the reduction of a number of oxidants to warrant further investigation.

FLEISCHMANN et al[23] have indicated that the three-phase problem incurred by gases may be overcome in the case of oxygen by injection as a saturated solution under pressure.

Other work on fluidised beds associated with the development of fuel cells is due to HIDDLESTON and DOUGLAS[19],[20], who found that low electronic conductivity between the particles in the bed is a limiting factor in its operation.

2.3.3. Hydrometallurgy of Copper

FLETT[41] has studied the electrowinning of copper from dilute copper sulphate solutions, employing a cell of the type depicted

in Figure 2.1.a. The bed particles were 40 mesh copper coated glass beads, and the initial copper concentration was 2 g/l.

Preliminary tests showed that reduction in pH increased the rate of deposition but did not affect current efficiencies. On the basis of these results he carried out all subsequent experiments with 1N sulphuric acid.

His results showed that by using a fluidised bed there is a gain in power consumption (compared with a plate cathode), and that current efficiency remains constant even when the copper concentration reaches p.p.m. levels, e.g. 27 p.p.m.

The current efficiencies are higher than 80% and he attributes the loss of current efficiency to a slow back dissolution of copper by the acidic electrolyte. An increase in current density should therefore cause a general increase in current efficiency.

KUHN[39] has calculated current efficiencies from the data given by SURFLEET[40] who employed a Chemical Electronic cell shown schematically in Figure 2.1.d. In general they are much lower than those found by FLETT, but they cannot be strictly compared since SURFLEET purposely used an electrolyte containing iron and traces of other metals.

FLEISCHMANN et al[24] used a cell similar to the one employed by FLETT, and they mentioned a 99% current efficiency for the deposition of copper from 10^{-4} Molar $CuSO_4$ (equal to 6 p.p.m. copper), in complete contrast with the current efficiency (less than 10%) mentioned by KUHN for the same concentration.

In practice there will be an economic limit set on the lower concentration of Cu^{++} for recovery, governed primarily by a balance between costs of cell and equipment and the rate of recovery of copper

rather than by current efficiency.

2.4. Comment

At this stage in the development of fluidised electrodes it is difficult to pass critical comment since the amount of experimental data available is relatively limited and scattered over so many different chemical systems. However, it is beginning to emerge that, particularly for anodic operation, there may be material problems. The more common anodic materials e.g. nickel, platinum and lead, have exhibited passivity in the fluidised state, particularly noticeable in the discharge of chlorine[51], and the oxidation of soluble fuel cell feeds[18].

Carbon particles, another possible anodic material, are of low density and consequently have poor fluidising characteristics. This may be overcome by coating on a dense core, but naturally the cost of the material will rise accordingly.

The scale up of fluidised electrodes has hardly yet begun, and will almost certainly throw up a number of engineering and design problems.

In this connection, however, the theoretical treatment of fluidised electrodes shows promise of facilitating the prediction of cell performance simply from a knowledge of polarisation, charge transfer coefficient and electrolyte conductivity. Of these, the value of charge transfer coefficient is as yet the most inaccessible, but as the accumulation of experimental data proceeds, empirical correlations, perhaps guided by the expression of FLEISCHMANN and OLDFIELD, may be possible.

CHAPTER 3. POLARISATION AND CURRENT EFFICIENCY DATA FOR THE DEPOSITION AND DISSOLUTION OF COPPER IN A SULPHURIC ACID-COPPER SULPHATE ELECTROLYTE

3.1. Introduction

A knowledge of the behaviour of a two-dimensional electrode in terms of polarisation and current efficienty characteristics is a necessary prerequisite to a thorough analysis of the performance of a three-dimensional system such as the fluidised electrode. Accordingly the initial stages of the work were devoted to this aspect.

In order to allow a comparison with existing data the first observations of this nature were carried out, following common practice, on a plane copper electrode immersed in a flowing electrolyte. In view of the objectives of the present work, however, it was thought necessary to take this basic study a stage further, and observe the behaviour of an electrode exposed to a flow regime akin to that encountered in a fluidised system. To this end, polarisation data have also been obtained for a wire immersed in a fluidised bed of glass beads.

3.2. Cell Design for Polarisation and Current Efficienty Observations

3.2.1. Polarisation Cell I

Polarisation curves and current efficiency data for a plane electrode with flowing electrolyte were obtained using the cell shown in Figure 3.1, which will henceforward be referred to as Polarisation Cell I.

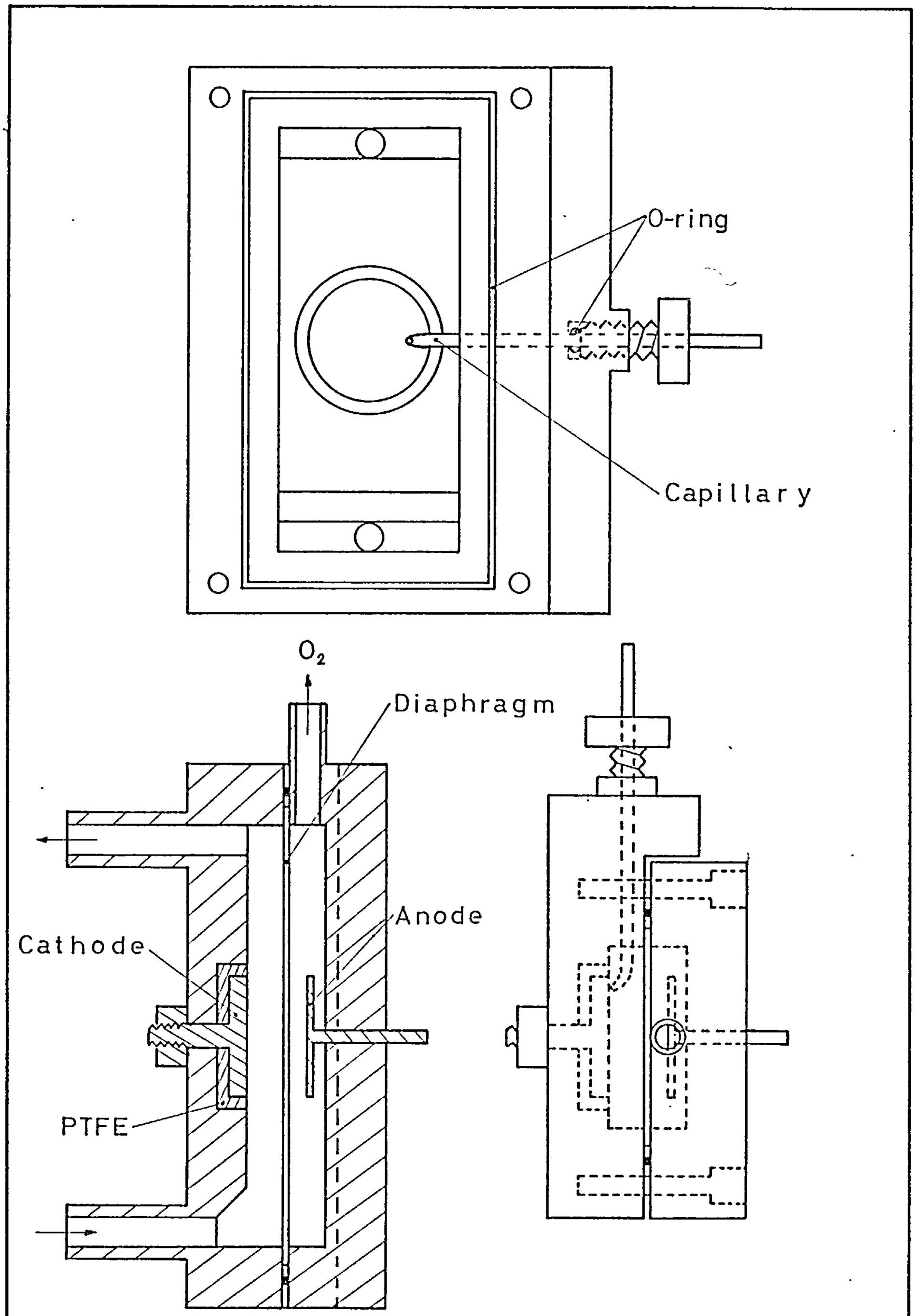

Polarisation Cell I

FIG. 3.1

The cell is constructed in perspex and is made in two parts which, when bolted together and sealed at the flange by an O-ring, enclose a rectangular cavity. Clamped between them is a diaphragm (porous PVC) which divides the cavity into anolyte and catholyte chambers, each chamber having the approximate dimensions 6 x 3 x 0.6 cm.

The cathode is removable and consists of a copper disc, 2 cm in diameter and 0.3 cm in thickness mounted axially on a threaded copper rod. The disc is received by a recess in the cell wall and rod passes through the wall to be secured by a nut. A good seal between the cathode assembly and the perspex is ensured by a P.T.F.E. liner as indicated in Figure 3.1. The dimensions of the recess and liner were arranged so that the surface of the cathode and the internal surface of the cell were flush. The precaution was taken of "lacomiting" the rear surface and the edge of the copper disc to prevent corrosion by trapped electrolyte and deposition by indeterminate secondary currents.

The anode is a disc of platinum foil, again 2 cm in diameter, attached to a brass rod covered with "lacomite" which passes through the cell wall and is sealed into it by "Tensol" cement.

When the cell is assembled the separation between the electrodes is 1 cm.

A Luggin capillary is introduced through the side of the cell as shown in Figure 3.1, and its tip is bent through an angle of 90^{o} to be adjacent to the cathode surface. A seal was made at the point of introduction by means of a screw fitting and an O-ring.

An inlet and outlet for continuous circulation of catholyte are provided, and also a vent for the escape of oxygen released at the anode.

3.2.2. Polarisation Cell II

Observations on the polarisation of an electrode in a fluidised bed of glass beads utilised a cell which was specifically designed for later experiments with conducting beads and therefore its description is left until a more appropriate section (4.3).

When used in the present context, however, it will be referred to as Polarisation Cell II.

Two cathodes were employed, both of which consisted of a platinum wire protruding from a glass sheath. At the point of exit the glass was fused around the platinum to form a seal. The cathodes differed only in their length, the protrusion in one case being 0.9 cm and in the other 2.5 cm. The diameter of the electrodes and the inert glass beads was selected to be approximately equal to that of the conducting beads, i.e. 550 microns, used subsequently in the active fluidised system.

The cell was open at the top and when making measurements the appropriate cathode was held in a clamp from which it dipped vertically into the cell to a point where the tip was approximately 6 cm above the apex of the distributor (c.f. Figure 4.4.(c)). A sufficient quantity of glass beads was placed in the cell such that under fluidised conditions the uppermost point of the cathode was immersed to a depth of at least 1 cm.

3.3. Materials

For all experiments double distilled water was used together with the following reagents:

(i) Copper Sulphate

Analar $CuSO_4$ 5 H_2O with limits of impurities of 0.005% Fe, 0.0005% Chloride, 0.002% Nitrogen compounds.

(ii) Sulphuric Acid

B.D.H. with limits of impurities of 0.01% HCl, 0.001% HNO_3 and 0.002% Fe.

(iii) Mercurous Chloride

B.D.H. not less than 99%

(iv) Potassium Chloride

Analar not less then 99.8%

(v) Agar

B.D.H. fine powder.

3.4. Reference Electrodes

The reference electrodes were of the saturated calomel type, having an electrode potential of + 0.242 V with respect to the hydrogen electrode. Two similar types were used, both employing an agar gel junction. The designs are shown in Figure 3.2. The gel was made with saturated aqueous potassium chloride, powdered agar, and approximately 0.05 grs. of mercurous chloride. The calomel paste was made with mercurous chloride, saturated aqueous potassium chloride, and a drop of mercury.

3.5. Instrumentation

Details of the instrumentation and equipment items are given in Appendix E. Reference is made to this Appendix by numbers preceded by the letter E.

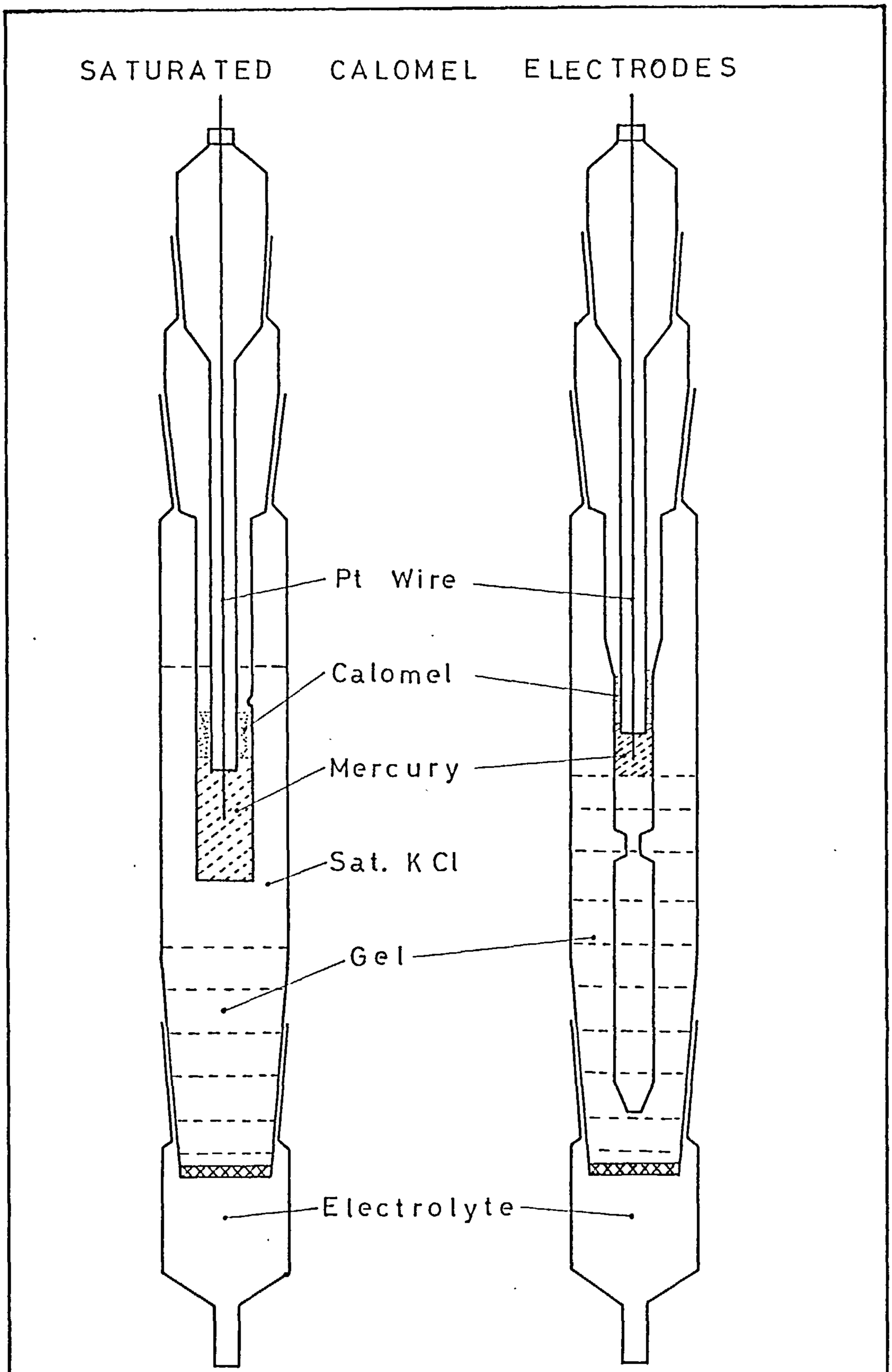
SATURATED CALOMEL ELECTRODES
Pt Wire
Calomel
Mercury
Sat. K Cl
Gel
Electrolyte

FIG. 3.2

3.6. Experimental Procedure and Results for Polarisation Cell I

3.6.1. Polarisation Curves

The copper cathode was polished with diminishing grades of emery paper until it presented a mirror-like finish, after which the cell was assembled and connected into the flow and electrical circuits shown in Figure 3.3. One litre of freshly prepared electrolyte was poured into the reservoir, and circulated through the catholyte chamber by switching on the pump. The electrolyte passed slowly through the porous membrane filling the anolyte chamber.

After closing the electrical circuit, a period of about 20 minutes was allowed to elapse during which the cathode achieved a steady rest potential. Readings of cell current over a range of electrode potential were then taken, an interval of 30 sec. being allowed between each reading to allow the system to settle down. This relatively rapid procedure was adopted in order to avoid undue changes in the electrode surface area arising from prolonged deposition.

The temperature of the electrolyte was maintained throughout the runs at $22^{o}C$.

The results for 0.1, 0.01 and 0.001 Molar Cu^{++} in 0.1 Molar sulphuric acid, and 0.01 Molar Cu^{++} in 1.0 Molar sulphuric acid are shown in Figure 3.4.

3.6.2. Current Efficiency

The equipment was set up in a manner identical to that described above for the polarisation observations. Deposition was

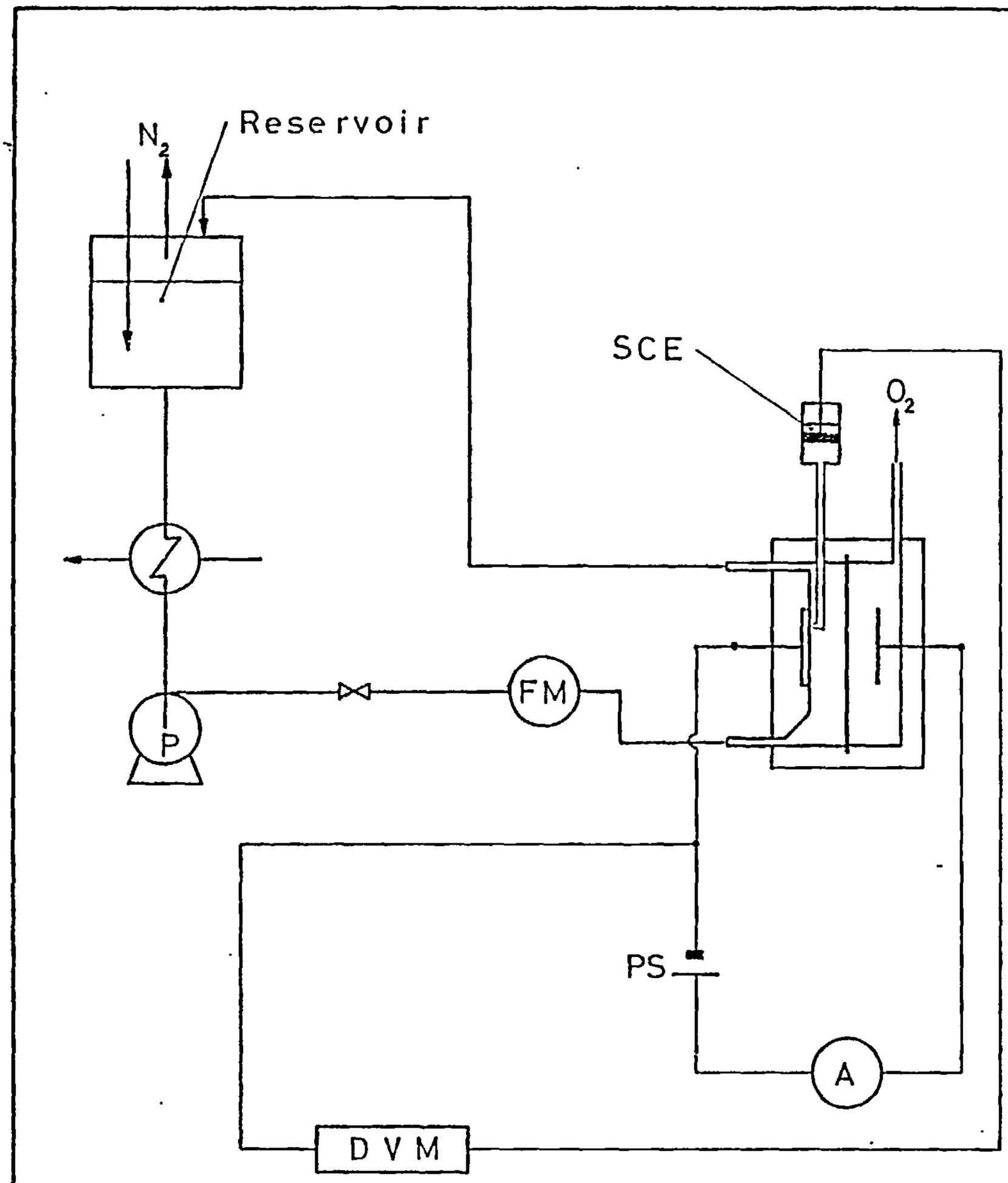

P pump(E1)

FM flow meter(E9)

PS power supply(E3) and (E6)

A ammeter(E5)

DVM (E7)

Polarisation Cell I

FIG. 3.3

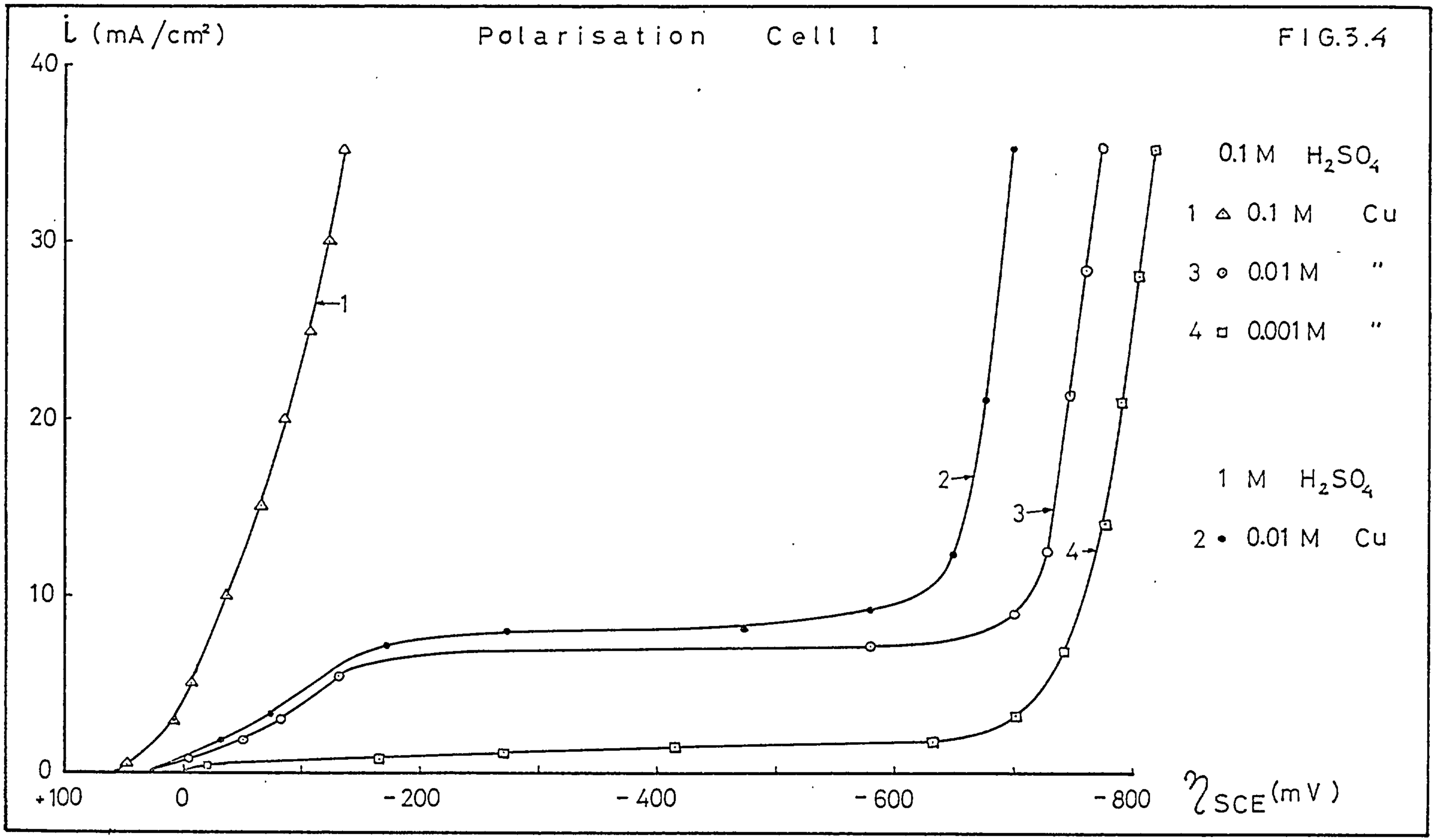
i (mA/cm²)
Polarisation Cell I
FIG.3.4
40
30
20
10
0
+100
0
-200
-400
-600
-800
η SCE (mV)
1
2
3
4
0.1 M H2SO4
1 △ 0.1 M Cu
3 ○ 0.01 M "
4 □ 0.001 M "
1 M H2SO4
2 • 0.01 M Cu

allowed to occur under potentiostatic conditions and the amount deposited was determined by gravimetric difference.

Temperature was again maintained at approximately 22°C. The quantity of electricity passed in each current efficiency determination was of the order of 50 coulombs.

The observed current efficiencies are shown in Figures 3.5 and 3.6 plotted against current density and electrode potential respectively.

3.7. Experimental Procedure and Results for Polarisation Cell II

The experiments were carried out with the same flow and electrical circuits previously used in conjunction with Polarisation Cell I and shown in Figure 3.3. After introducing the required amount of glass beads into the cell, the electrolyte was circulated to produce fluidisation. The appropriate platinum cathode was then lowered into the bed and connected to the electrical circuit. Flow control and hence bed expansion was exercised through a valve (Figure 3.3). The temperature of the system was maintained at approximately 22°C.

Polarisation was observed under a variety of conditions differing one from another according to the history of the electrolyte, bed expansion and electrode pretreatment and size. Pretreatment was carried out either by holding the potential of the electrode at a set value until the cell current became steady or by exposing the electrode to a potential sweep of 1 cycle between the limits 0.03 - 0.28 V, the cycling time being one minute.

After its pretreatment, the polarisation characteristics of

Polarisation Cell I

0.1 M H_2SO_4

FIG. 3.5

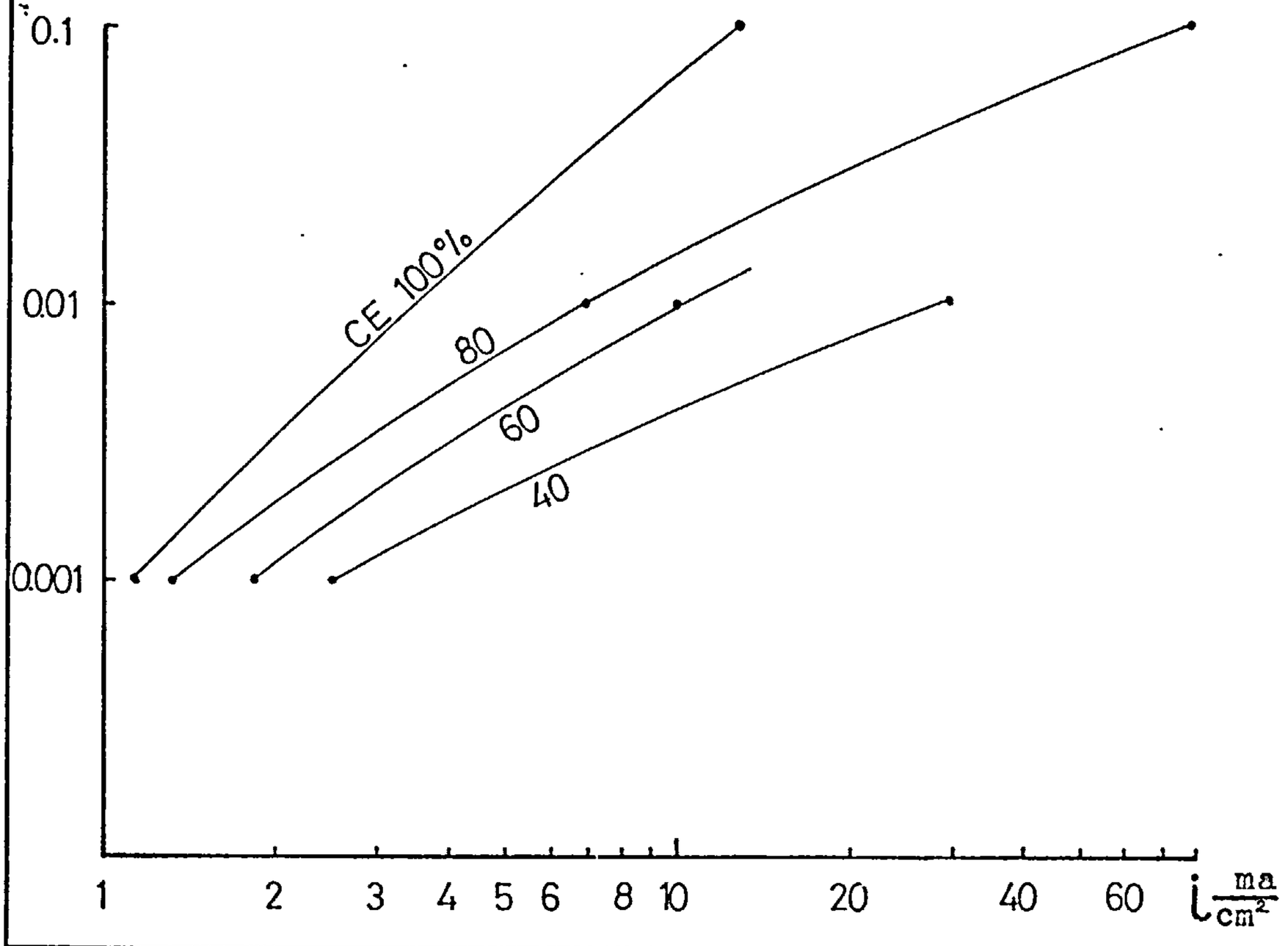

FIG. 3.6

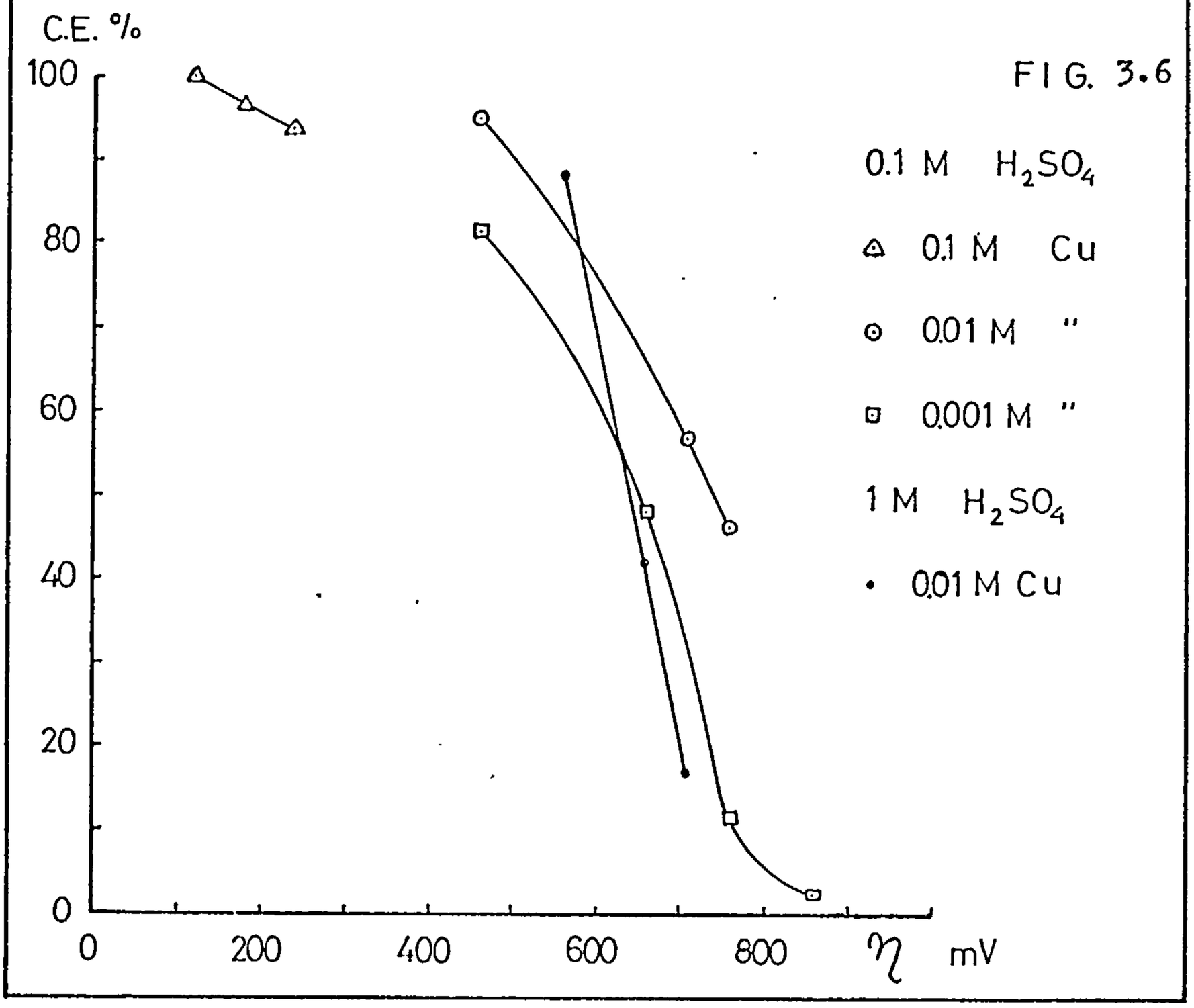

the electrode were determined by noting the cell current at discrete intervals of potential. Readings were taken in the directions of both increasing and decreasing potential, and at each potential level the polarisation parameters were noted as quickly as possible to minimise the effect of electrode growth. Electrode area was taken to be that on completion of a run and not that of the platinum wire core.

The various conditions under which polarisation data were acquired are listed for convenience in Table 3.1.

TABLE 3.1. Experimental Conditions for Polarisation

Experimental Run (see Fig. 3.7)	Electrolyte	Cathode Length cm	Pretreatment
1	Fresh	0.9	Fixed Potential 0.14 V for 40 mins.
2	Fresh	0.9	Fixed Potential 0.04 V for 20 mins.
3	2 weeks old	2.5	Fixed Potential 0.04 V for 20 mins.
4	Fresh	2.5	Potential Cycled

Results were obtained for solutions containing 0.1 Molar Cu^{++} in 0.1 Molar sulphuric acid and are plotted in Figure 3.7. Included in Figure 3.7 are comparable results from Polarisation Cell I.

A rather cursory observation of the anodic behaviour of copper was also carried out. A copper wire replaced the platinum wire of the previous experiments and the results obtained are also given in Figure 3.7.

Polarisation Cell II FIG. 3.7

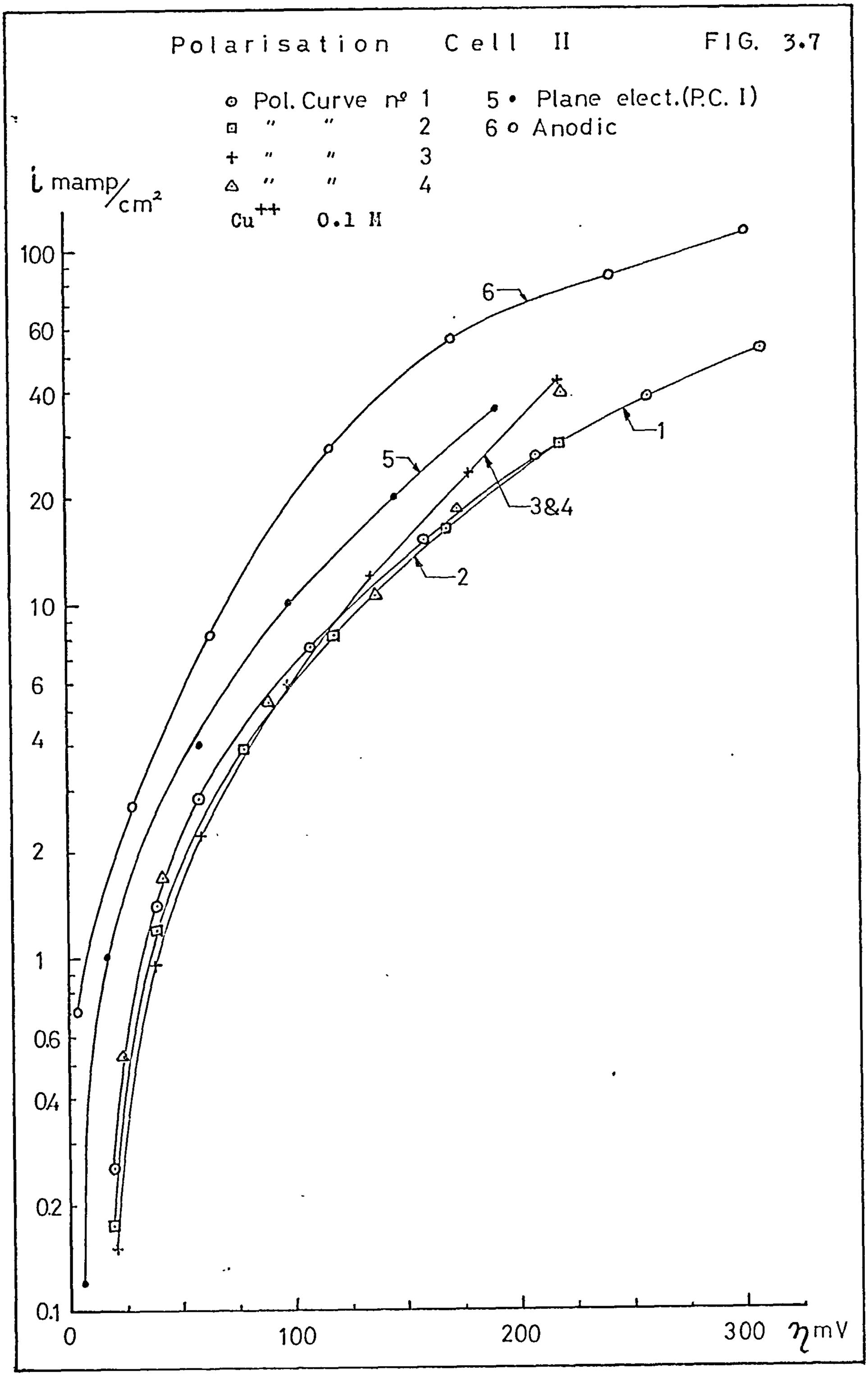

3.8. Discussion of the Polarisation Data

3.8.1. Plane Electrode with Flowing Electrolyte

Several authors have studied the deposition of copper from an aqueous copper sulphate-sulphuric acid electrolyte, and a summary of the conditions they used in terms of electrolyte composition is given in Table 3.2. Curves representative of their results are shown in Figure 3.8 along with a typical curve arising from the present work.

TABLE 3.2. Summary of Polarisation Conditions in the Literature

Authors	Electrolyte Composition		Ref.
	Cu^{++} (Molar)	H_2SO_4 (Molar)	
Shreir and Smith	0.25	0.5	34
Marie and Thon	-	-	36
Gauvin and Winkler	-	-	35
Mattsson & Lindstrom	0.5	0.5	9
Mattsson & Bockris	0.075	0.05	10
Hurlen	0.1	0.05	12
Kimber et al	1.0	0.55	32
Gnusin	0.77 (app.)	0.49 (app.)	37
Lopez Cacicedo	0.1	0.1	Present work
	0.01	0.1	
	0.001	0.1	
	0.01	1.0	
	0.1	0.1*	

* Electrode immersed in a fluidised bed of glass beads

FIG. 3.8

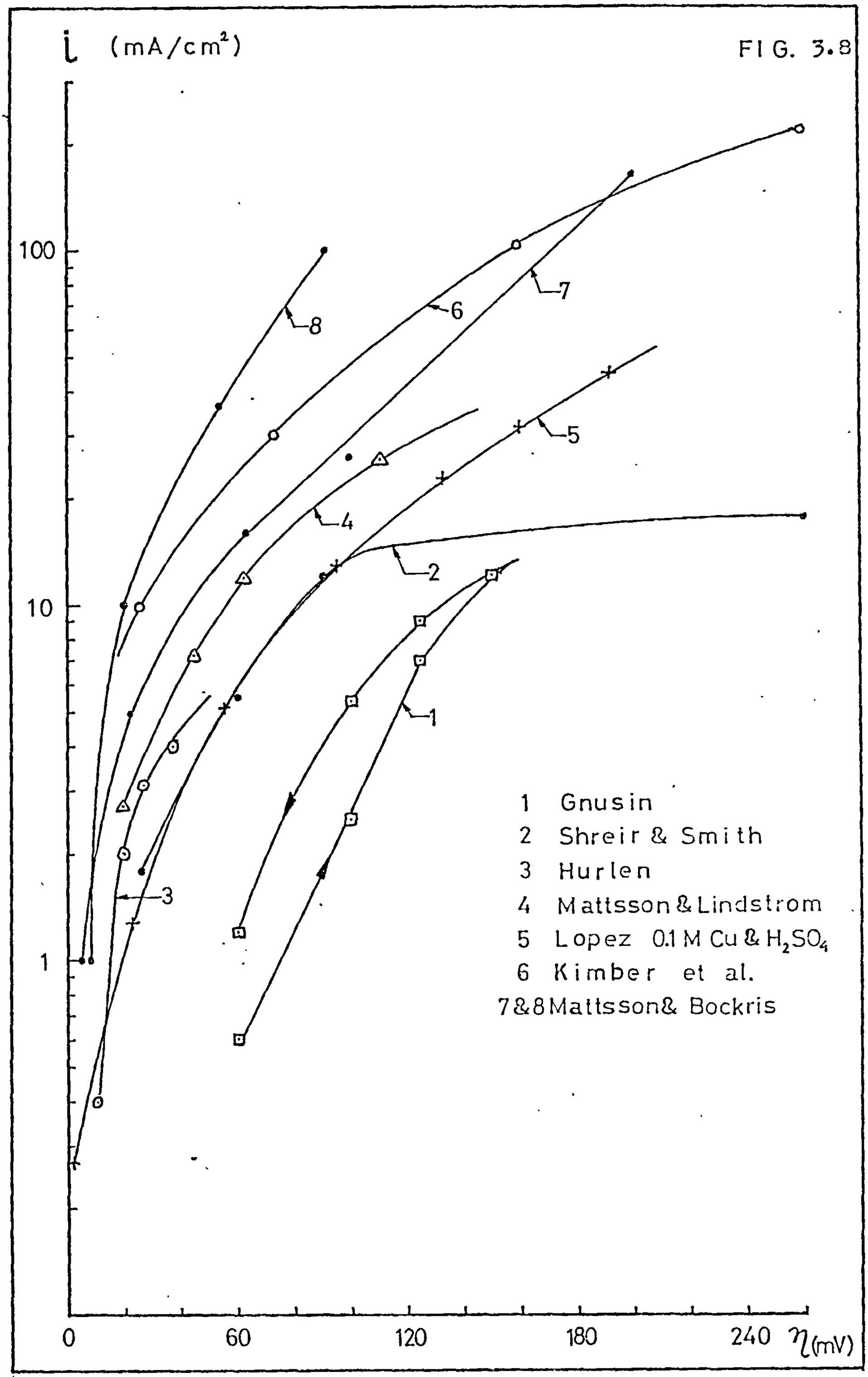

1 Gnusin
2 Shreir & Smith
3 Hurlen
4 Mattsson & Lindstrom
5 Lopez 0.1 M Cu & H_2SO_4
6 Kimber et al.
7&8 Mattsson & Bockris

The picture they present is far from uniform and cannot be accounted for simply by variation of electrolyte strength. Published discussion on this point looks, for explanation, to the effects of surface structure and aging of the electrolyte.

It is common knowledge that the true surface area of an electrode is dependent to a greater or lesser extent upon its surface microstructure, and by following the normal practice of calculating current densities on the basis of apparent area, this dependency is ignored. Although this may be relatively inconsequential under circumstances where the electrode forms no more than an active interface of somewhat permanent geometry, its effects in metal deposition where the surface is in continuous state of change may be much more marked. GAUVIN and WINKLER[35] have placed particular emphasis on this possibility and suggest that it would explain the drift in electrode potential during the deposition of copper carried out amperostatically. By using d.c. transients MATTSSON and BOCKRIS[10] have been able to avoid electrode growth and therefore significant surface change and in this way were able to observe differences in behaviour arising from pretreatment procedures. They found that a copper cathode formed electrolytically had significantly different characteristics from one formed by melting in purified helium, (Figure 3.8: curve 7, electrode produced by electrodeposited copper and curve 8, electrode produced by melting in purified helium), and although it may be argued that this can again be accounted for by dissimilar surface areas, the possibility must not be discounted that the mode of forming may affect the surface in a thermodynamic sense. Either way, these observations are a reminder that electrode pretreatment can be very influential,

and since in all experimentation of this nature some method of pretreatment, usually electrolytic, is practised, the type and duration of the treatment may well explain much of the scatter in the reported data. This opinion is also shared by SHREIR and SMITH[34].

The effect of aging of the electrolyte is not so well established, although firmly claimed by SHREIR and SMITH[34] and MARIE and THON[36]. The present work, however, has failed to produce any supporting evidence for their claims.

Curve 5 in Figure 3.8 describes results derived in this work from Polarisation Cell I and is appropriate to Cu^{++} and H_2SO_4 concentrations of 0.1 Molar. This curve, in relation to the others, follows what may be called a "middle" course, and may therefore be considered to fit satisfactorily into the somewhat vague picture which the literature presently conveys.

Experimental results for the more dilute solutions of Cu^{++} have been omitted from Figure 3.8 because no comparable data have been reported. The general effects of dilution are, however, well known and the present results, which are plotted in Figure 3.4, merely serve to give quantitative definition to them with regard to the particular case of copper. As the potential is raised cathodically the rate of deposition increases until, at approximately -0.2 V SCE, a maximum is reached corresponding to diffusion control. As would be expected the diffusion limited current density is roughly proportional to the Cu^{++} concentration. Thus for concentrations of 0.01 and 0.001 Molar, values of 8 and 1 mA cm^{-2}, respectively, were observed. The diffusion limited condition was never attained for a Cu^{++} concentration of 0.1 Molar since it lay outside the range of current densities investigated. It

may be presumed, however, to have a value in the region of 80 mA cm^{-2}.

The limiting current densities observed are broadly supported by the relationship

$$i_d = \frac{Dz\,F}{\delta}\,a$$

in which it is implied that the bulk of the ionic transport is due to H^+ migration. If average values for D and δ of 10^{-5} cm^2 sec^{-1} and 10^{-3} cm are assumed, the diffusion limited current densities are calculated to be 2 and 20 mA cm^{-2} for 0.001 and 0.01 Molar Cu^{++} respectively.

The rest potentials were + 58, + 25 and 0 mV with respect to SCE for 0.1, 0.01 and 0.001 Molar in Cu^{++} respectively. These values obey the Nernst relationship, which predicts a change of 30 mV for each tenfold change of concentration.

Curves 2 and 3 in Figure 3.4 refer to electrolytes of equal Cu^{++} concentration but differing acidity. They indicate that the rate of copper deposition is enhanced by the presence of sulphuric acid, but not to any great degree. These findings are supported by FLETT[41].

The sharp rise in the curves of Figure 3.4 at approximately - 0.7 V SCE marks the evolution of hydrogen.

3.8.2. Wire Electrode Immersed in an Inert Fluidised Bed

The experimental observations made on platinum wire cathodes immersed in a fluidised bed of glass beads are shown on Figure 3.7, the legend for which, in respect of curves 1 - 4, is defined in Table 3.1. Discussion of the curves is conducted under appropriate headings as follows.

Effect of Fluidisation

For an assessment of the effects of fluidisation, attention is drawn to curves 1 and 5, the latter of which has been transposed from Figure 3.4, and corresponds to the hydrodynamic conditions of Polarisation Cell I. These curves are selected because the catholyte composition and electrode pretreatment were roughly the same in each case.

Inspection of the curves shows that the presence of fluidisation produces a fall in current density of approximately 30%.

An explanation in terms of mass transfer rates is most unlikely because, firstly, the curves lie outside the diffusion controlled region where mass transfer plays a key role, and secondly, it would be anticipated that fluidisation with its associated high transfer rates would produce a rise in current density rather than the reverse, as confirmed by LE GOFF et al[49] and VERGNES et al[50]. It could possibly arise from differences in surface structure, since the deposit formed in the absence of fluidisation was noticeably different from that on the wire electrode when viewed under the microscope. These findings echo to some extent the results of MATTSSON and BOCKRIS.

Effect of Cathode Pretreatment

Curves 1 and 2, Figure 3.7, highlight the effects of cathode pretreatment. As indicated in Table 3.1, the first curve corresponds to pre-electrolysis carried out at 0.14 V (Cathodic potential) for 40 minutes, and the latter to one at 0.040 V for 20 minutes. No significant difference in the results can be discerned. It may be

that any possible differences in surface structure normally arising from this source have been damped out by the fluidised bed.

It was stated earlier that on completion of pre-electrolysis the potential of the electrode was raised (sweep 1) and then lowered (sweep 2) cathodically in small steps, and at each step a note was made of the cell current. Immediately sweep 2 was completed, the cycle was repeated through sweeps 3 and 4, the odd numbers corresponding to a rising potential and the even to a falling potential, again, in a cathodic sense. When the pre-electrolysis was carried out at a relatively low potential it was noticeable that the curve resulting from sweep 1 was considerably lower in terms of current density than the results of the other sweep. A similar effect was reported by GNUSIN[37] whose results for the conditions given in Table 3.2 are in Figure 3.8, curve No. 1.

The data corresponding to the falling sweeps were much more reproducible and have been used exclusively in formulating Figure 3.7.

Effect of Potential Cycling

It has been observed[15] that the spatial distribution of potential in the dispersed phase of a fluidised bed is non-uniform. It follows, therefore, that if a particle in its peregrinations within the bed takes up the local potential of its environment it will suffer in consequence a potential cycle. The pretreatment conditions of curve 4 are an attempt to simulate this phenomenon and thereby register its effect on the polarisation characteristics. It can be seen by the agreement between curve 4 and curves 1, 2 and 3 that again no significant effect was detected.

It should be mentioned that although repeated reference is made to "curve" 4, an actual line drawn through the relevant points has been omitted from Figure 3.7 for the sake of clarity, although if drawn it would follow approximately the path of curve 3.

Anodic Polarisation

Curve 6 of Figure 3.7 describes the anodic behaviour of a copper electrode and was determined using a copper wire immersed in a fluidised bed of glass beads. Although it is plotted on the same potential scale as the cathodic curves, it is of course of opposite polarity. It is included here for the sake of completeness.

3.9. Current Efficiencies

Current efficiencies measured with a plane electrode in Polarisation Cell I are shown in Figures 3.5 and 3.6. Figure 3.6 clearly shows that provided cathode potentials are maintained below 0.4 V, current efficiencies in excess of 80% might be expected down to copper concentrations of approximately 60 p.p.m., and that this is little affected by tenfold changes in acid concentration. As the concentration falls, however, the high efficiencies are gained at the expense of current density. Thus in Figure 3.5, 80% current efficiency at the lowest concentration, 0.001 Molar Cu^{++}, corresponds to a deposition rate of 1.5 mA cm^{-2}. It is quite obvious, therefore, that an electrolytic operation designed to strip copper from solution down to tens of p.p.m. will almost certainly demand a high specific area device if capital outlay is not to be inordinately high.

Loss of efficiency, particularly at the higher potentials, is largely due to hydrogen evolution, but there is a contribution at all potentials due to chemical oxidation under acidic conditions. More will be said of this later.

The results described compare favourably with those of MEYER, reported by KUHN[39], who made observations under similar conditions except for acid concentration.

CHAPTER 4. CELL DESIGN FOR THE FLUIDISED ELECTRODES

4.1. Introduction

The experimental work was carried out with relatively small laboratory cells, the effect of scale up being left to a second phase of the work now in progress. Two cell geometries were investigated, namely, cylindrical and planar, and in both cases the behaviour of the bed has been observed in terms of cell current, current efficiency and electrode potential.

The present chapter is concerned only with cell design, the results and discussion being considered separately.

4.2. Cylindrical Cell

Cylindrical geometry was investigated using the perspex cell shown in Figure 4.1. The cell comprised a cavity of circular cross section, divided into two chambers - one annular and one central - by a cylindrical diaphragm. The central chamber contained the fluidised cathode and the annular chamber a cylindrical carbon anode. A copper rod mounted in the cell cap and dipping downwards into the cell, supplied current to the bed. Electrical contact with the anode was made by means of a platinum wire which pierced the cell wall.

The bed was supported in the cell by the electrolyte distributor, the design of which is taken up later. When assembled, the anode, diaphragm, and copper rod were arranged to be concentric with the cell's axis. Nozzles were provided for the circulation of the catholyte, and a vent was inserted into the anolyte chamber to take off evolved oxygen.

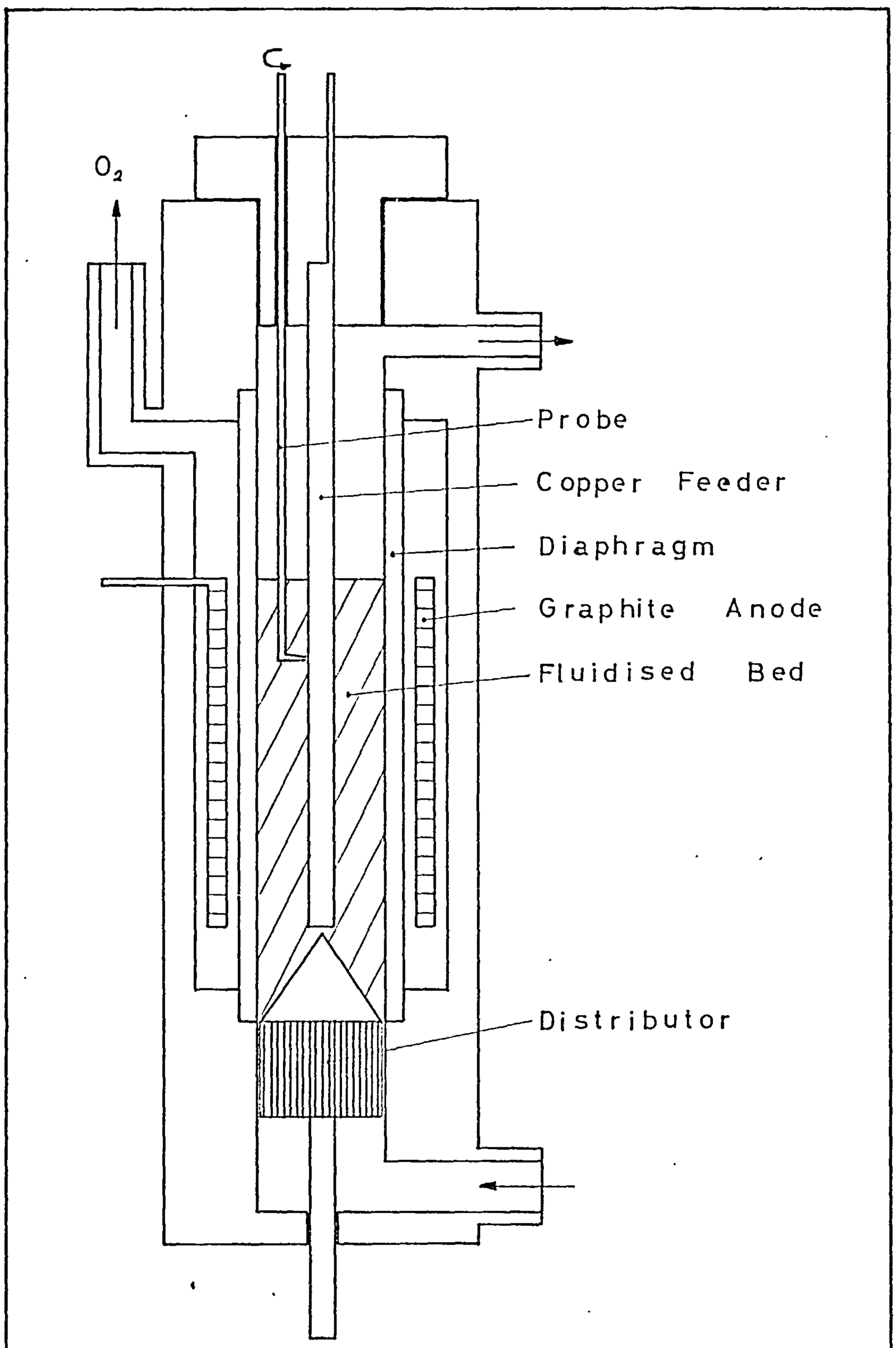

CONCENTRIC CELL

FIG. 4.1

A P.V.C. diaphragm was used initially, but owing to its high permeability it was unable to prevent undue mixing of the anolyte and catholyte, with the result that dissolved oxygen passed into the cathode compartment and caused dissolution of copper under the acidic conditions obtaining there. Coating the diaphragm with Plaster of Paris supplied only a temporary expedient, erosion rendering the treatment ineffective after no more than a few hours service. A satisfactory solution was eventually achieved by using Celloton (E 10 Appendix E), which combines low permeability with high conductance.

The cell henceforward referred to as Cylindrical Cell I utilizes the P.V.C. diaphragm covered with Plaster of Paris, and its dimensions vary somewhat from the one utilizing the Celloton diaphragm, henceforward referred to as Cylindrical Cell II.

The salient dimensions of the cells are given in Table 4.1.

TABLE 4.1. Dimensions of Cylindrical Cells

	Cell I	Cell II
Cell:		
Height	35 cm	35 cm
Diameter	9	9
Cathode chamber:		
Diameter	4.3	3.6
Height	20	20
Diaphragm thickness	0.5	0.6
Anode:		
Internal diameter	6	5.7
Height	12	11.5
Feeder:		
Diameter	0.6	0.6

4.3. Planar Cell

Planar geometry was investigated using the perspex cell shown in Figure 4.2. The catholyte and anolyte chambers, both of rectangular cross section, are separated by a Celloton diaphragm. The current feeder is a copper plate parallel to the diaphragm and inserted in a recess of the catholyte chamber. The thickness of the copper plate is such that the surface of the plate facing the bed and the internal surface of the catholyte chamber are flush.

Special care was taken in the design of the catholyte chamber in order to avoid any protrusion that could interfere with the fluidisation characteristics, and thus the diaphragm and the catholyte chamber wall were also flush.

The electrolyte distributor supports the bed, and its design will be described below.

The graphite anode is parallel to the diaphragm and its dimensions are the same as the copper feeder.

The salient dimensions of the cell are given in Table 4.2.

TABLE 4.2. Dimensions of Planar Cell

Catholyte chamber:	
length	10 cm
width	2
height	12
Anolyte chamber:	
length	10
width	1
height	14
Feeder and Anode:	
length	10
height	6
Celloton Diaphragm:	
length	11
height	19.5
thickness	0.3

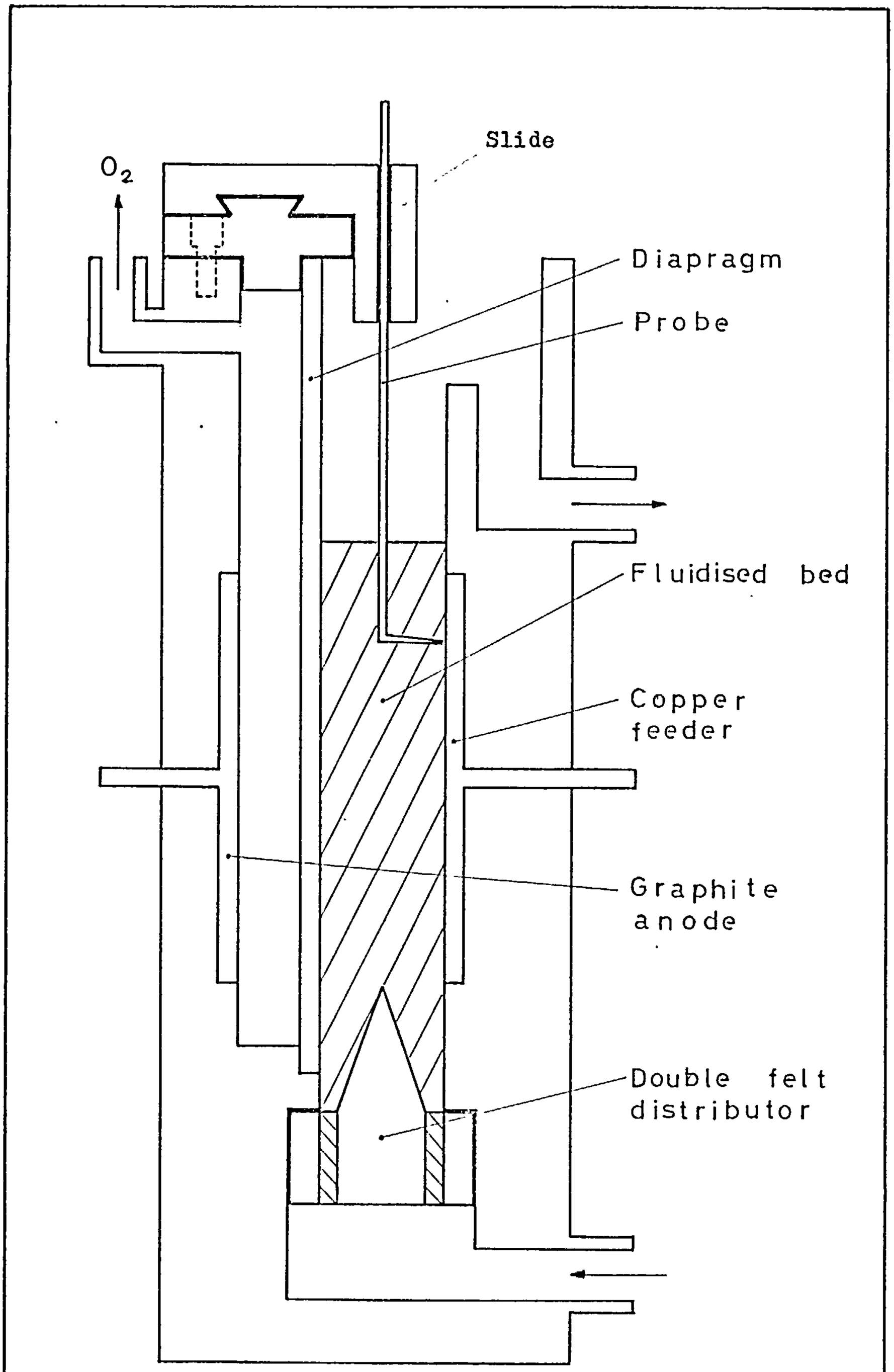

RECTANGULAR CELL

FIG. 4.2

The electrolyte enters the cell through a nozzle, and an overflow system along the whole length of the catholyte chamber is provided for the outlet of electrolyte, thus avoiding end conditions that could introduce undesired effects into the fluidisation.

4.4. Distributor Design

In most previous laboratory studies on fluidised electrodes, the electrolyte has been fed into the bed through a porous body, commonly a sintered glass plate or a P.V.C. disc or strip.

From an industrial point of view, however, they are not particularly attractive, since any chance suspended matter in the electrolyte is collected in the pores and causes either a total or partial blockage. This effect, particularly in thin porous distributors would contribute to channelling.

Cleaning by flow reversal has not proved satisfactory, and the remedy of replacement, especially if the operation requires withdrawal of the bed, may give rise to undue down-time. The other alternative, meticulous filtration, would undoubtedly carry high investment costs.

For these reasons other devices are in the course of development, which may be broadly classified into sieve plates and slots, a selection of which is shown diagrammatically in Figure 4.3. In each case the orifice dimensions are made small enough to retain the particulate mass of the bed, and large enough to give easy passage to fine suspensions. The path length through the distributor is set by

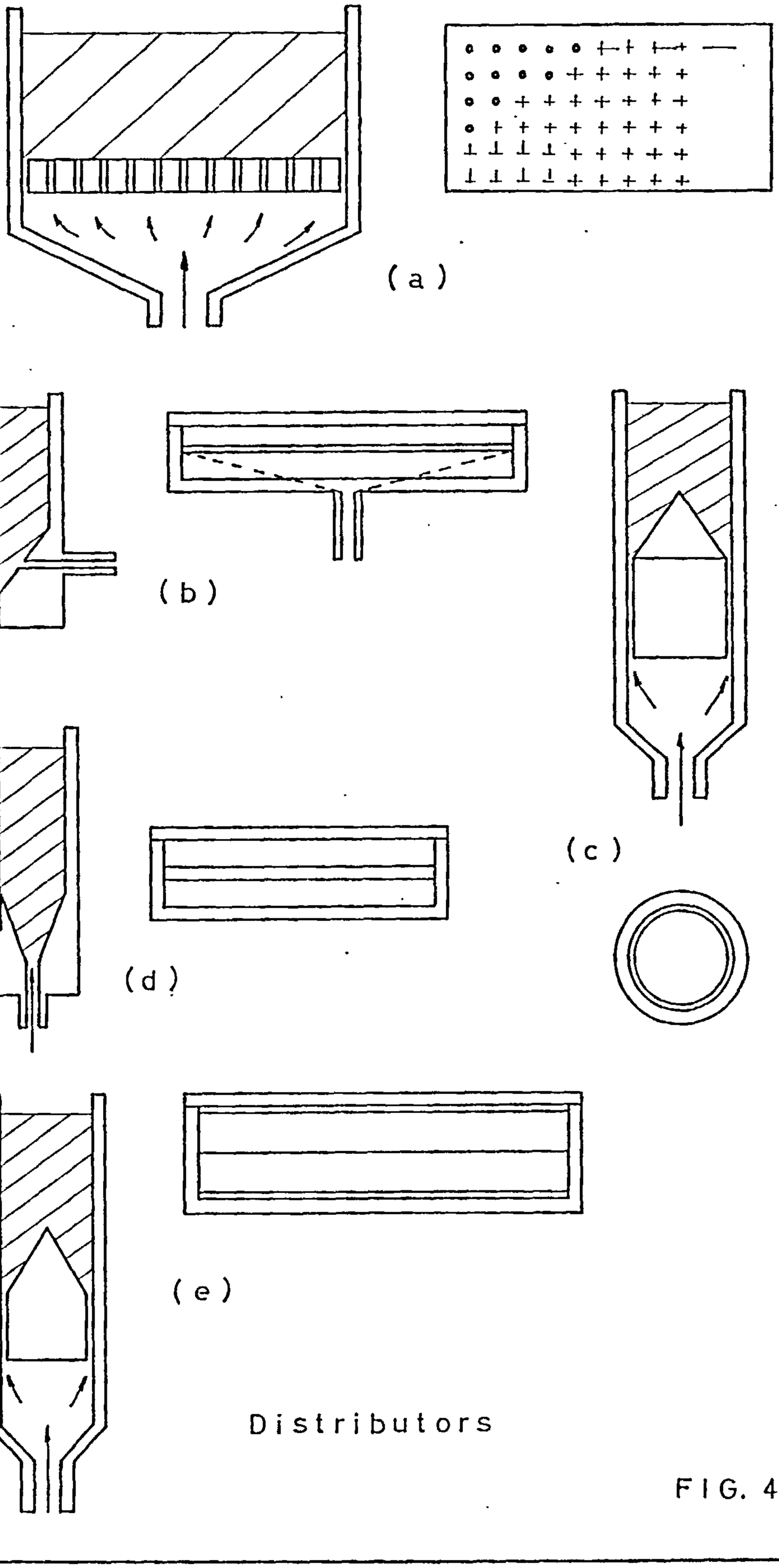

Distributors

FIG. 4.3

the necessary pressure drop, which must be at least comparable to that across the bed, otherwise the electrolyte passes through the system by preferred routes.

Although these designs might solve difficulties of a mechanical nature, they may well introduce others of a hydrodynamic one which affect electrode behaviour. The entry of electrolyte through a porous body is diffuse and occurs across the whole section of the bed, whereas in the devices just described it enters at selected points and its expansion into the rest of the bed occurs as a subsequent step. This point may at first seem trivial, but it must be remembered that observations on the entrance region of these electrodes[26] indicate their performance to be extremely sensitive to flow pattern. It cannot be assumed, therefore, that results obtained with one form of distributor are directly applicable to another. Consequently the distributors used in the present work, which is part of a continuing program leading ultimately to a scaled up engineering study, represent a deliberate departure from porous plates in order that the results acquired might be the more appropriate to the long term effort. The distributors employed embodied the principles of those shown in (c), (d) and (e) of Figure 4.3 and are described in detail below.

4.4.1. Distributor Employed in the Cylindrical Cell

The design for the cylindrical cell was based on Figure 4.3.(c), but in translating the principle to practice the annular slot was divided up into grooves. This served two purposes. Firstly, the high spots, which made a push fit with the cell walls, located the device and secondly, the narrow channels thus provided raised the

pressure drop to a more acceptable value. This distributor is shown diagrammatically in Figure 4.4.(a).

4.4.2. Distributors Employed in the Planar Cell

The designs for the Planar Cell were based on Figures 4.3.(d) and 4.3.(e).

The distributor based on Figure 4.3.(d) was made with two perspex blocks as shown in Figure 4.4.(b). The pressure drop was attained by placing a piece of felt 0.5 cm thick and 2.5 cm long (this distance is the path the electrolyte has to travel through the felt) between the perspex blocks and it was fixed by means of two screws. This distributor will henceforward be referred to as Single Felt Distributor.

The distributor based on Figure 4.3.(e) was made with two pieces of felt 0.3 cm thick and 2.5 cm wide and positioned between three blocks of perspex as indicated in Figure 4.4.(c). This distributor will henceforward be referred to as Double Felt Distributor.

In both distributors the pieces of felt were 2.5 cm wide and 11 cm long. The felt can be obtained in different thicknesses and grades and was supplied by Dolman James & Co. Ltd. (E 11 Appendix E).

The electrolyte was guided through the felt by sealing the zone of contact between the cell and the distributor with an O-ring, as indicated in Figure 4.4.(b).

With this design it is possible to adjust the pressure drop through the distributor "in situ", and each screw can be adjusted independently to exercise a measure of local control on fluidisation.

Distributors

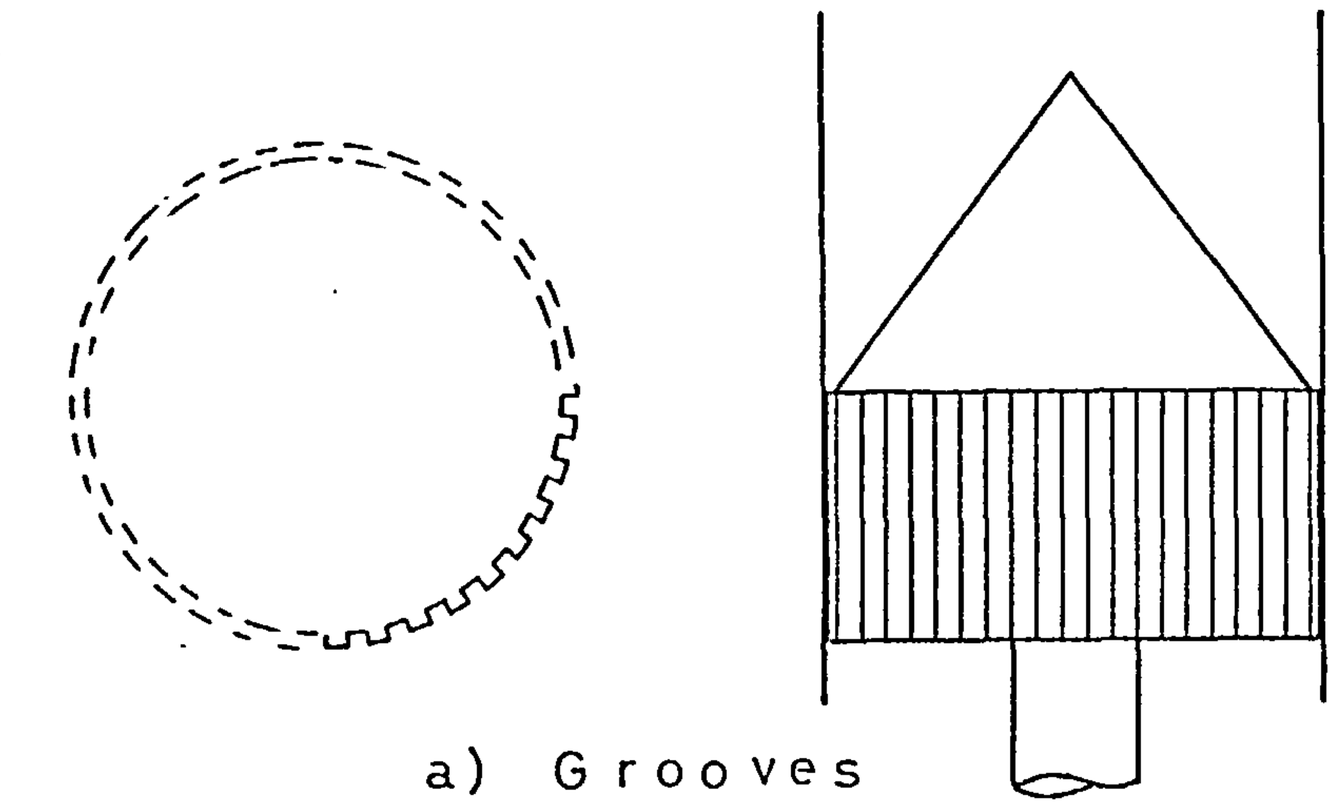

a) Grooves

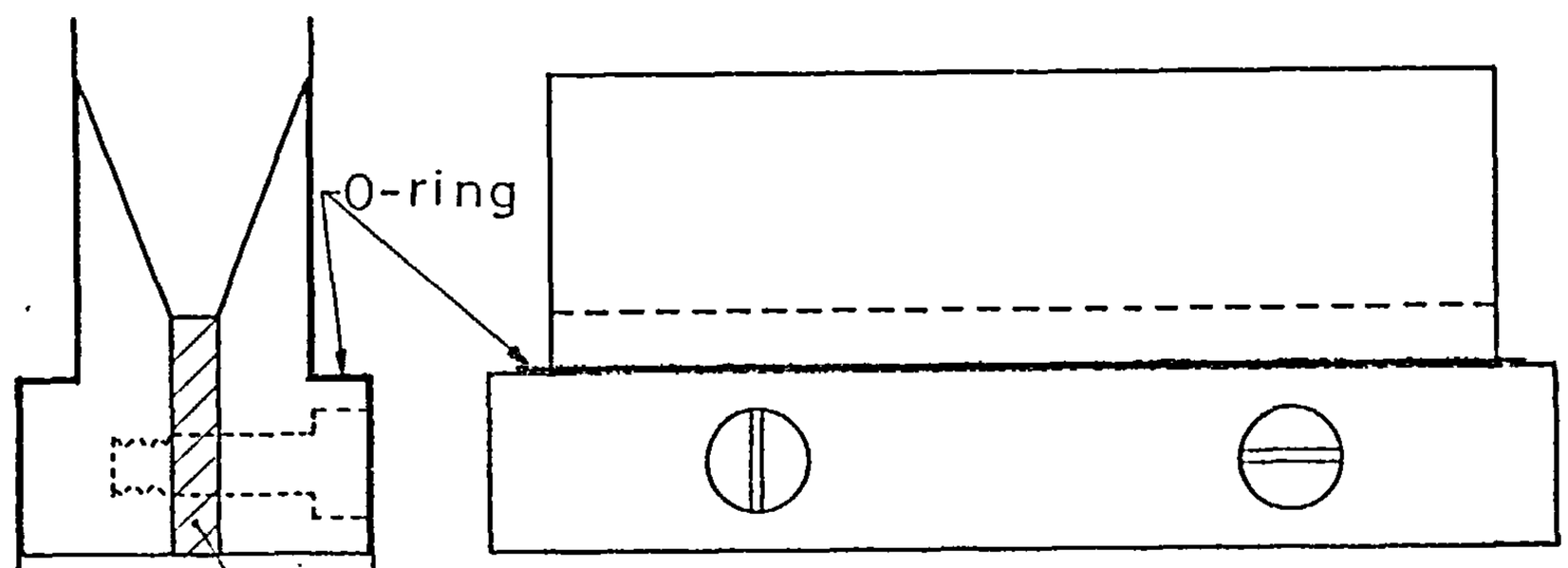

b) Single Felt

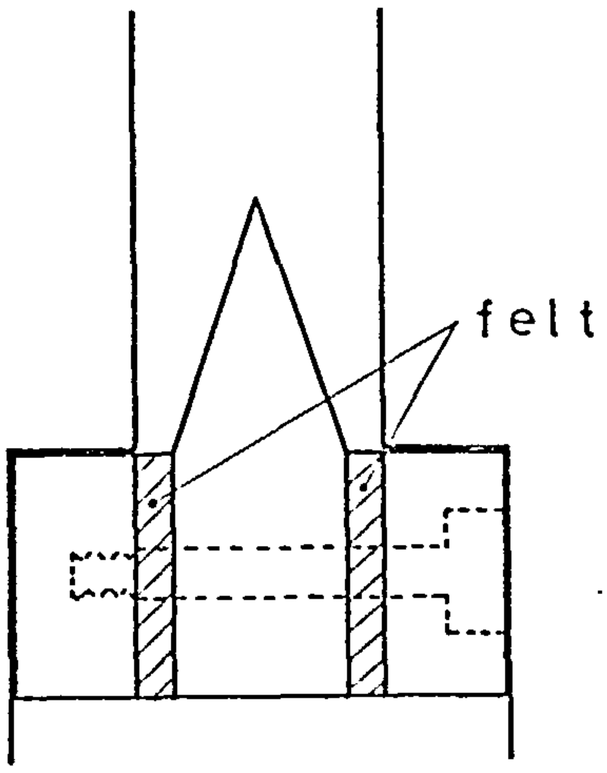

c) Double Felt

FIG. 4.4

4.5. Design of the Potential Probes

The same set of probes were used for the experimental measurement of potential distribution in both the planar and cylindrical cells.

For sensing electrolyte potentials the probe illustrated in Figure 4.5 was used. It was made as follows. The upper end of a glass tube, outside diameter 0.4 cm, was jointed to a perspex tube by tensol cement, and the lower end was drawn out into a Luggin capillary of length 1.5 cm. The tip of the capillary was approximately 0.03 cm in diameter and was bent through an angle of 90^{o} as shown. In operation the Luggin and connecting tubing was filled with electrolyte to provide an electrically conducting link with a saturated calomel electrode. This in turn was wired up to the feeder to produce a closed circuit.

Although two probe designs were used formeasuring potential distributions in the dispersed phase, they differed only in the shape of their sensing elements (Figure 4.5) and broadly speaking were made in the same way. Copper wire was soldered to a short length of platinum wire and then threaded through a sleeve of glass tubing, 0.4 cm outside diameter, which had been slightly extruded at one end, and again attached to a perspex tube at the other. A portion of the platinum wire was left projecting from the extruded end which was then fused to give a platinum-to-glass seal. The protruding platinum constituted the sensing element of the probe, both types of which are illustrated in their final form, with dimensions, in Figure 4.5. The platinum "T" piece which was required for one of the probes was readily made by

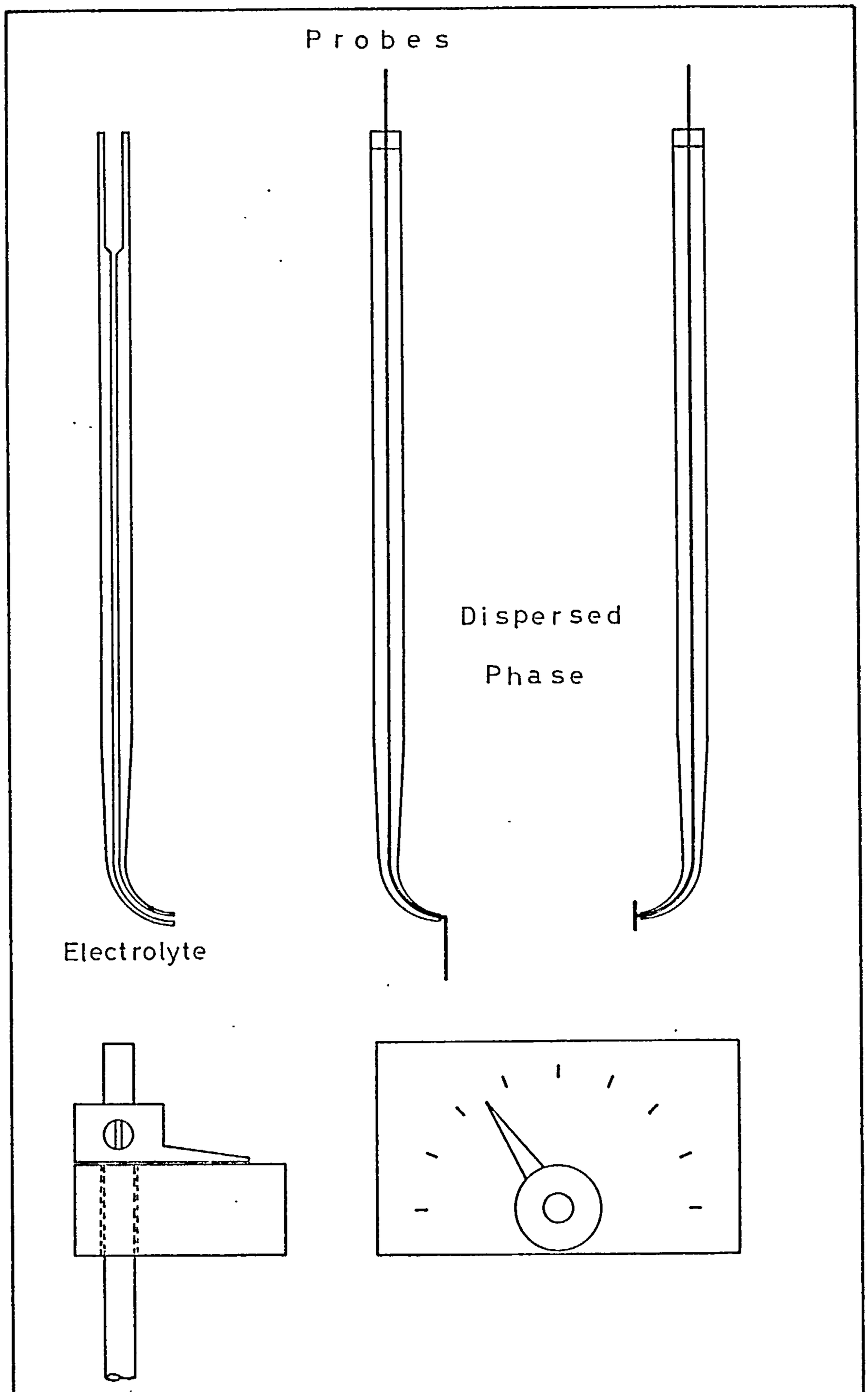

FIG. 4.5

heating two pieces of platinum wire to red heat and welding them together by a sharp blow. For obvious reasons this step was completed before the probe was made up. In operation the probes were connected to the feeder by an external circuit containing a Digital Voltmeter (E 7 Appendix E).

The reason for using the two designs is as follows. The sensing element is essentially a length of wire immersed in a system of conducting particles. At any instant in time there may be a distribution of potential along the element reflecting the distribution of potential among the particles making contact with it. The reading indicated on the DVM at the same instant would correspond, not to the average potential, but to that of the platinum wire at the point where it entered the glass seal. In one case this would be at the extreme end of the sensing element and in the other at the middle. Any significant systematic error arising from this source could therefore be detected by comparing the readings of the two probes under the same experimental conditions. In reference the probes will be distinguished as one- and two-end probes.

In practice the electrolyte and dispersed phase potentials were measured in separate experiments, so that the same supporting device could be used for both sets of probes. In the case of the cylindrical cell the perspex portion of the probe passed through a hole in the cell cap as a sliding fit and was held in place by a bush and locking screw, as shown in Figures 4.1 and 4.5. The position of the probe in a vertical sense was indicated on a scale mounted externally to the cell and could be altered at will by loosening the locking screw. Its horizontal location could be altered by simple rotation, causing the tip to traverse the bed along an arc, as indicated in Figure 4.1.

Its position in this sense was indicated by a pointer attached to the bush which moved over a horizontal scale as shown in Figure 4.5. Calibration of this scale was carried out with the cell empty. A further degree of adjustment was possible by rotation of the cell cap. The equivalent freedom of movement in the planar cell was achieved by carrying the probe on a slide (see Figure 4.2), but in other respects the mounting was identical to that in the cylindrical cell.

4.6. Electrode Particles

The particles forming the electrode were in all experiments spherical glass beads coated with a thin layer of copper.

The method employed for coating the glass beads is a chemical reduction used by several workers and described in detail in Appendix C. Some of the beads' properties relevant to the present work are summarised in Appendix D.

Unless otherwise specified it should be assumed that the size of beads used in the experiments is 550 microns mean diameter (sieved between 500 and 600 μ).

CHAPTER 5. CURRENT EFFICIENCIES IN FLUIDISED BED ELECTRODES

5.1. Introduction

In the present work current efficiency has its generally accepted meaning, which, in respect of copper deposition, is the ratio of the mass of copper deposited to that which should have been deposited according to Faraday's law. Since one faraday discharges 31.77 g of Cu^{++} it follows that current efficiency, η , may be calculated from

$$\eta = 3.0372 \times 10^{3} \times \omega / I_c \theta$$

where ω is the mass of copper deposited, in grams, over an interval of θ secs with cell current of I_c amps.

The experiments described in this chapter were conducted to determine current efficiencies for copper deposition on fluidised electrodes from dilute solutions of cupric ions. Of the factors which might influence current efficiency special emphasis has been placed on copper ion concentration, bed expansion, and current density at the diaphragm. The latter requires definition, and in the present work it is the ratio of total cell current to the area of diaphragm in contact with the fluidised bed. Diaphragm current density has been preferred to electrode potential as a measure of the electrical characteristics of the bed for two reasons. Firstly, both true current density and electrode potential vary in a complex way throughout the particulate mass and therefore a unique value of either of them can at best offer only a rough guide to the electrical condition of the bed. Under these circumstances the choice fell on the one which was more

readily observed, namely, diaphragm current density. Secondly, it is felt that a parameter defined in this way is much more meaningful in a commercial context, since it allows a more or less direct comparison to be made between the performance of cells employing plate and fluidised electrodes.

In general the experimentation was arranged such that current efficiencies were determined for two levels of each of the variables. It is fully realised that this approach is capable of providing only a broad picture of the dependency of current efficiency on the selected variables. No more than this was intended, since, in the opinion of the author, a clear understanding of the behaviour of a three dimensional electrode requires a detailed study of potential distribution, to which much of the present work has therefore been devoted. Nevertheless the type of information contained in the present chapter, albeit somewhat qualitative serves the important function of pin-pointing any obvious disadvantages, technical or economic which might discourage the use of fluidised electrodes in copper recovery.

5.2. Experimental Procedure

Current efficiencies were determined for both the cylindrical and planar cells and in each case the experimental system was set up as shown in Figure 5.1. The experimental procedure adopted, however, varied according to the parameter under investigation, procedure A being used to study the effect of copper ion concentration, and procedure B for the effect of bed expansion and diaphragm current density.

FIG. 5.1

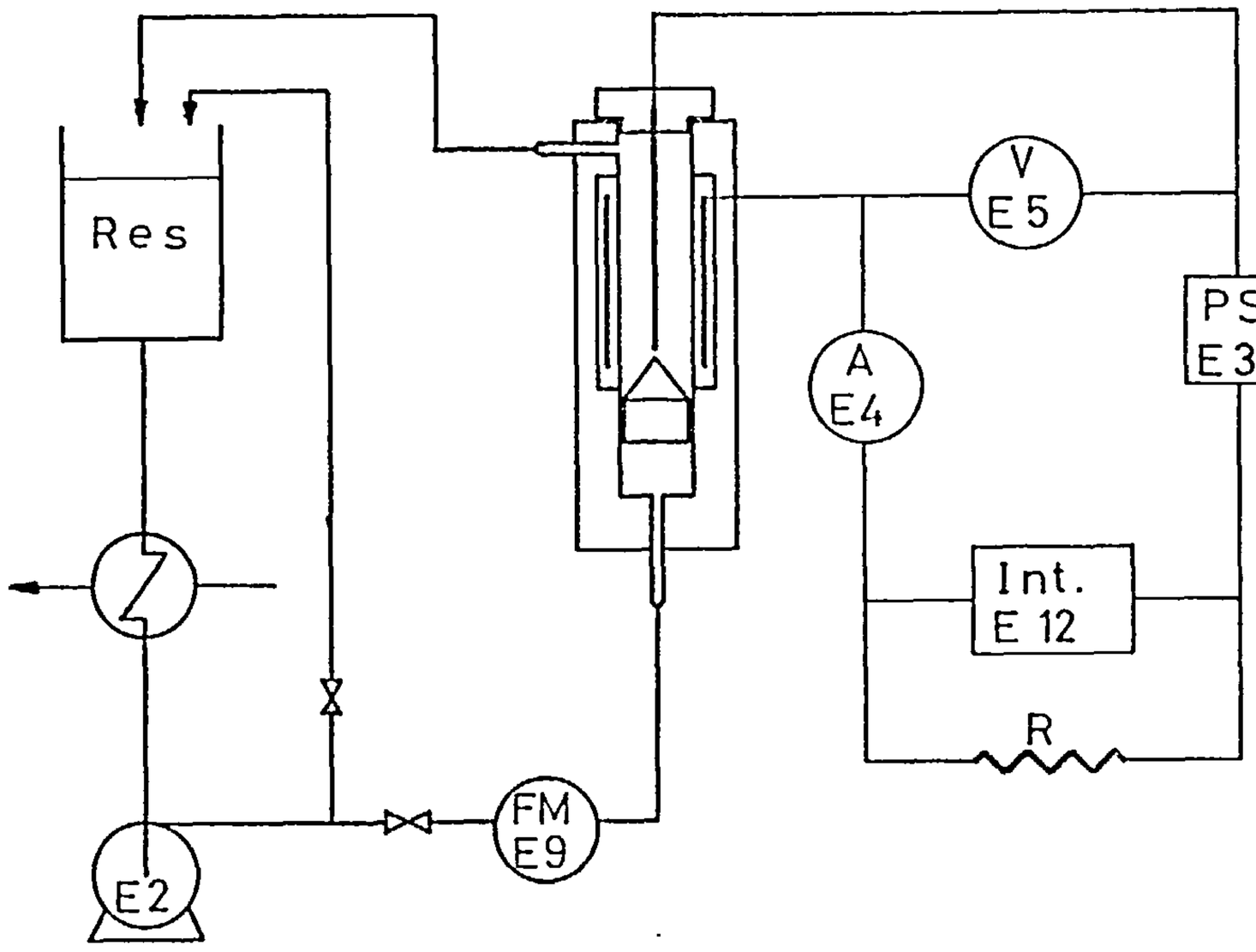

Concentration Decay FIG. 5.2

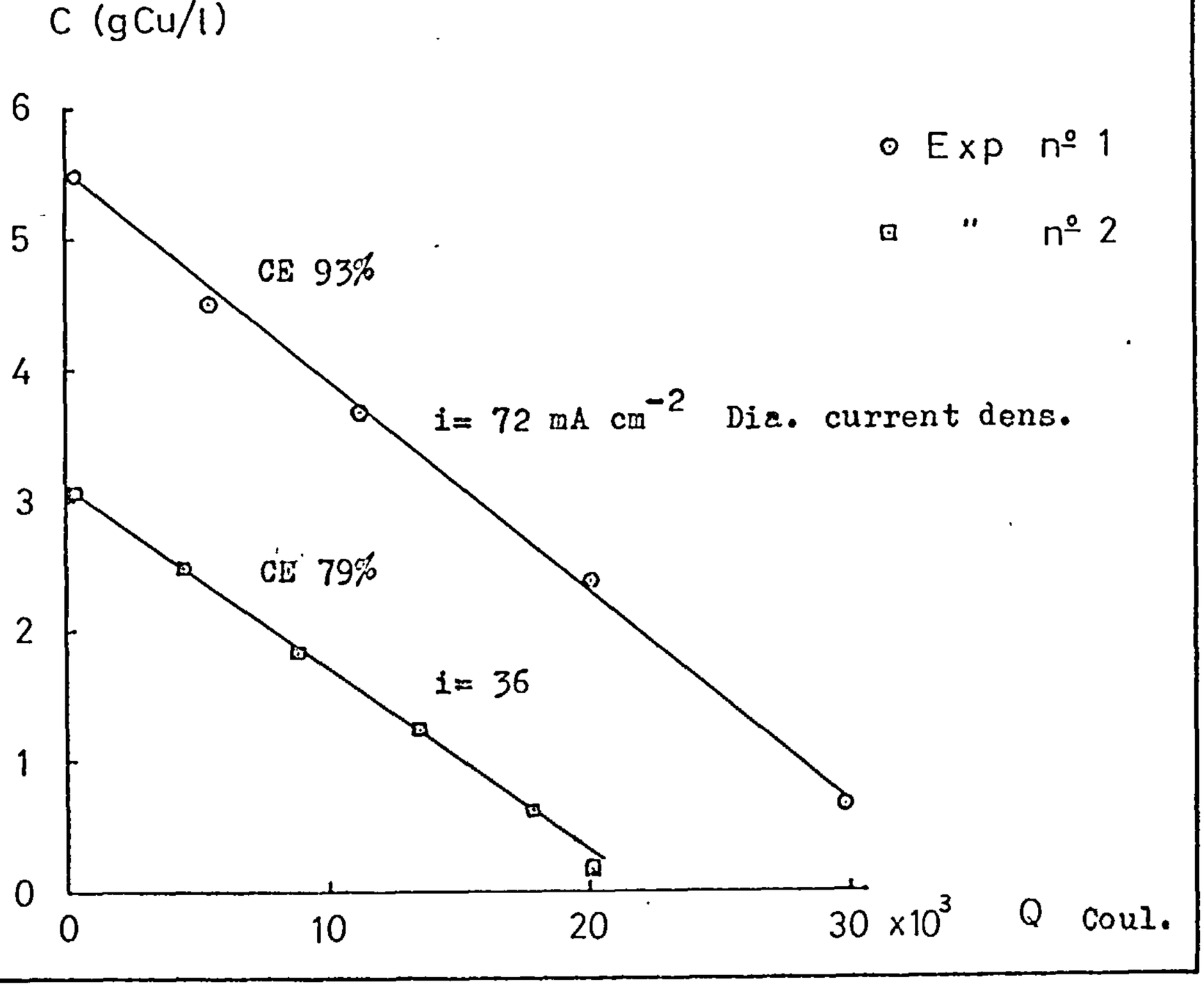

Procedure A

The electrolyte pump was first switched on and after adjusting the circulation rate to achieve the required bed expansion the cell circuit was closed. Electrolysis was carried out at constant current and after a settling down period of 10 minutes had elapsed electrolyte samples were taken at regular intervals together with the corresponding readings of the current integrator. The samples were analysed for copper according to the method described in Appendix B, and current efficiencies were determined from the rate of decay of copper ion concentration, corrected for volume of each sample, and the corresponding instantaneous value of integrated cell current.

An example of the calculations is summarised in Table 5.1. In practice these calculations are reduced to the determination of the slope of the line arising from a plot of electrolyte copper concentration against integrated current, assuming that the volume of electrolyte remains constant, i.e. the volume of a sample is negligible when compared with the volume of the electrolyte.

TABLE 5.1. Current Efficiencies. Procedure A

t (min)	C (gr/l)	$-\Delta C$	V (ml)	ω (g)	Q(coul)	CE(%)
0	3.08	0	1920	0	0	-
15	2.49	0.59	1890	1.12	4500	76
30	1.85	0.64	1860	2.31	8960	78
45	1.26	0.59	1830	3.37	13500	76
60	0.63	0.63	1800	4.51	17900	77
68	0.18	0.45	1770	5.31	20260	79

Procedure B

This procedure commenced in the same way as Procedure A up to the point where a sample of electrolyte and the current integrator reading had been taken. No further samples were then taken, however, until a sharp rise in cell voltage was observed and massive hydrogen occurred. At this point a second and final sample of electrolyte was taken, together with the reading on the current integrator. The samples were analysed for copper and current efficiency determined from a mass balance on the electrolyte between its initial and final condition.

This procedure strictly gives an average current efficiency for the operation, and not point values corresponding to specific copper ion concentrations. It was justified, however, after previous tests, conducted according to Procedure A, had shown that for any given set of operating conditions the current efficiency of copper deposition exhibited a steady value over a wide range of copper ion concentration, provided that this remained over a certain minimum level. This minimum level corresponds to the "end-point" of the above experimental procedure and was quite readily recognised by the rise in cell voltage, which took place over the space of 30 seconds or so, to attain the new value required by hydrogen evolution. The concentration of copper ion at which this occurred is termed, in the present work, the limiting concentration, and its value is given by the analysis of the final sample.

In Table 5.2 a calculation of the current efficiency according to this procedure is summarised. The cell used was the Cylindrical Cell I.

TABLE 5.2. Current Efficiency. Procedure B

Bed expansion	=	20%
Cell current	=	2.4A
time	=	40 minutes
C_o	=	1.55 g/l
C limiting	=	0.105 g/l
Electrolyte volume	=	850 ml
Quantity of electricity	=	5810 coulombs
$-\Delta C$	=	1.445 g/l

CE = $(3.0372 \times 1.445 \times 0.85) \times 10^5/5810$ = 64.2%

5.3. Effect of Cupric Ion Concentration

The effect of cupric ion concentration on current efficiency was determined using cylindrical cell I. The experiments were carried out according to Procedure A and were terminated at the limiting copper ion concentration. Two levels of diaphragm current density were investigated, and the experimental conditions are summarised in Table 5.3. The results are plotted in Figures 5.2 and 5.3 together with an indication of the limiting copper ion concentrations for each of the diaphragm current densities used.

TABLE 5.3. Operating Conditions for Experiments of Figures 5.2 and 5.3

	⊙	⊡
Volume of expanded bed	143 cc	143 cc
Temperature	21°C	21°C
Electrolyte volume (initial)	1.9 ℓ.	1.9 ℓ.
Bed expansion	10%	10%
Cell current	9.7A	4.8A
Diaphragm current density	72 mA cm^{-2}	36 mA cm^{-2}

Current Efficiency dependency on Copper ion concentration

Fig. 5.3

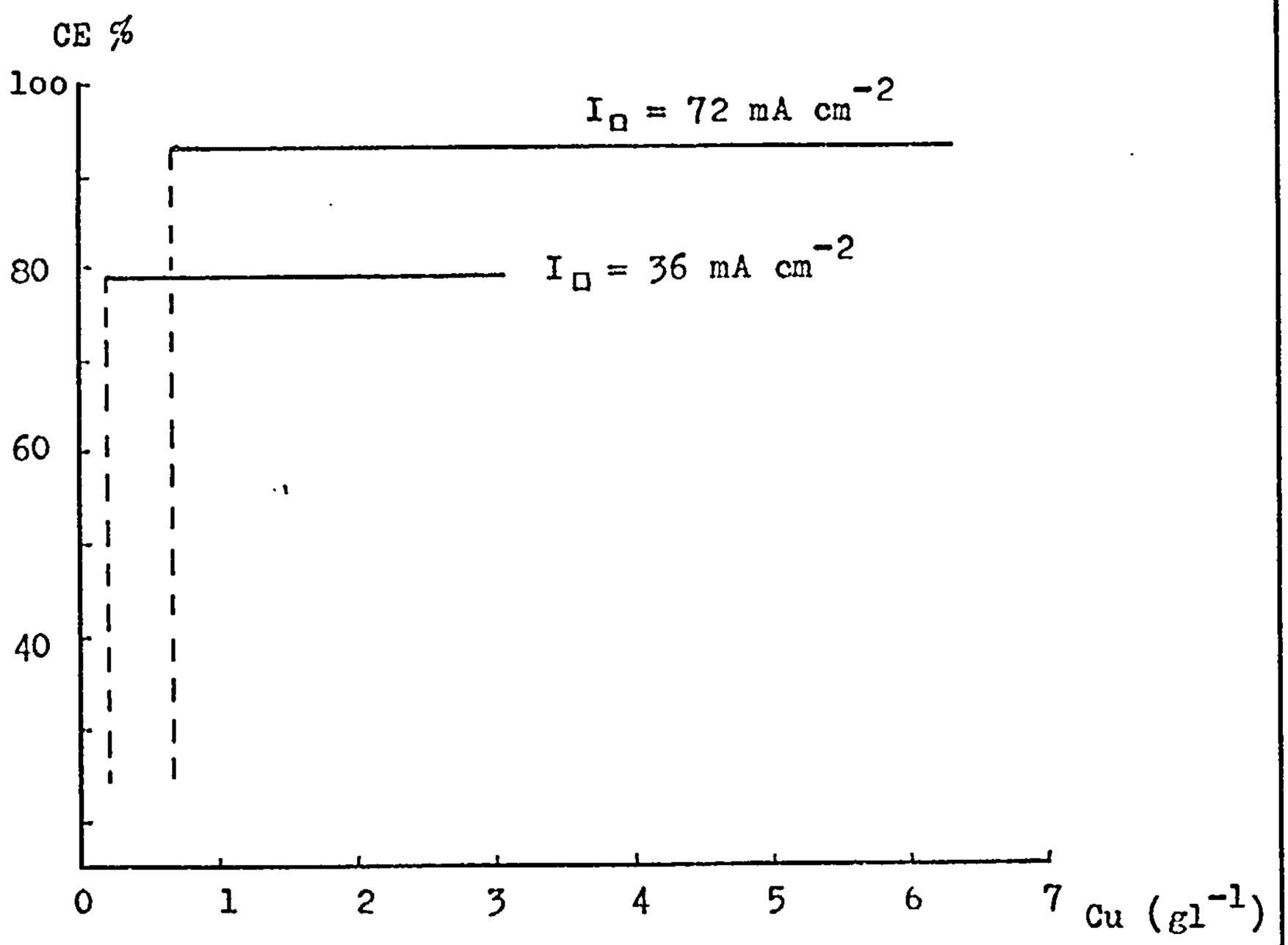

Current Efficiency dependency on Bed Expansion

Fig. 5.4

Cylindrical ————

Planar — — —

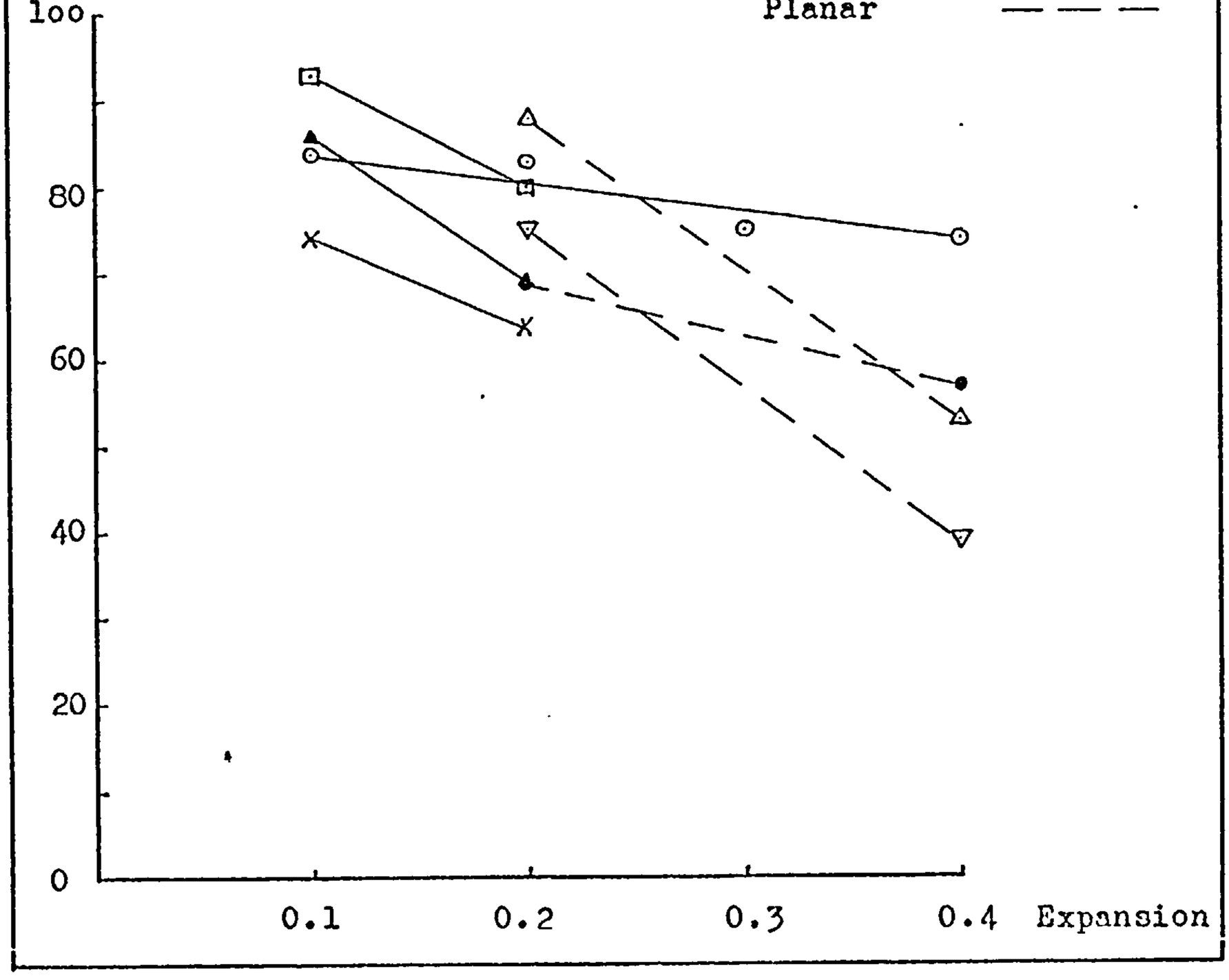

It can be seen from Figure 5.3 that for any given set of operating conditions it is likely that current efficiency is independent of copper ion concentration until the limiting value is reached, at which point it suffers a rapid decline. So rapid, in fact, that this condition is indicated in Figure 5.3 by a vertical broken line. This assertion was supported by separate experiments using the cylindrical cell II where current efficiencies of 83% and 75% attained before massive hydrogen evolution occurred, dropped to 30% and 16% when hydrogen evolution had been taking place for a short period of time (5 and 10 mins. respectively). These observations were not entirely unexpected since they are not inconsistent with the data for plane electrodes in Figure 3.6.

The significant effect of diaphragm current density on current efficiencies brought out by Figure 5.3 will be discussed under a separate heading.

Although it would appear appropriate to give some discussion under this heading to the limiting copper ion concentration, it is felt more helpful to do so later in conjunction with potential distribution, to which it is particularly sensitive. However, it can be recorded that in cylindrical cell II deposition was achieved down to copper ion concentration of 50 and 17 p.p.m. (diaphragm current density 22 and 11 mA cm^{-2} respectively) with current efficiencies in excess of 70%

These conclusions corroborate the findings of FLETT[41] who asserts that the current efficiency remains constant, even when the copper concentration reaches p.p.m. levels, e.g. 27 p.p.m.

SURFLEET (see KUHN[41]) found that the efficiency does not decrease sharply until some 10 p.p.m. Cu levels are reached.

5.4. Effect of Bed Expansion

Using Procedure B, current efficiencies were determined for cylindrical cells I and II, and the planar cell with both single and double felt distributors. The results are shown in Figure 5.4 and summarised in Table 5.4, for a number of levels of diaphragm current density, and although they are not entirely self consistent it is clear that there is in all cases a fall in current efficiency with increase in expansion. As far as the results will allow a quantitative examination, they indicate that there is roughly a linear drop in current efficiency, over the range of expansion considered, (10% - 40%), amounting to 10% for every 10% rise in expansion. Actual efficiencies in any particular case apparently depend upon the geometry of the cell and the current density at the diaphragm, but over the whole range of variables investigated, current efficiencies were for the large part better than 70% at an expansion of 20%.

It cannot be over-emphasised, however, that only a broad picture can be discerned from this type of experiment, and that a thorough understanding requires a detailed study of potential distribution.

TABLE 5.4. Variation of Current Efficiency with Bed Expansion

	Fig. 5.4	Exp.	CE %	$I_{\square}$ (mA cm^{-2})
Cylindrical Cell I	□	0.1	93	72
		0.2	80	72
	▲	0.1	86	36
		0.2	69	36
	×	0.1	74	18
		0.2	64	18
Cylindrical cell II		0.1	84	22
	○	0.2	83	22
		0.3	75	22
		0.4	69	22
Planar Single Felt	△	0.2	88	36
		0.4	53	36
	▽	0.2	75	18
		0.4	39	18
Planar Double Felt	●	0.2	69	36
		0.4	57	36

Copper ion concentration 0.1 Molar

Sulphuric acid concentration 0.1 Molar

Temperature $20^{o}C \pm 2^{o}C$

5.5. Effect of Diaphragm Current Density

The effect of diaphragm current density on current efficiency has been examined using all the cells according to Procedure B. The results are summarised in Table 5.5 and plotted in Figure 5.5, and correspond, with one exception, to a bed expansion of 20%. Within the range over which the variables were investigated, all the curves show a tendency to improved current efficiency with increase in diaphragm current density. In particular it may be concluded that for diaphragm current densities below 20 mA cm^{-2} a sharp drop in efficiency is experienced. This may be partly due to lack of adequate cathodic protection of some parts of the bed at the correspondingly low cathodic potentials, and partly due, at low deposition rates to the greater relative significance of chemical dissolution by the action of oxygen.

A short digression in the experimental work was made at this point to confirm the corrosive effect of oxygen on copper, in the presence of sulphuric acid. The planar cell with double felt distributor was used, and a number of experiments were conducted to determine the effect of oxygen when transferred from the anode to the cathode chamber by diffusion and bulk flow. In the latter case a slight leakage was allowed to occur around the diaphragm, which, although it could not be measured when the cell was in operation, was arranged to simulate what could happen in a faulty possible commercial cell. To observe the behaviour of the cell under the lowest possible level of oxygen content, the anolyte chamber could be swept continuously with oxygen-free nitrogen. A summary of the results is given in Table 5.6,

Current Efficiency dependency on Particle Size

Fig. 5.6

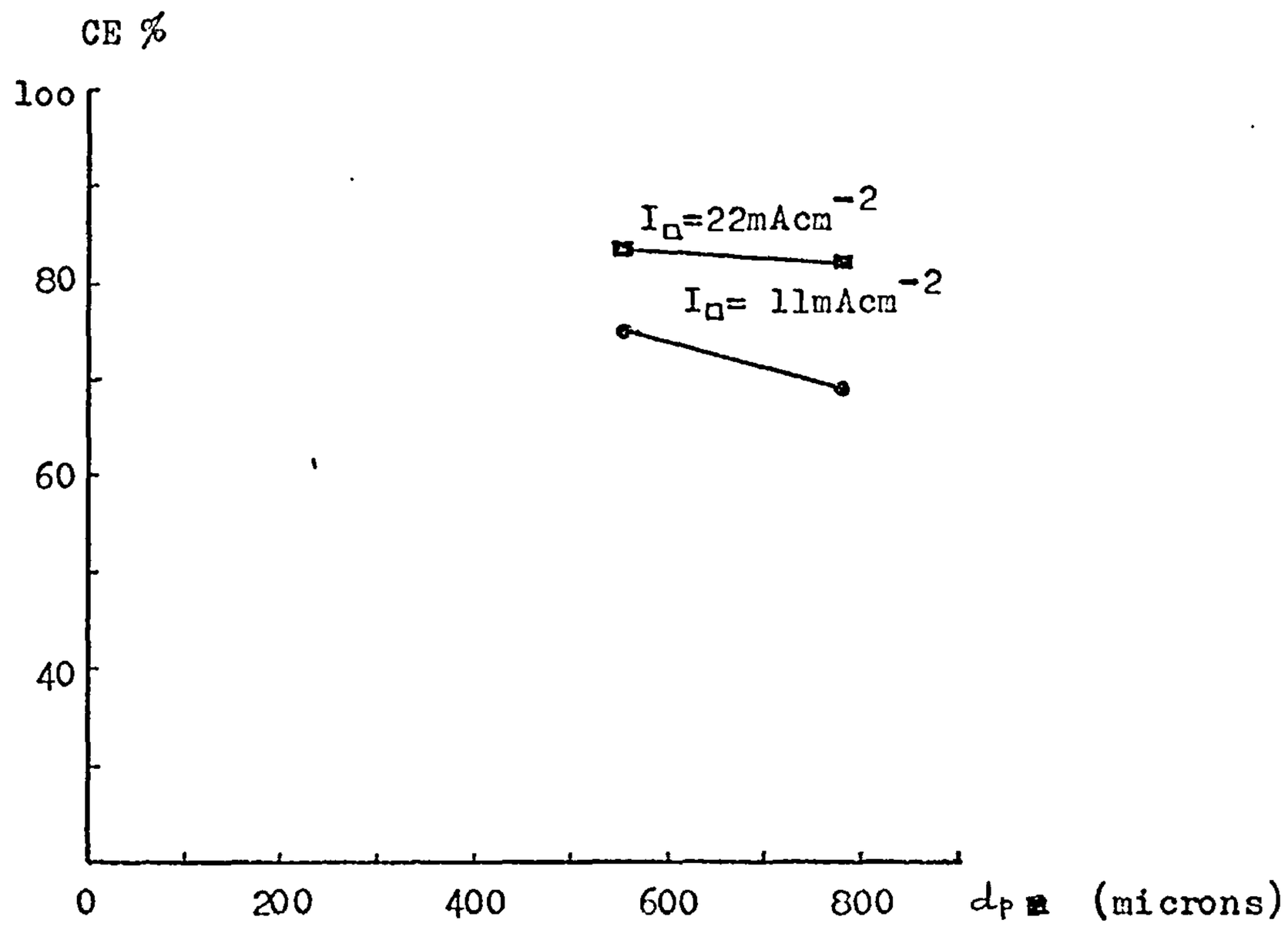

Current Efficiency dependency on Diaphragm Current Density

E = 0.2

Fig. 5.5

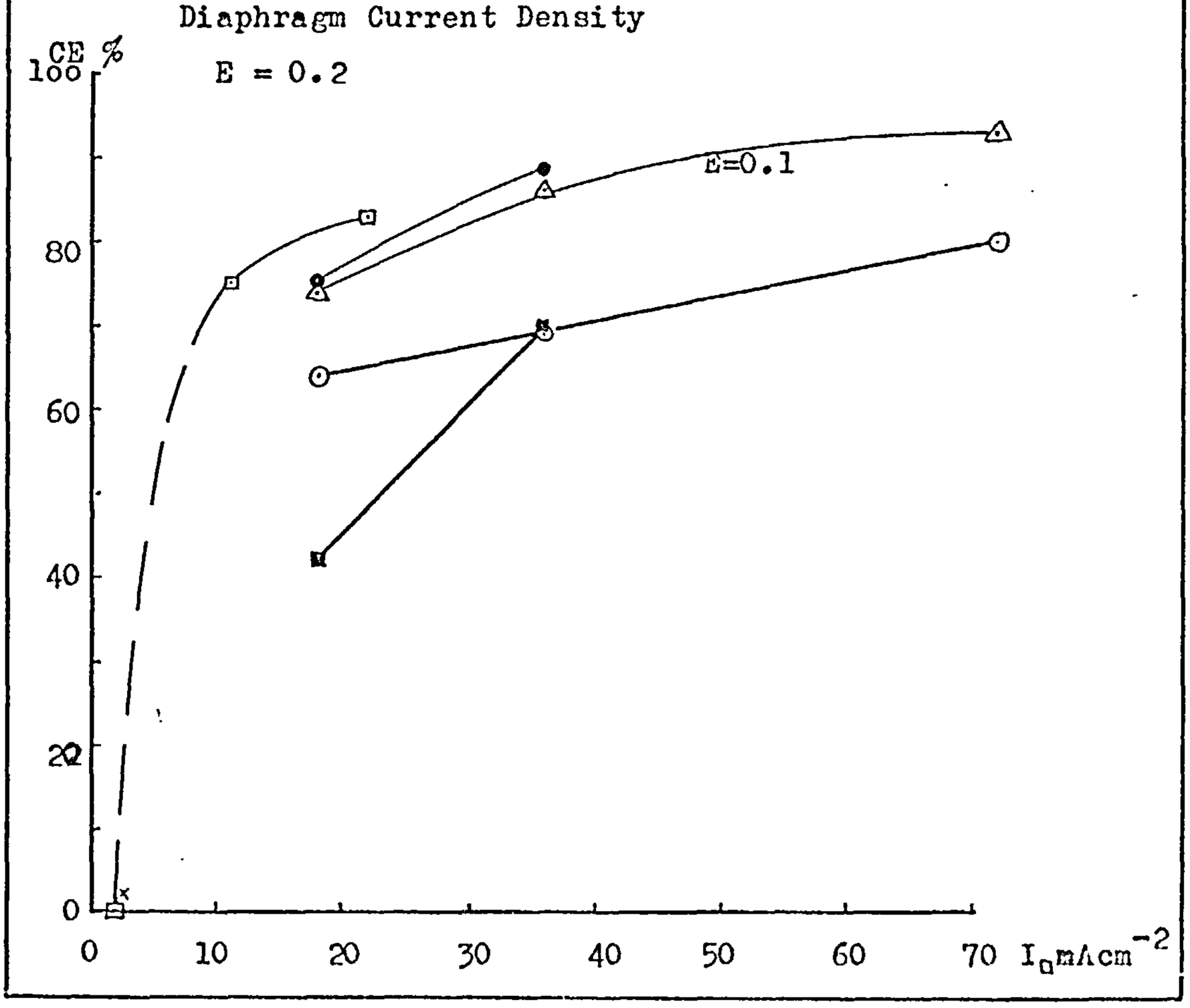

which show that even with only slight bulk mixing of anolyte and catholyte, a serious reduction in current efficiency arises, strongly indicating therefore that oxygen is a powerful corrosion agent in acid media. This is given further support by the fact that the introduction of oxygen-free nitrogen into the system significantly lessens the effect. Nitrogen had no influence, however, when the separation of the anode and cathode chambers was made perfect, from which it may be deduced that both oxygen diffusion and bulk flow through the Celloton diaphragm are negligible, and that diaphragms of this type may be eminently suitable for this type of operation.

The conclusions of this section are in agreement with those of FLETT[41]. He arrives at the conclusion that the variation in the current efficiencies for the fluidised cathode relates to a slow back dissolution of copper by the acidic electrolyte, thus causing a general increase in current efficiency as the current density is increased. Incidently he found that reduction in pH did not affect current efficiency, thus a pH of about 0.5 (1.0 N) was chosen for his studies.

In a plane electrode, however, current density has the reverse effect on current efficiency, i.e. it decreases with increasing current density. This is due to hydrogen evolution, but it should be remembered that the fluidised electrode experiments were deliberately carried out at concentrations where no hydrogen evolution occur, therefore the losses in current efficiency were due to a different cause, namely, copper dissolution.

TABLE 5.5. Variation of Current Efficiency with Diaphragm Current Density

Exp.	I_D (mA cm^{-2})	CE %	Fig. 5.5
Cylindrical Cell I	0.1	72	93	
	0.1	36	86	△
	0.1	18	74	
	0.2	72	80	
	0.2	36	69	○
	0.2	18	64	
Cylindrical Cell II	0.2	22	83	
	0.2	11	75	□
	0.2	2	*	
Planar Cell Single Felt	0.2	36	88	●
	0.2	18	75	
Planar Cell Double Felt	0.2	36	69	■
	0.2	18	42	

* Copper Dissolution; 1.9 mg Cu hr^{-1} cm^{-3} of bed

Copper ion concentration 0.1 Molar

Sulphuric acid concentration 0.1 Molar

Temperature $20^{o}C \pm 2^{o}C$

TABLE 5.6. Effect of Oxygen on the Current Efficiency of Copper Deposition

Anode/Cathode Separation	Nitrogen Presence	C.E. (%)
Imperfect	No	45
Imperfect	Yes	58
Perfect	No	69
Perfect	Yes	69

Experimental Conditions:

Expansion	20%
Diaphragm current density	36 mA cm^{-2}
Temperature	22°C
Copper ion concentration	0.1 Molar
Sulphuric acid concentration	0.1 Molar

5.6. Effect of Particle Size

The effect of particle size on current efficiency was carried out in Cylindrical Cell II according to Procedure B, using particles of two sizes, namely, 550 and 780 microns. The results are tabulated in Table 5.7 and plotted in Figure 5.6. From the limited data obtained it is tentatively concluded that particle size has only a slight, if any, effect on current efficiency, although a more detailed study is necessary before this could be stated with certainty. Table 5.7 also shows that at low currents, and therefore low cathodic potentials, both particle sizes exhibited a net dissolution which was slightly, but perhaps not significantly, higher in the case of the largerparticles.

It should be mentioned at this point that the coating of 550 microns glass beads by the electroless method described in Appendix C, produced practically 100% coated beads. However, with 780 microns particles, a small proportion of the beads was not totally coated, this proportion was much higher when using 1 mm beads, and therefore this size was not examined.

TABLE 5.7. Variation of Current Efficiency with Particle Size

Particle size (microns)	Expansion (%)	$I_{\square}$ (mA cm^{-2})	C.E. (%)	Fig 5.6
780	20	22	82	■
550	20	22	83	
780	20	11	69	●
550	20	11	75	
780	20	2	(1)	
550	20	2	(2)	

(1) Dissolution 2.7 mg Cu hr^{-1} cm^{-3} of bed
(2) Dissolution 2.2 mg Cu hr^{-1} cm^{-3} of bed

5.7. Agglomeration

Agglomeration of particles occurs when two or more particles of the fluidised bed are permanently linked either by cohesive deposition or surface tension. Accumulative agglomeration is not only detrimental to flow distribution but in the extreme may cause partial or total "freezing" of the bed.

Qualitative observation of its occurrence was made in all experiments and was found to be absent at low diaphragm current densities and high expansions.

Between 5 and 10% of the bed was agglomerated at 10% expansion and 72 mA cm^{-2} diaphragm current density in Cylindrical Cell I, but at 36 mA cm^{-2} no agglomeration occurred. In the planar cell, single felt distributor, agglomeration was observed at the edges of the distributor where particles were trapped between the distributor and the catholyte chamber's walls.

It appears therefore that agglomeration is favoured by:

(i) low bed expansions,

(ii) high cell currents, and

(iii) non-homogeneous fluidisation, dead spaces within the bed, etc.

Anticipating the findings of Chapter 6, it is suggested that cell designs with flow directed to the feeder and diaphragm might be desirable since these surfaces are generally associated with the higher rates of deposition.

5.8. Summary

Conclusions and comments made in this chapter are strictly applicable to the cells used in the experimental work, particularly in

regard to dimensions in the direction of current flow, which for convenience are tabulated below in Table 5.8.

TABLE 5.8. Cell dimensions parallel to the direction of current flow

Cell	Cylindrical Cell I	Cylindrical Cell II	Planar Cell Single Felt	Planar Cell Double Felt
Dimension cm	1.85	1.50	2.0	2.0

Bearing this in mind, the following points emerge from the investigations described so far.

Firstly, and most important, it has been demonstrated that copper deposition can be carried out satisfactorily in a fluidised bed of conducting particles with current efficiencies in excess of 90%. This claim is based on experimental runs in which the copper ion concentration exceeded the limiting value, the diaphragm current density was in excess of 20 mA cm^{-2} and the bed expansion was 20%. Outside this condition current efficiencies far below 90% may be encountered, particularly at very low copper ion concentrations where low diaphragm current densities are required to avoid hydrogen evolution. At these current densities a further difficulty can arise from copper dissolution by oxygen corrosion giving net efficiencies well below 90%. Even so copper ions were discharged at a concentration of 17 p.p.m. with an efficiency better than 70%. It is noteworthy that these results were achieved in Cylindrical Cell II which, compared to the other cells, had the smallest dimension in the direction of current flow. This tends to

point out to careful choice of cell geometry as an important criterion in the efficient processing of very dilute solutions.

Secondly, the occurrence of agglomeration in prolonged runs may be troublesome, and may need a great deal of development in cell design to be overcome.

Thirdly, there is no evidence to suggest that change in particle size due to deposition would have a detrimental effect on the deposition process, provided, presumably, that the usual minimum ratio of bed width to particle size is observed.

CHAPTER 6. ELECTRODE POTENTIAL DISTRIBUTION IN THE FLUIDISED BED ELECTRODE

6.1. Introduction

The behaviour of a fluidised bed electrode is the summation of the behaviour of each of its constituent particles. In turn, the rate of deposition on each particle at any instant will be directly related to its electrode potential in accordance with the polarisation characteristics already determined for the plane electrode system (Chapter 3).

The analysis of the performance of a fluidised electrode by experimental observation of each of the entire population of particles is obviously impracticable, but there are two other approaches. Firstly, it can be assumed that all particles over a sufficiently long interval of time experience an identical "electrical" history, and therefore the behaviour of one particle in the bed is representative of the whole. A detailed knowledge of the performance of the bed could therefore be deduced from the experimental observation of just one, or perhaps a few, of its constituent particles. The second approach makes use of the assumption that, all other conditions being equal, the electrical condition of a particle depends primarily on its spatial location in the bed. On this basis the performance of the electrode can be analysed in terms of the average distribution of electrode potential as interpolated from values measured at a number of specific fixed points. Of these two approaches, the second is not only much simpler from a practical point of view but has already been

justified by GOODRIDGE et al[25,26]. On these grounds it was selected for the present work, and potential distributions have been observed in cylindrical and planar cell geometries and for a number of electrolyte compositions, particle sizes, bed expansions and diaphragm current densities.

The results and discussion relating to the cylindrical cell geometry are treated separately from those from the planar cell geometry, and in the latter case opportunity has been taken to emphasize any differences which were observed between the two geometries. It can also be pointed out at this juncture that discussion of the results in the present ~~chapter~~ section is restricted to the experimental evidence, and further interpretation in terms of the mathematical model proposed by GOODRIDGE et al[25,26] is left to a later one ~~(Chapter 7)~~. In this way it is hoped to eliminate any confusion which might otherwise occur between deductions drawn from observation and those derived from hypothesis.

As a preliminary exercise, electrolyte potential distributions were also measured in fluidised beds of glass beads to determine effective electrolyte conductivities and to substantiate the use of BRUGGEMAN'S relationship[43].

6.2. Experimental Procedure

The appropriate cell was connected into the flow and electrical circuits shown schematically in Figure 6.1. Electrolyte was circulated by switching on pump E2, and the rate adjusted to produce the required bed expansion. The electrical supply circuit was closed, and the cell

run at constant current using manual control. This procedure was preferred to automatic potentiostatic control because slight variations in the local condition of the bed at the point of control required relatively large compensating changes in cell current, with the result that the cell never attained steady operation.

Throughout all the runs the copper ion concentration was maintained at an approximately constant level ($\pm$ 5%) by continuous injection of concentrated aqueous copper sulphate (1 Molar). The injection was made by a variable stroke micrometering piston pump at a rate determined by the cell current and an assumed current efficiency of 75%.

When the system had settled down, the continuous and dispersed phase potentials were measured successively by the probes described in Section 4.5. In practice it was found that the dispersed phase potential was much more prone to fluctuation than that of the continuous phase, and the readings quoted later are in nearly all cases the mean of twenty readings. The exception to this general rule concerns the planar cell with single felt distributor for which special steps were taken to reduce the effect of the fluctuations on the probe, but more will be said of this in the appropriate discussion.

A typical batch of twenty readings is shown in Table 6.1.

Fig. 6.1

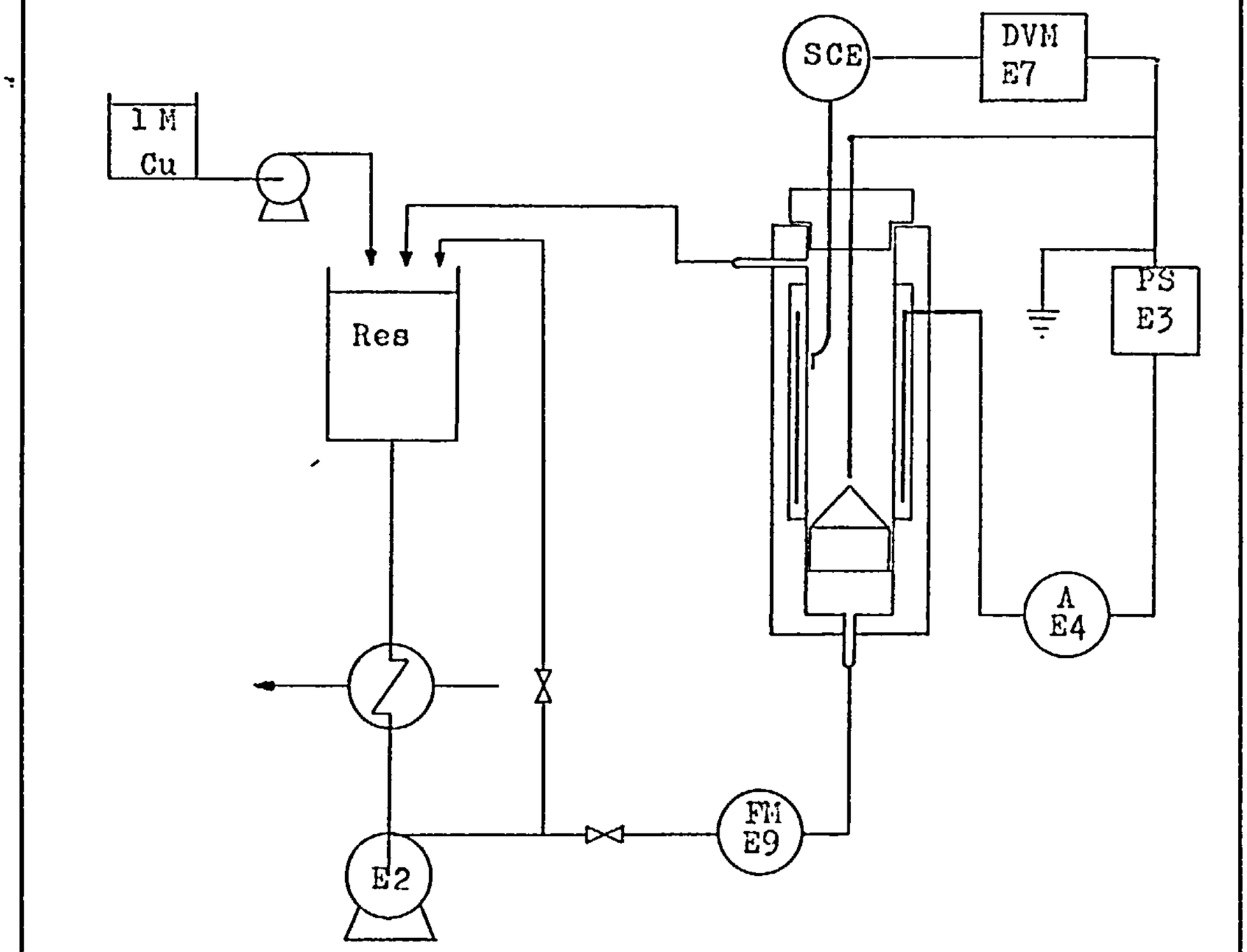

Planar Cell

0.1 M Cu E 20%

Fig. 6.2

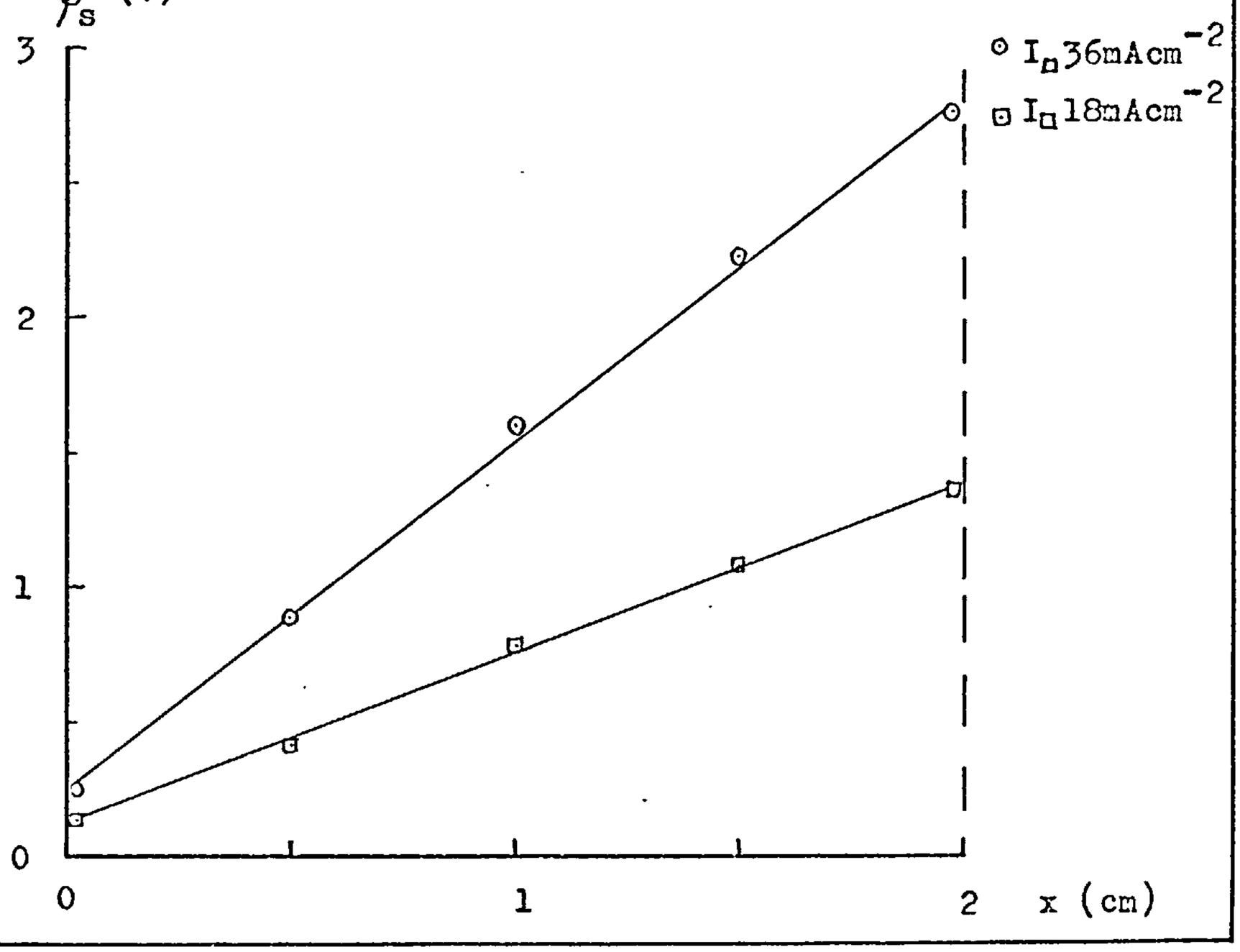

TABLE 6.1. Typical Readings of Continuous Phase Potential ϕ_s

ϕ_s (mV)			
129	148	131	126
130	123	116	130
122	112	114	141
120	131	115	122
129	134	137	129

Experimental Conditions:	
Copper ion concentration	0.1M
Sulphuric acid concentration	0.1M
Bed expansion	20%
Diaphragm current density	36 mA cm^{-2}
Reference Electrode:	Saturated Calomel

6.3. Results and Discussion

6.3.1. Effective Electrolyte Conductivity

It has become the general practice for a conducting medium forming the continuous phase in a heterogeneous system to be treated as a continuum, with the true conductivity replaced by an effective conductivity which takes into account the heterogeneity (see, for instance, ref. 43).

It follows, therefore, that in a fluidised bed the flow of current I in the electrolyte across a plane of area A, will be given by

$$I = - K_s A \frac{d \phi_s}{dn} \qquad \ldots\ldots\ldots(1)$$

where n represents distance, measured normal to the plane and ϕ_s

the electrolyte potential at the plane. The sign convention requires that I be treated as positive when flowing in the positive direction of n. K_s is the effective conductivity of the electrolyte.

For an electrode of cylindrical symmetry with current flowing radially, the above equation may be written in the form,

$$I = - K_s \; 2\pi r h \; \frac{d \phi_s}{dr} \qquad \ldots\ldots\ldots(2)$$

where I now represents the flow of current across a cylindrical plane, axially symmetrical with the feeder of height h and radius r. If h is equal to the total height of the electrode then, for an inert electrode of glass beads, I becomes I_c, the cell current, and it follows that

$$I_c = - K_s \; 2\pi r h \; \frac{d \phi_s}{dr} \qquad \ldots\ldots\ldots(3)$$

Designating $\phi_s^{\,o}$ as the electrolyte potential at points adjacent to the feeder, radius r_o, integration gives

$$\phi_s - \phi_s^{\,o} = - \frac{I_c}{2\pi K_s h} \ln \left(\frac{r}{r_o} \right) \qquad \ldots\ldots\ldots(4)$$

A corresponding equation can be developed similarly for the planar cells and is expressed by

$$\phi_s - \phi_s^{\,o} = - \frac{I_c}{K_s A_D} x \qquad \ldots\ldots\ldots(5)$$

where x is distance measured parallel to the current flow, origin at the feeder surface, and A_D is the cross sectional area of the bed,

normal to current flow.

The variation of $\emptyset_s$ with r and x was observed experimentally in cylindrical cell II and the planar cell with double felt distributor. In both cases an inert bed of glass beads was used, and the experimental procedure followed was that described in Section 6.2, with minor modifications. The experimental details are given in Tables 6.2(a) and 6.2(b) and the results plotted in Figures 6.2, 6.3 and 6.4. In all cases the plots are linear as required by Equations (4) and (5), and the slopes allowed values of K_s to be determined. These are tabulated in Table 6.3.

TABLE 6.2. Experimental Conditions for the Determination of Effective Electrolyte Conductivity

a) Planar Cell with Double Felt Distributor

b) Cylindrical Cell II

	a)	b)
Particle size, microns	550	550
Temperature, ^oC	18	18
Bed Expansion, %	20	10,20,30 and 40
Cell Current, Amps	2.0 & 1.0	0.1
Copper ion concentration, molar	0.1	0.1 & 0.01
Sulphuric acid concentration, molar	0.1	0.1
Effective cross sectional area of bed, cm^2	60	
Effective height of bed, cm		8
Radius of feeder, r_o, cm		0.3
Internal radius of diaphragm R, cm		1.8

Cylindrical Cell II

0.1 M Cu

Fig. 6.3

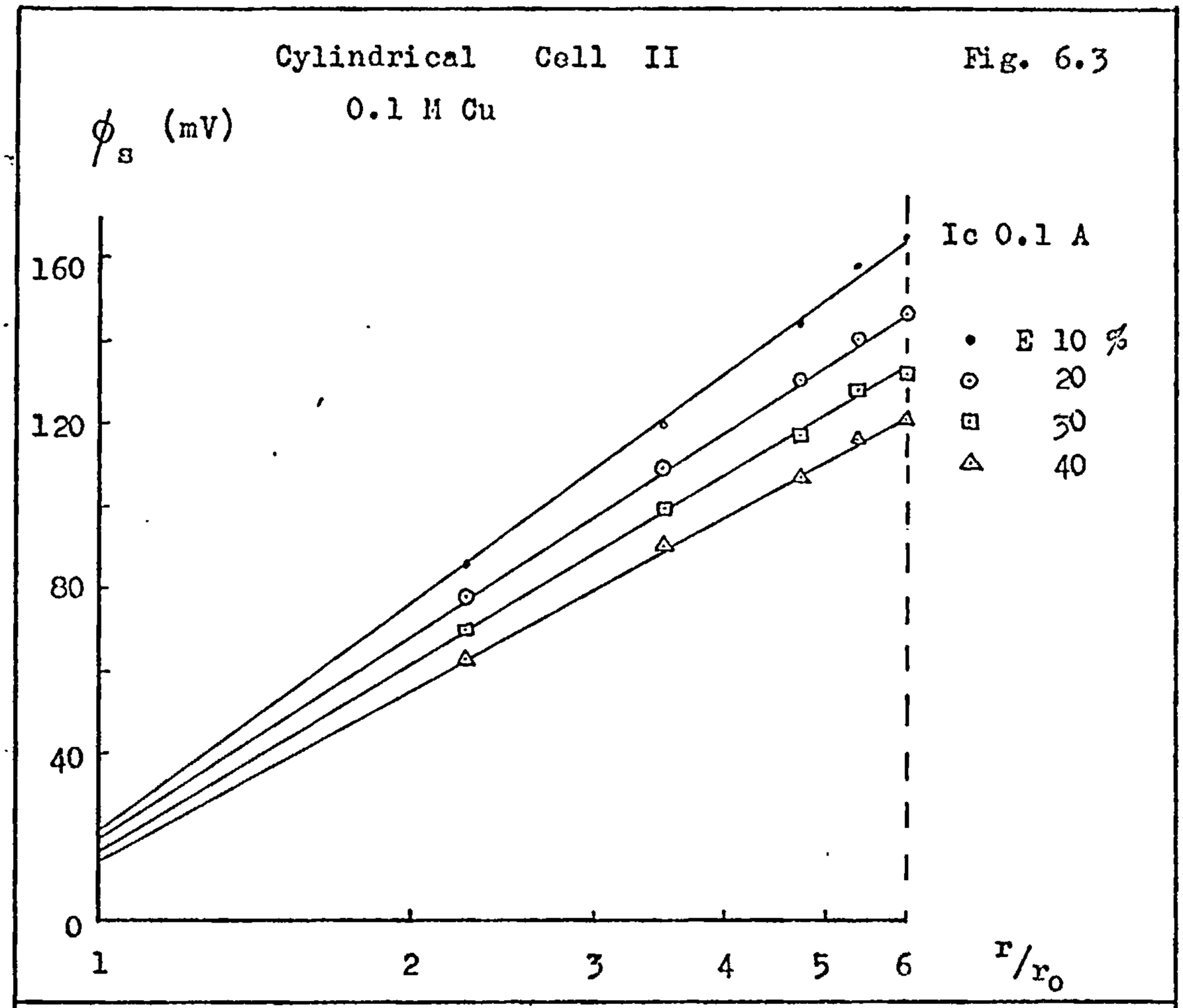

Cylindrical Cell II

0.01 M Cu

Fig. 6.4

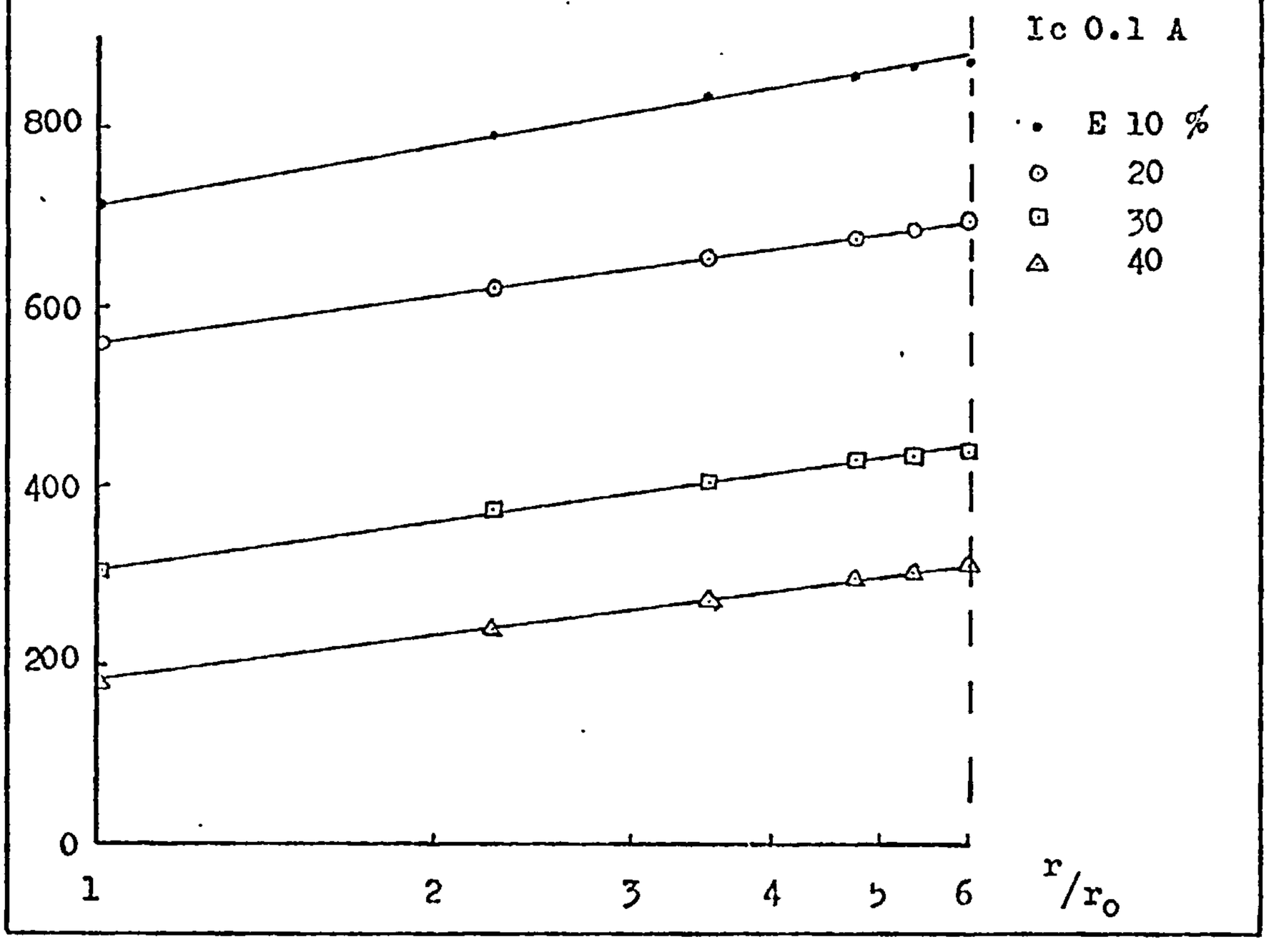

TABLE 6.3. Values of Effective Electrolyte Conductivity K_s ($ohm^{-1}\ cm^{-1}$)

Bed Expansion, %	Copper ion Concentration	
	0.1 M	0.01 M
10	0.0236	0.0205
20	0.0274	0.0239
30	0.0308	0.0268
40	0.0339	0.0295

The values are associated with spherical particles, diameter 550 microns, and a sulphuric acid concentration of 0.1 M.

In previous studies[25] values of K_s have been determined using the BRUGGEMAN equation[16], which proposed that, for a conducting medium occupying the interstices of a matrix of random spherical particles of uniform size, K_s is given by

$$K_s = \rho\ \varepsilon^{1.5}$$

where ρ is the true conductivity of the medium, and ε is the void fraction which it occupies. The present results have been used to test the validity of this equation in the context of the fluidised bed, and for this purpose values of K_s/ρ have been calculated from the data of Cylindrical Cell II, and are plotted in Figure 6.5 against $\varepsilon^{1.5}$. Values for ρ were obtained from the literature[44] and

are 0.089 and 0.072 ohm^{-1} cm^{-1} for 0.1 M H_2SO_4 containing 0.1 M and 0.01 M Cu^{++} respectively. The former is an extrapolated value since no reported experimental data in this range could be found.

Figure 6.5 shows that for the lower concentration of copper ions the BRUGGEMAN equation is a very faithful representation of the data, and accepting only slight experimental errors could be described as exact. For the higher concentration of copper ions, however, it gives values some 5% too high. This latter discrepancy may only be apparent, in view of the fact that an extrapolated value of ρ was used in calculating the data. On balance it may be regarded that the present work confirms the use of the Bruggeman equation for fluidised systems at least for expansions up to 40%.

6.3.2. Experimental Results for the Distribution of Electrode Potential in Cells of Cylindrical Configuration

Potential distribution in the electrolyte and dispersed phases were observed in cylindrical cells I and II for a range of bed expansion, diaphragm current density, copper ion concentration and particle size.

The electrolyte and dispersed phase potentials were measured with respect to the feeder (i.e. earth), the former against a saturated calomel electrode and the latter directly.

In preliminary tests with cylindrical cell I, potential distributions were measured in a number of x-planes for various values of r and γ (cf. Figure 6.6). From the results it was concluded that ϕ_s and ϕ_m were significantly dependent only upon $\frac{r}{a}$, and in subsequent investigations readings were, in consequence, confined to one x-plane.

Verification of the Bruggeman Relationship

Fig. 6.5

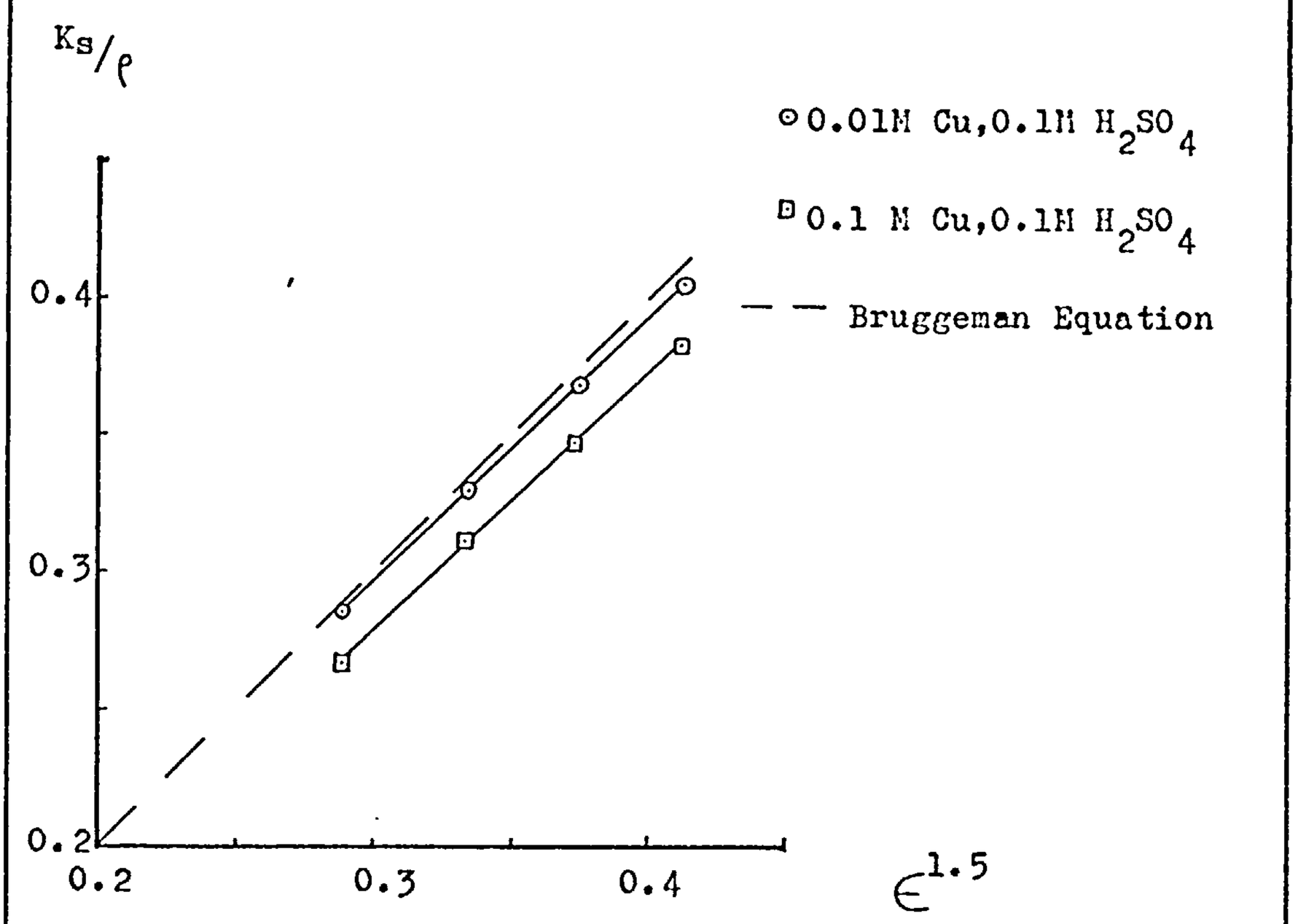

Cylindrical and Planar Cells Coordinates

Fig. 6.6

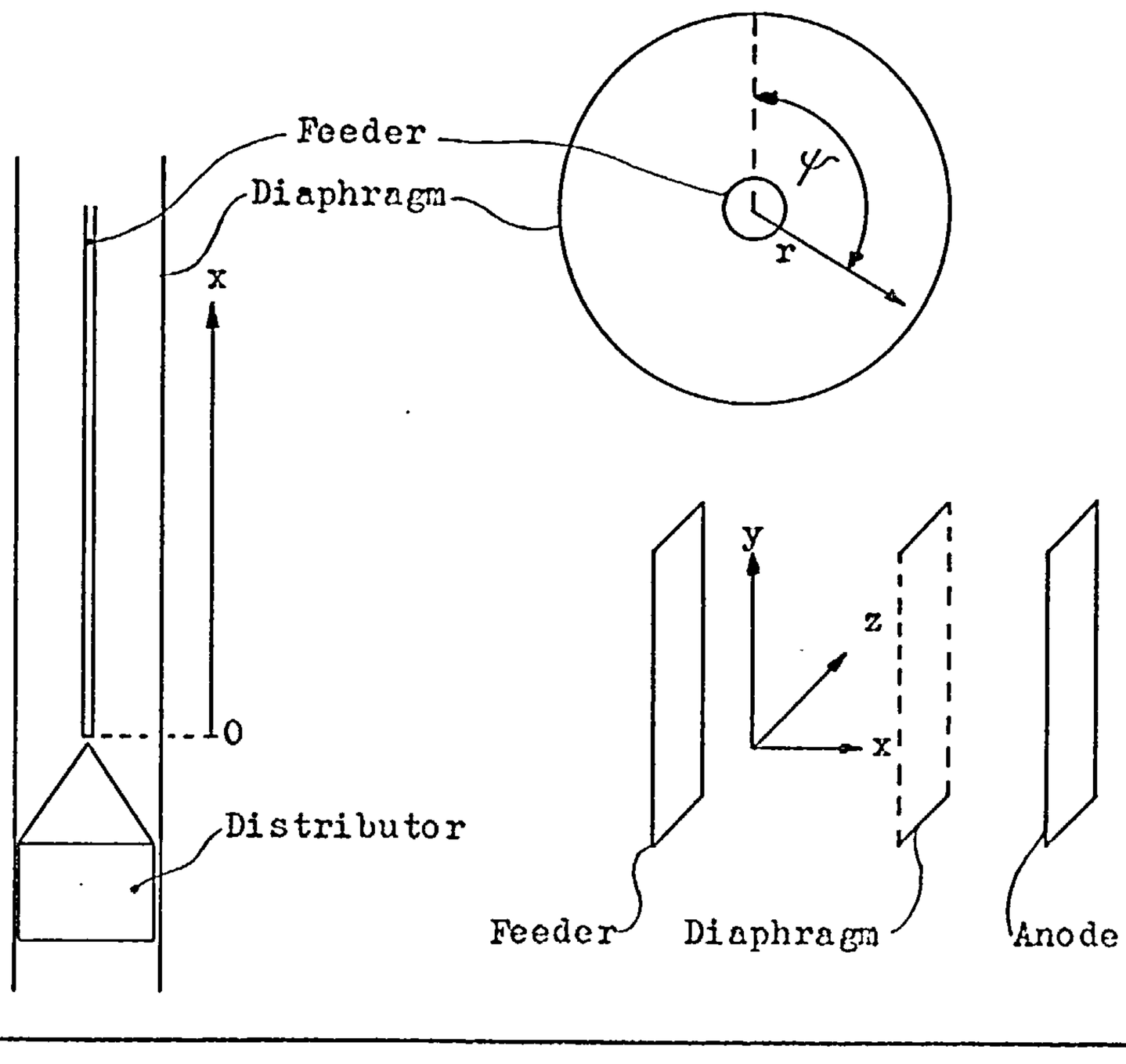

These findings are not contrary to those of GOODRIDGE et al[26] who report a typical behaviour in the entrance region, since the lowest value of x, for which potentials were measured is some 5 cm above the distributor and therefore in all probability outside the entrance region.

Subtraction of electrolyte potentials from those of the dispersed phase gives the distribution of electrode potential. The subtraction is carried out in a cathodic sense, i.e. $\phi_s - \phi_m$ to conform with the earlier presentation of the polarisation data, and the values are quoted using rest potential as an arbitrary datum. All ϕ_s data is presented as the potential (cathodic) with respect to rest potential, and values of ϕ, the electrode potential are calculated from

$$\phi = \phi_s - \phi_m$$

With this convention ϕ and i approach zero together. The values of the rest potentials for 0.1 Molar Cu^{++}, 0.01 M Cu^{++} and 0.001 M Cu^{++} all in 0.1 M H_2SO_4 are given in Appendix F with respect to the saturated calomel electrode and hydrogen electrode.

As a general rule it may be assumed that the higher the numerical value of the electrode potential the greater the rate at which deposition occurs, and in later sections a qualitative interpretation of the electrode potential profiles has been made on that basis.

Tables 1 to 18 of Appendix F present the potential profiles measured in Cylindrical Cells I and II.

Typical ϕ_s, ϕ_m and ϕ profiles are presented in Figure 6.7,

where each ϕ_s and ϕ_m value is the arithmetic mean of 20 readings.

A summary of the experimental conditions is given in Table 6.4.

TABLE 6.4. Experimental Conditions for Potential Profiles in the Cylindrical Cells

Conditions	Cell I	Cell II
Particle size, microns	550	550 and 780
Diaphragm current	36 and 72	2,11 and 22
Density, mA cm^{-2}	4.8 and 9.6	0.2,1 and 2
Cell current, Amps.	10,20 and 30	10,20,30 and 40
Bed expansion, %		
Copper ion concentration, Molar	0.1 and 0.01	0.1,0.01 and 0.001
Sulphuric acid concentration, Molar	0.1	0.1

6.3.3. Experimental Results for the Distribution of Electrode Potentials in Cells of Planar Configuration

In this cell geometry the electrode potential profiles were determined for a range of bed expansions and diaphragm current densities, but the copper ion concentration was fixed at 0.1 Molar (in 0.1 Molar H_2SO_4) and the particle size used throughout was 550 microns.

Preliminary tests with the planar cell and single felt distributor (c.f. Section 4.4.2) showed a significant dependency of potentials on x, the direction normal to the feeder, but were little affected by y and z locations (see Figure 6.6). In subsequent experiments readings were therefore confined to a traverse along an x-axis at fixed values of y and z. A typical set of profiles is shown in Figure 6.8 in which the slope of the ϕ_m curve displays a

Cylindrical Cell I

Fig. 6.7

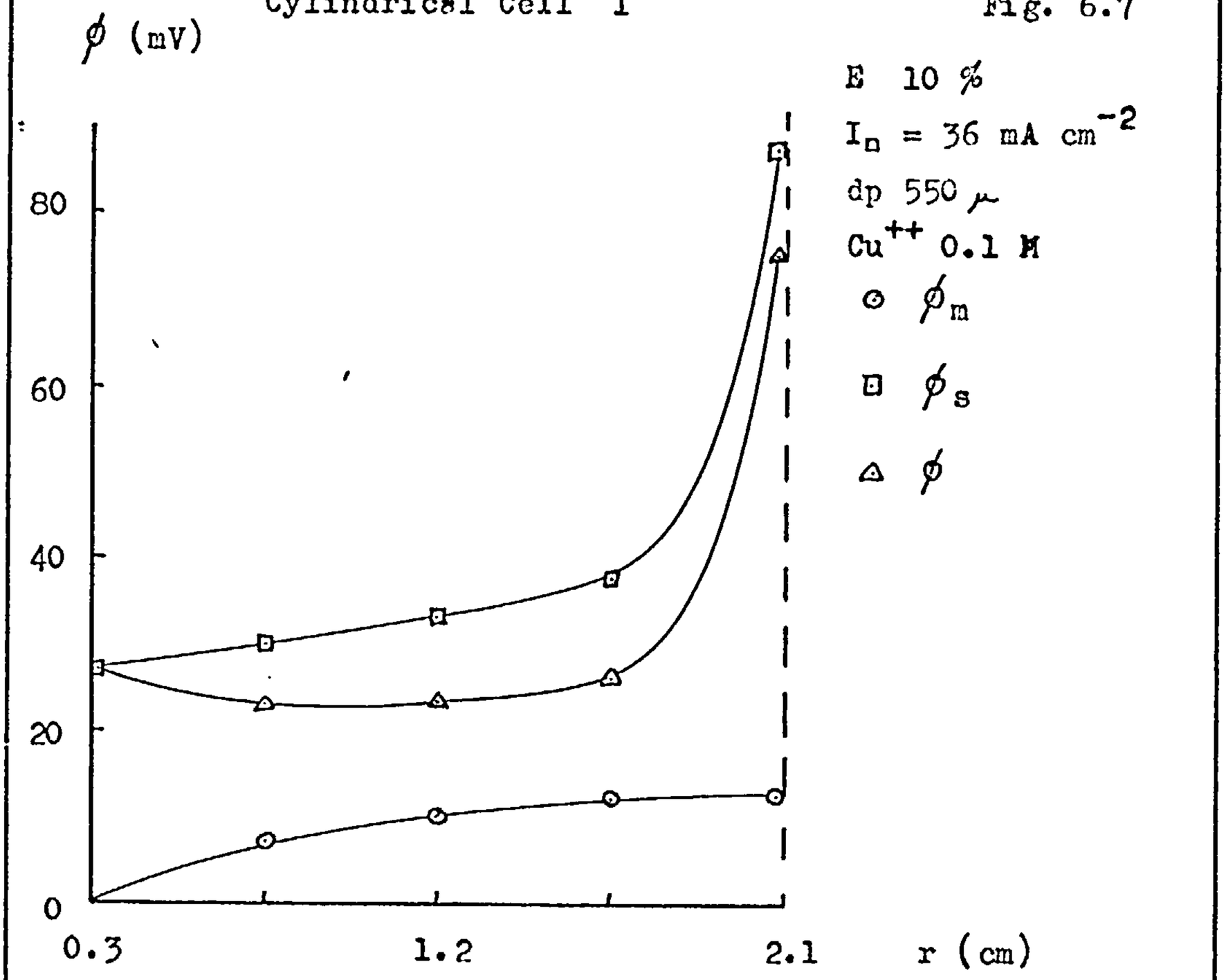

Planar Cell

Fig. 6.8

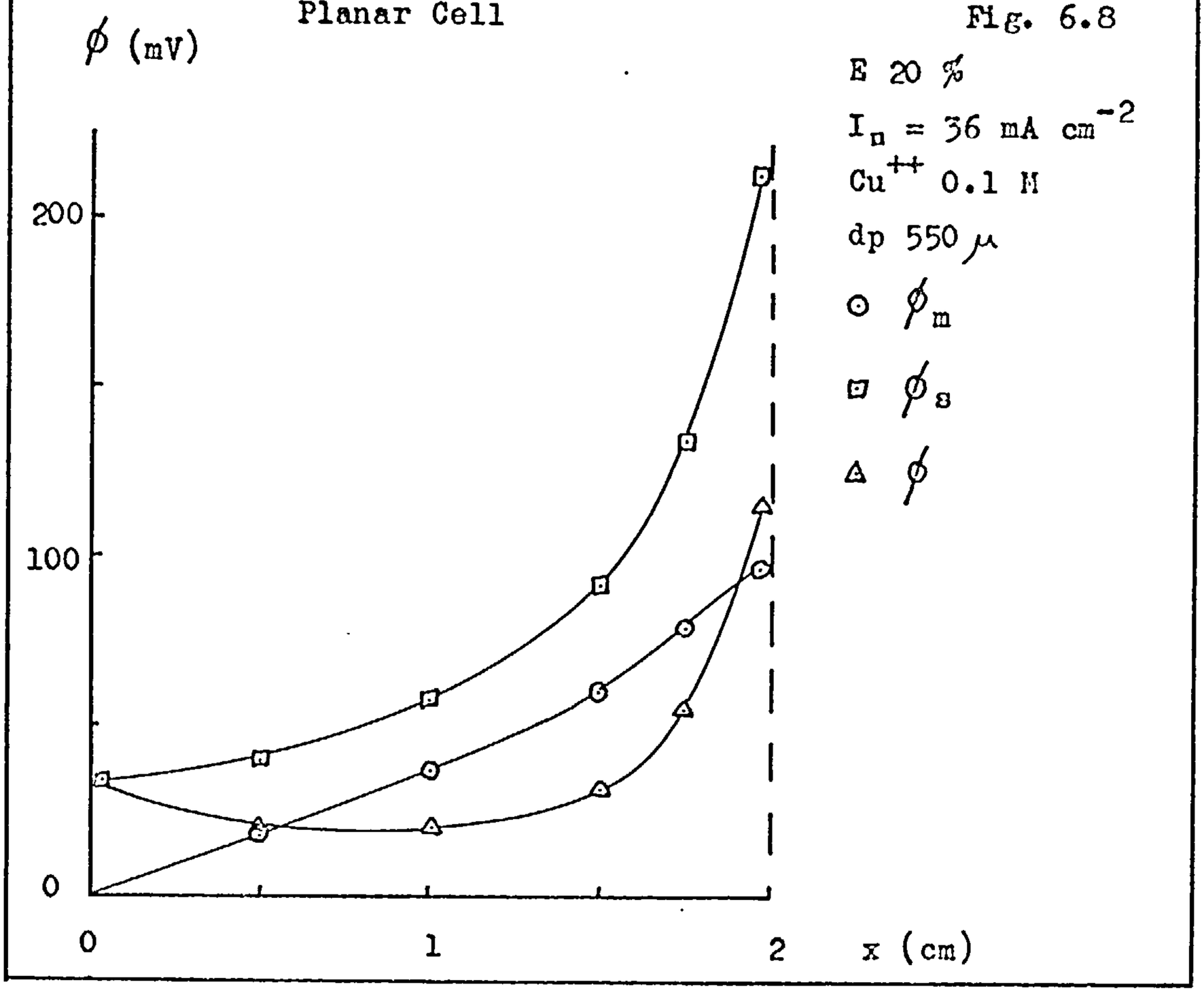

rather unexpected characteristic. It had been anticipated that, broadly speaking, the flow of current in the dispersed phase across any x-plane would be proportional to $d\phi_m/dx$ at that plane. It follows, therefore, that since this current falls continuously from a maximum at the feeder to zero at the diaphragm, the slope $d\phi_m/dx$, would do likewise. This, however, is patently not the case and it was concluded that either the effective conductivity of the dispersed phase varied from one region to another as a result of non-homogeneous fluidisation or the observations were unreliable. The latter possibility was investigated by introducing a number of modifications to the technique of measurement.

Firstly, the two-end probe described in Section 4.5 was used instead of the single ended probe but the results obtained were only a confirmation of those already obtained.

Secondly, one hundred readings were taken at each location instead of twenty, again with no effect.

Thirdly, the fluctuations in the observed potentials were damped by means of an RC filter as shown in Figure 6.9. The time constant of the filter,50 secs, was selected to be much greater than that incorporated in the Electronic Digital Voltmeter (E7). The high time constant required a lapse of 15 to 20 minutes before each reading attained a steady value. As can be seen in Figure 6.10 these readings again confirmed the original results.

It was concluded that the profiles were a true picture of conditions existing in the bed,but it was not clear whether this phenomenon was implicit in a planar configuration or arose from the

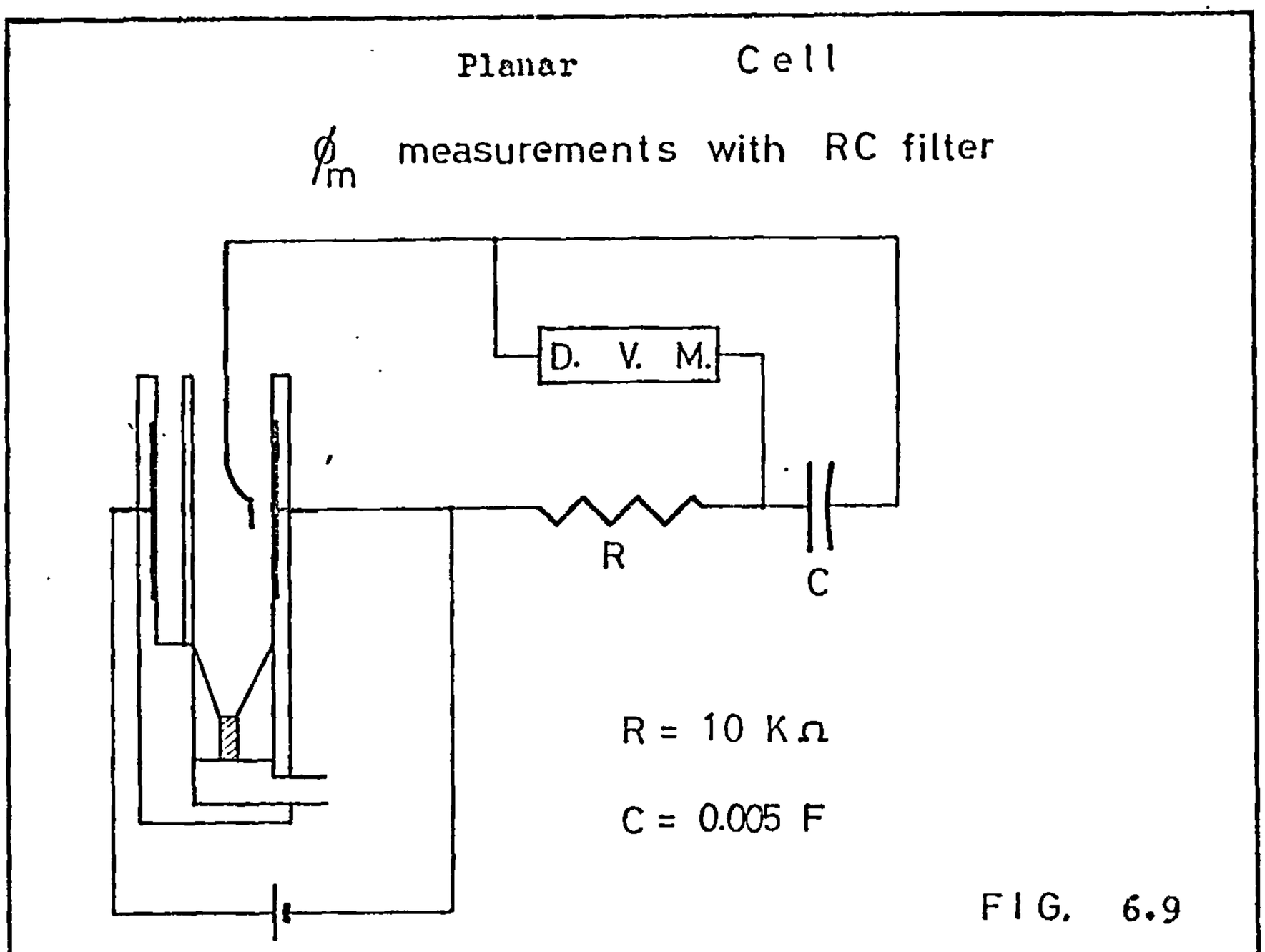

FIG. 6.9

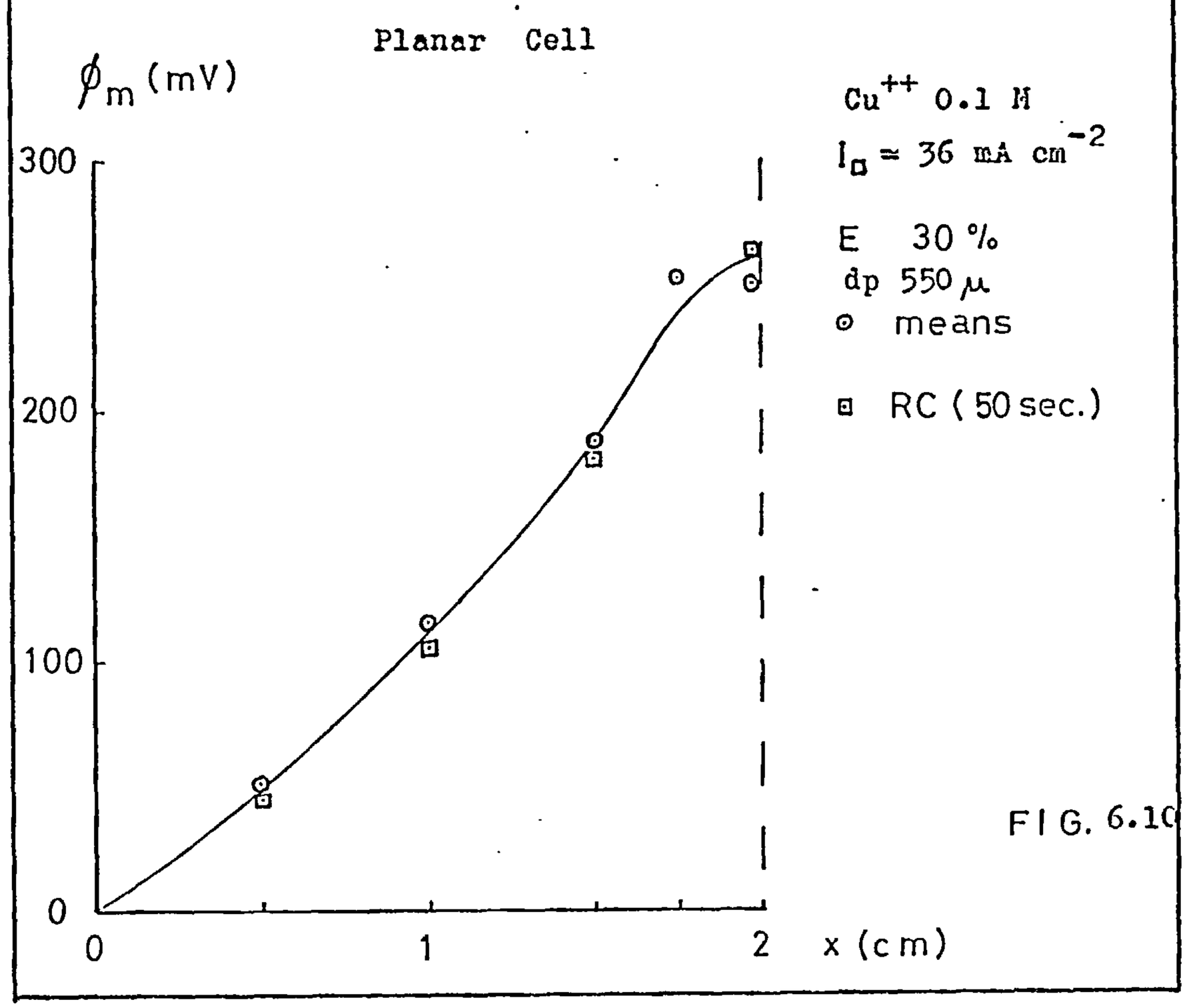

FIG. 6.10

design or location of the distributor. It was important, however, to distinguish between these alternative possibilities and for this reason the double felt distributor was designed. Potential profiles for this cell are tabulated in Tables F19 and F20 and shown in Figures 6.11 and 6.12, where it can be seen that the slope of the ϕ_m curve now falls continuously as would be expected under conditions of uniform fluidisation. It may be deduced, therefore, that uniform fluidisation can be achieved in a planar configuration, but that distributor design is a sensitive factor in producing it. It is also interesting to note that no visual differences in the fluidisation was apparent between the single and double felt distributors.

A comparison between the planar cell with double felt distributor and the cylindrical cell can be made using the standard deviations of the experimental readings about the mean. It will be remembered that the potential in the dispersed phase at each point was taken as the average of twenty readings. The standard deviation from the mean for the planar cell with double felt distributor was about 1% whereas for the cylindrical cell it was 5%. If one interprets these values as a measure of the stability of the behaviour of the electrodes it is apparent that the planar cell is the more preferable.

6.3.4. Discussion and Interpretation of the Electrode Potential Distribution

An inspection of Figures 6.7 to 6.22 shows that in general the electrode potential distribution in the fluidised bed electrode is largely uniform with a sharp rise to significantly higher values near

Planar Cell

FIG. 6.11

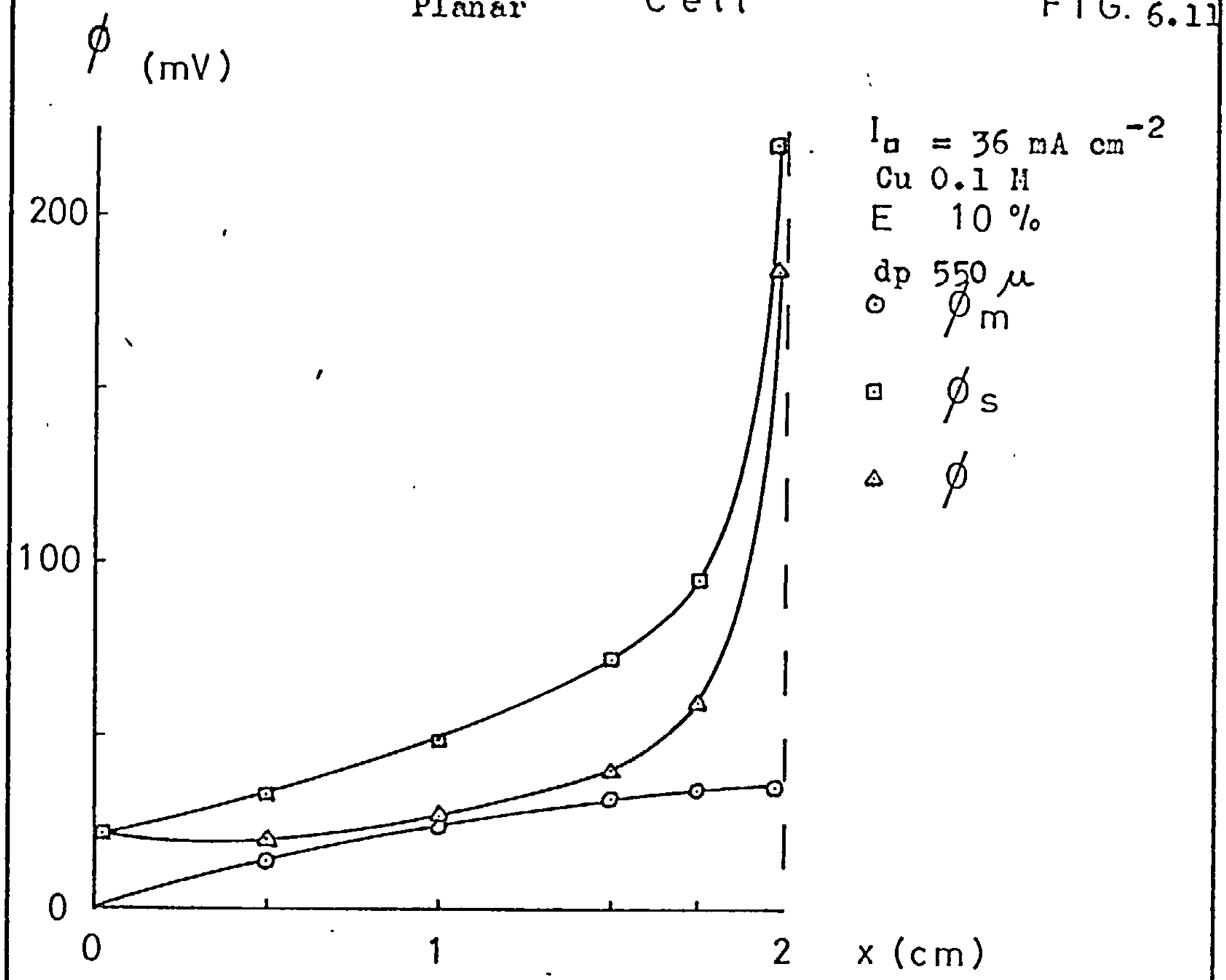

Planar Cell

FIG. 6.12

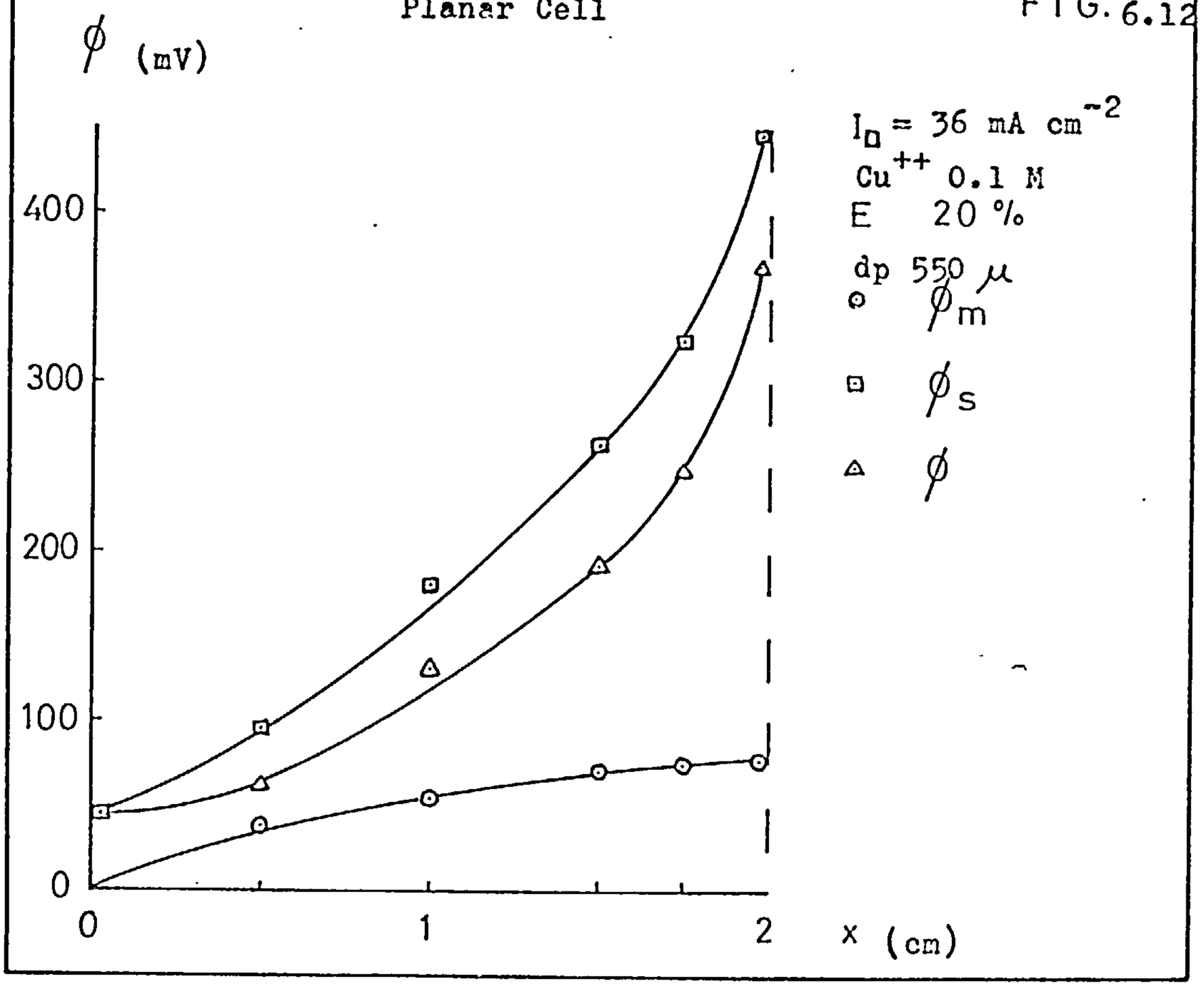

the diaphragm, and that this picture, within the limits of the experimental variables, is relatively unaffected by particle size (Figures 6.21, 6.22), copper ion concentration (Figures 6.13, 6.14) and diaphragm current density (Figures 6.19, 6.20). Only under extreme conditions of low copper ion concentration, low diaphragm current density and high bed expansion (30 - 40%) did the electrode potential in the inner region of the bed and near the feeder approach or equal that observed at the diaphragm (see Figures 6.17 and 6.16).

On the supposition that bed activity, i.e. rate of deposition, is roughly proportionalto electrode potential the general picture conveyed by the electrode potential profiles is one in which the majority of the deposition process takes place preferentially in the region near the diaphragm, whilst the "inner" part of the bed remains practically inactive. Cell geometry had no effect, and only at high expansions (30 - 40%) was there any noticeable tendency for other regions of the bed to become active. This interpretation has been confirmed by experiments where small (2 cm x 0.8 cm) platinum plates were immersed in the fluidised electrode at fixed points. They were mounted so that their only electrical contact with the system was through the surrounding fluidised particles. In the cylindrical cells the plates were concentric with the feeder each one being located in a fixed radial plane, and in the planar cell they were arranged to be parallel to the feeder and located in fixed x-planes. They were also offset to prevent mutual shielding. In both types of cells one of the plates was placed close to the diaphragm. Copper deposits were observed in all cases on the plates near the diaphragm, but on the other plates the deposits were small or non-existent.

Cylindrical Cell I

Fig. 6.13

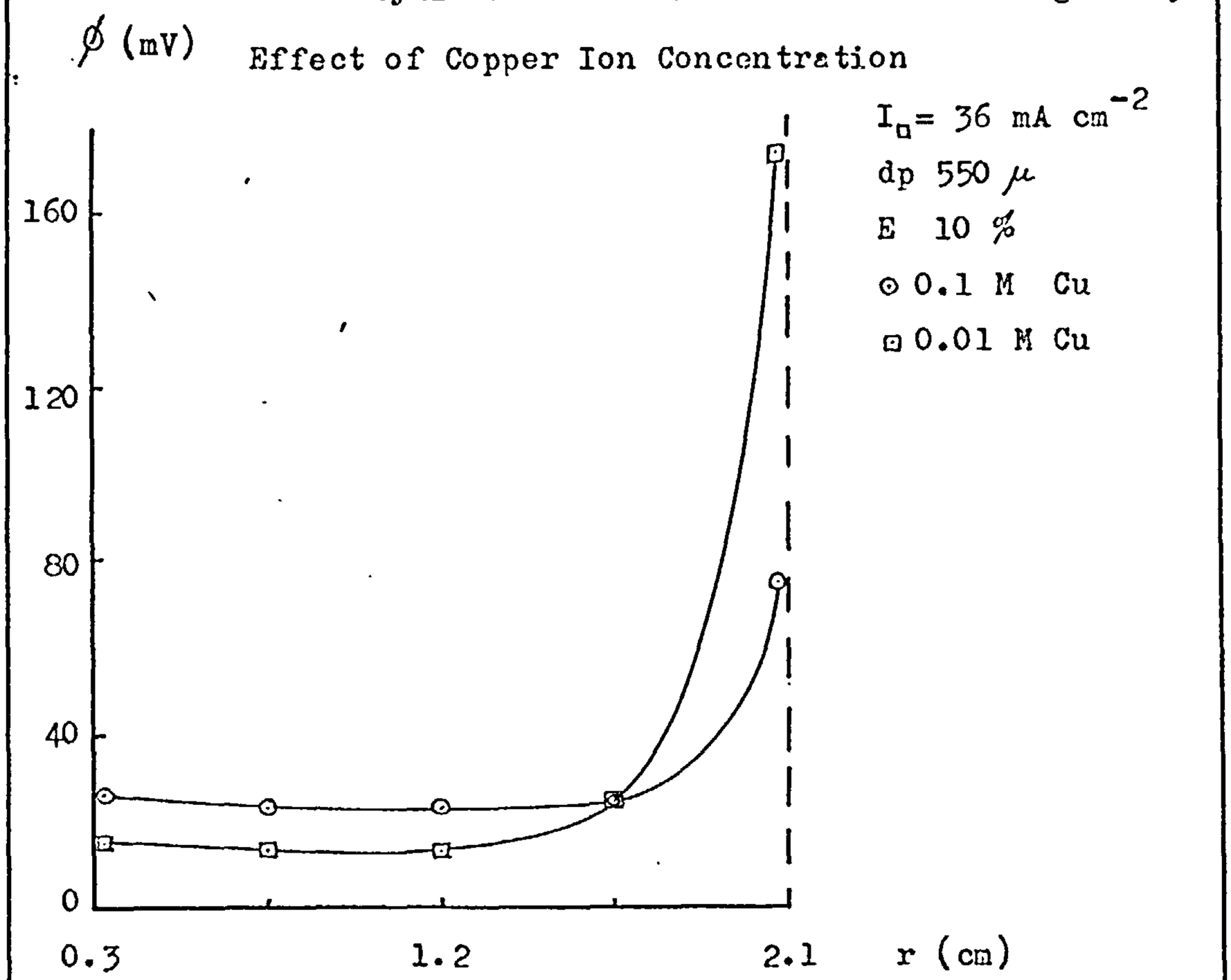

Cylindrical Cell II
Effect of Cupric Ion Concentration

Fig. 6.14

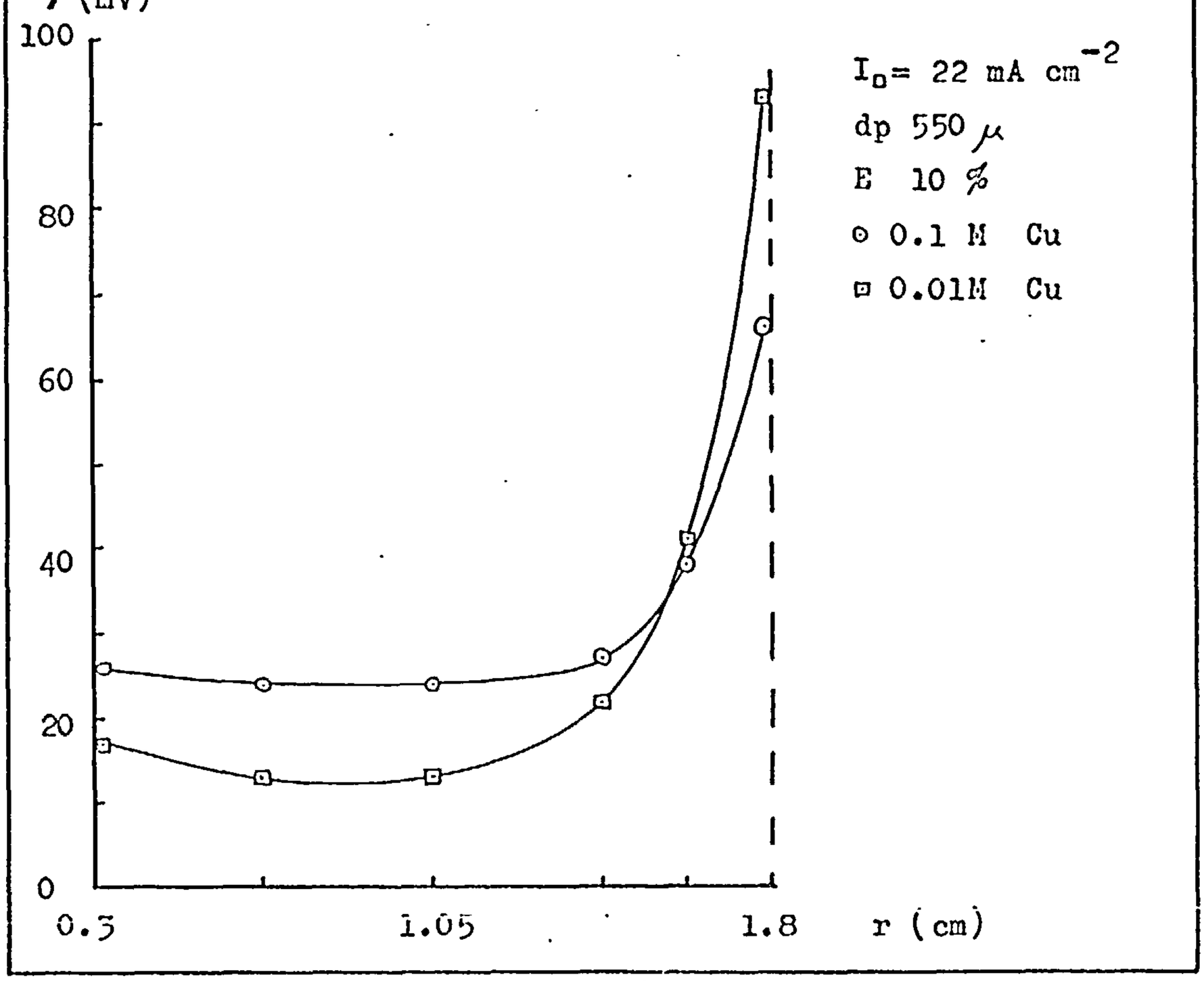

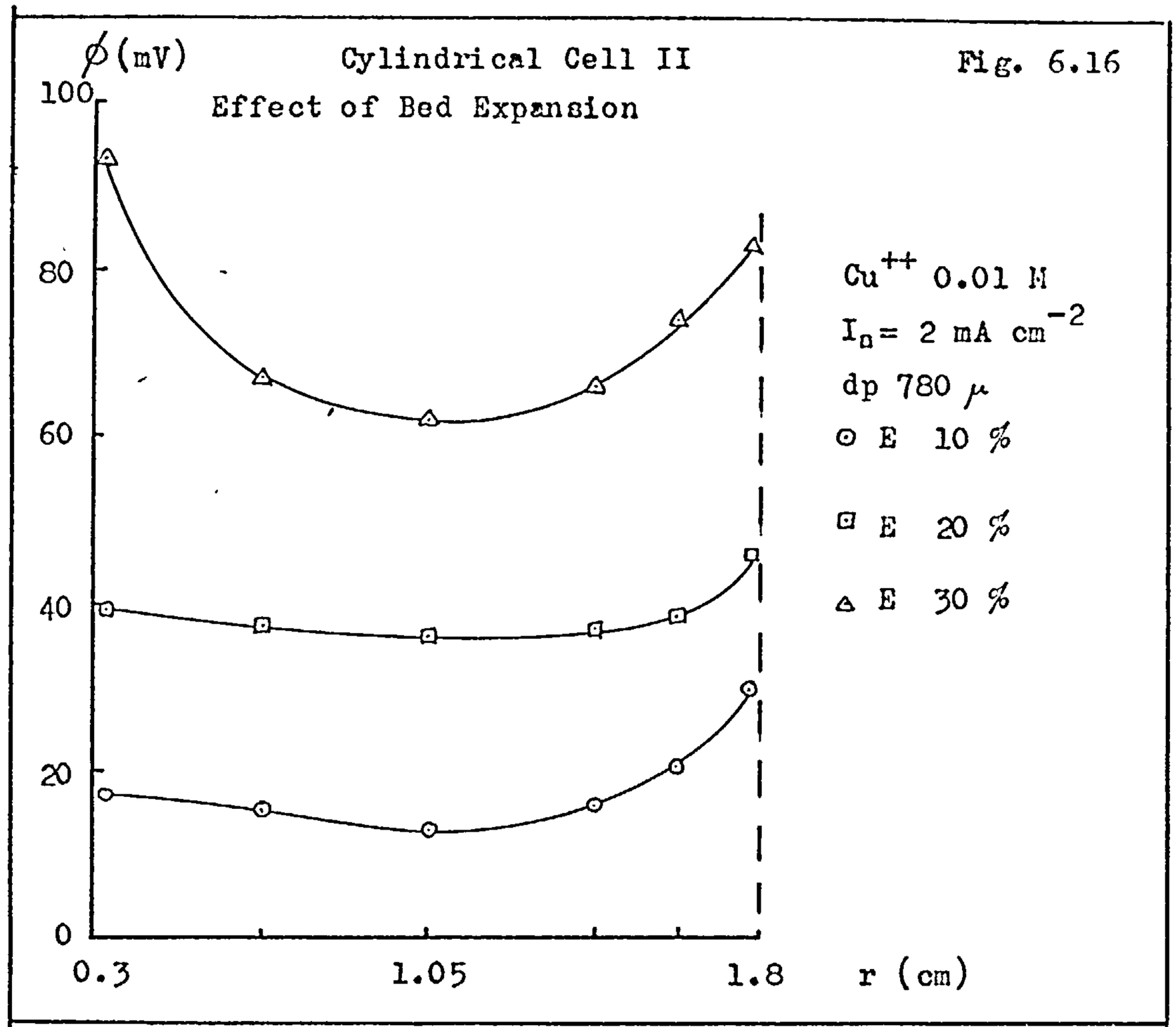
ϕ (mV)
Cylindrical Cell II
Effect of Bed Expansion
Fig. 6.16
100
80
60
40
20
0
0.3
1.05
1.8
r (cm)
Cu++ 0.01 M
In= 2 mA cm-2
dp 780 μ
⊙ E 10 %
□ E 20 %
△ E 30 %

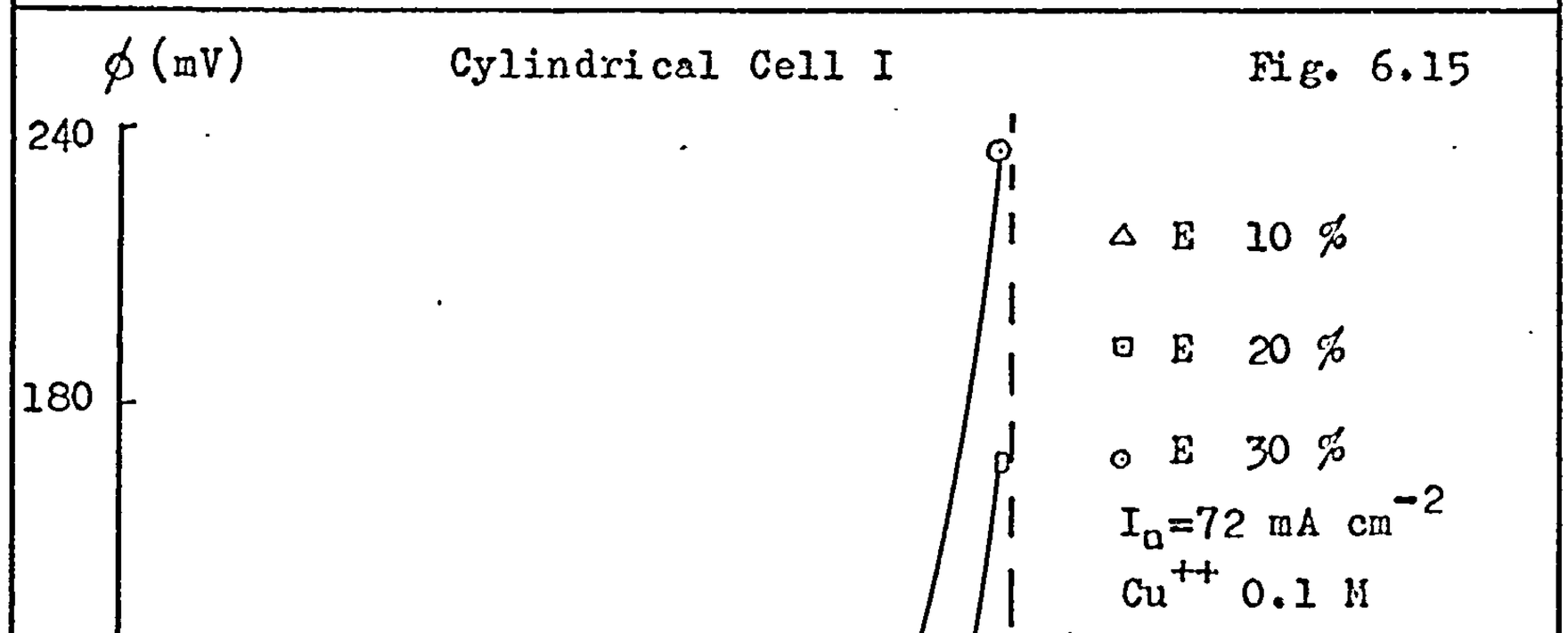
ϕ (mV)
Cylindrical Cell I
Fig. 6.15
240
180
120
60
0
0.3
1.2
2.1
r (cm)
△ E 10 %
□ E 20 %
⊙ E 30 %
In=72 mA cm-2
Cu++ 0.1 M
dp 550 μ

Planar Cell

Effect of Bed Expansion

Fig. 6.17

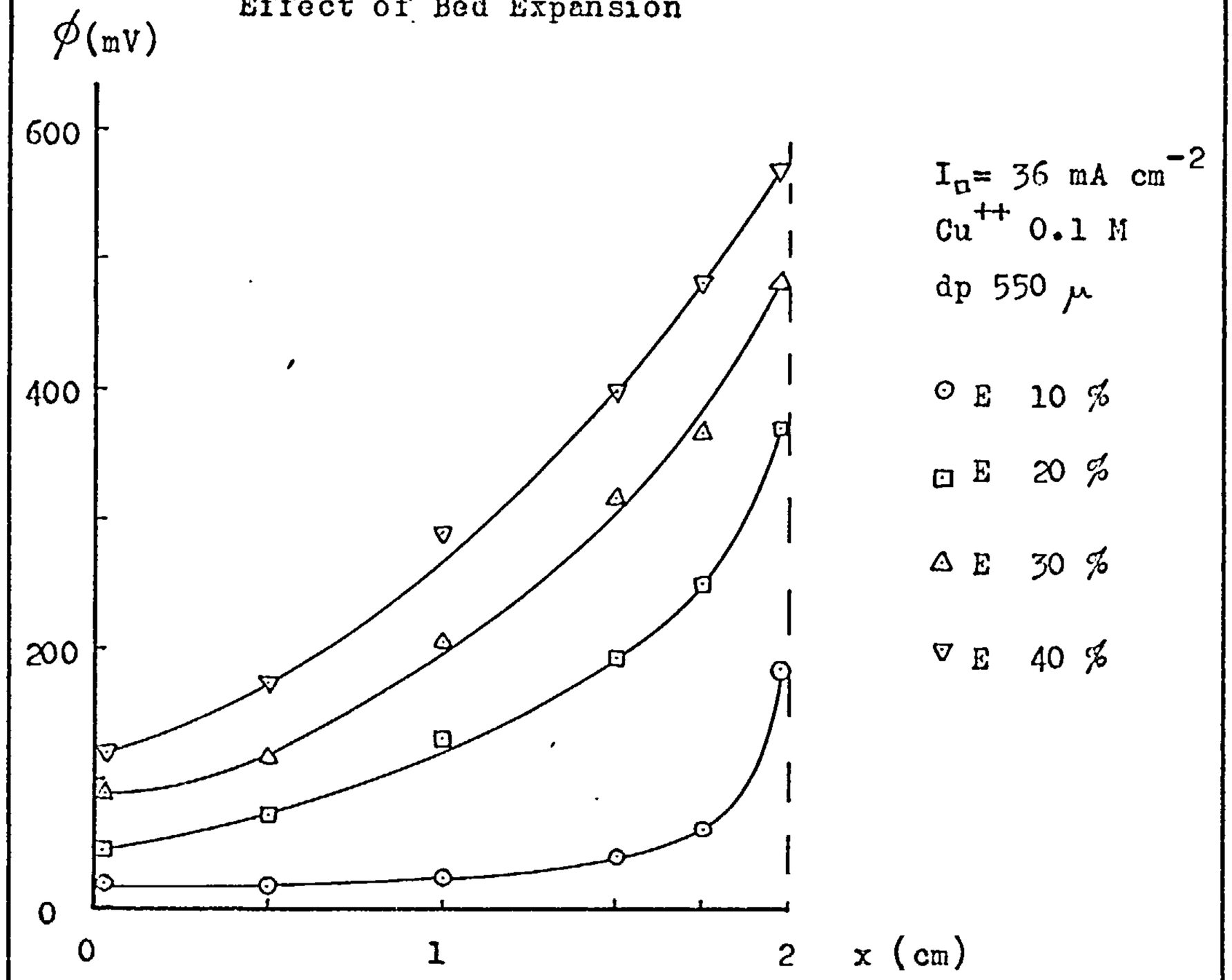

Cylindrical Cell I

Effect of Diaphragm Current Density

Fig. 6.18

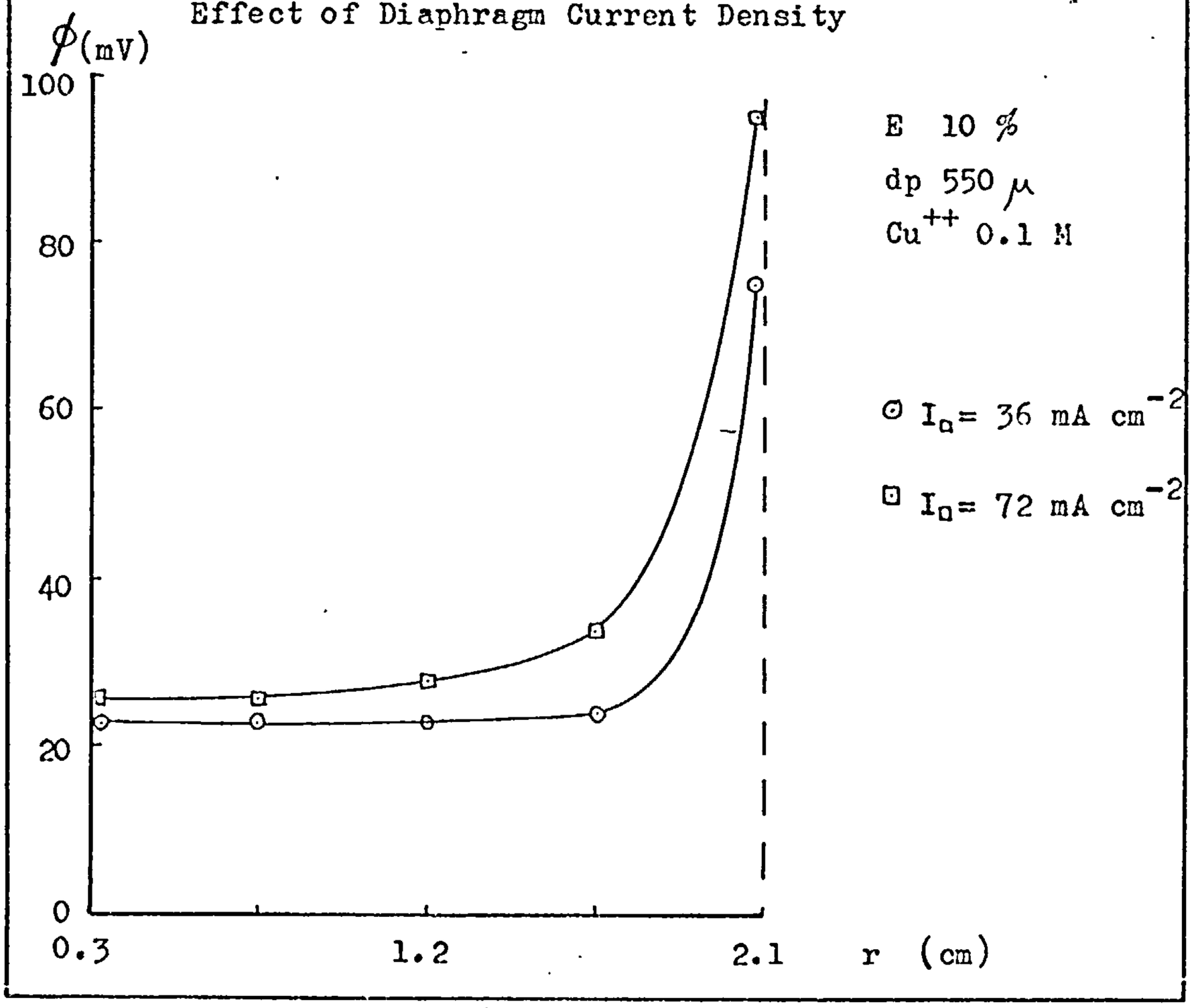

Cylindrical Cell II

Fig. 6.19

Effect of Diaphragm Current Density

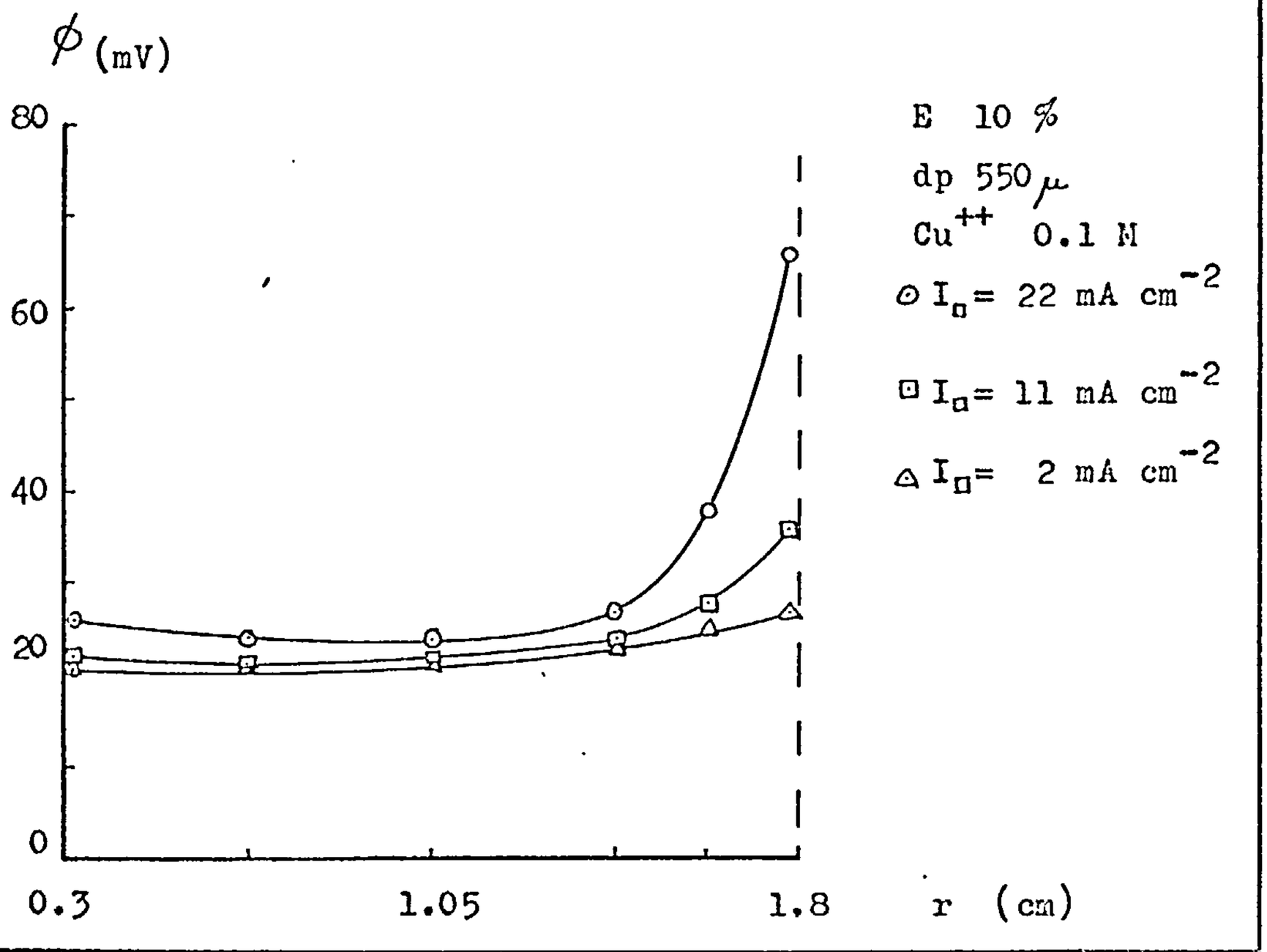

Planar Cell

Fig. 6.20

Effect of Diaphragm Current Density

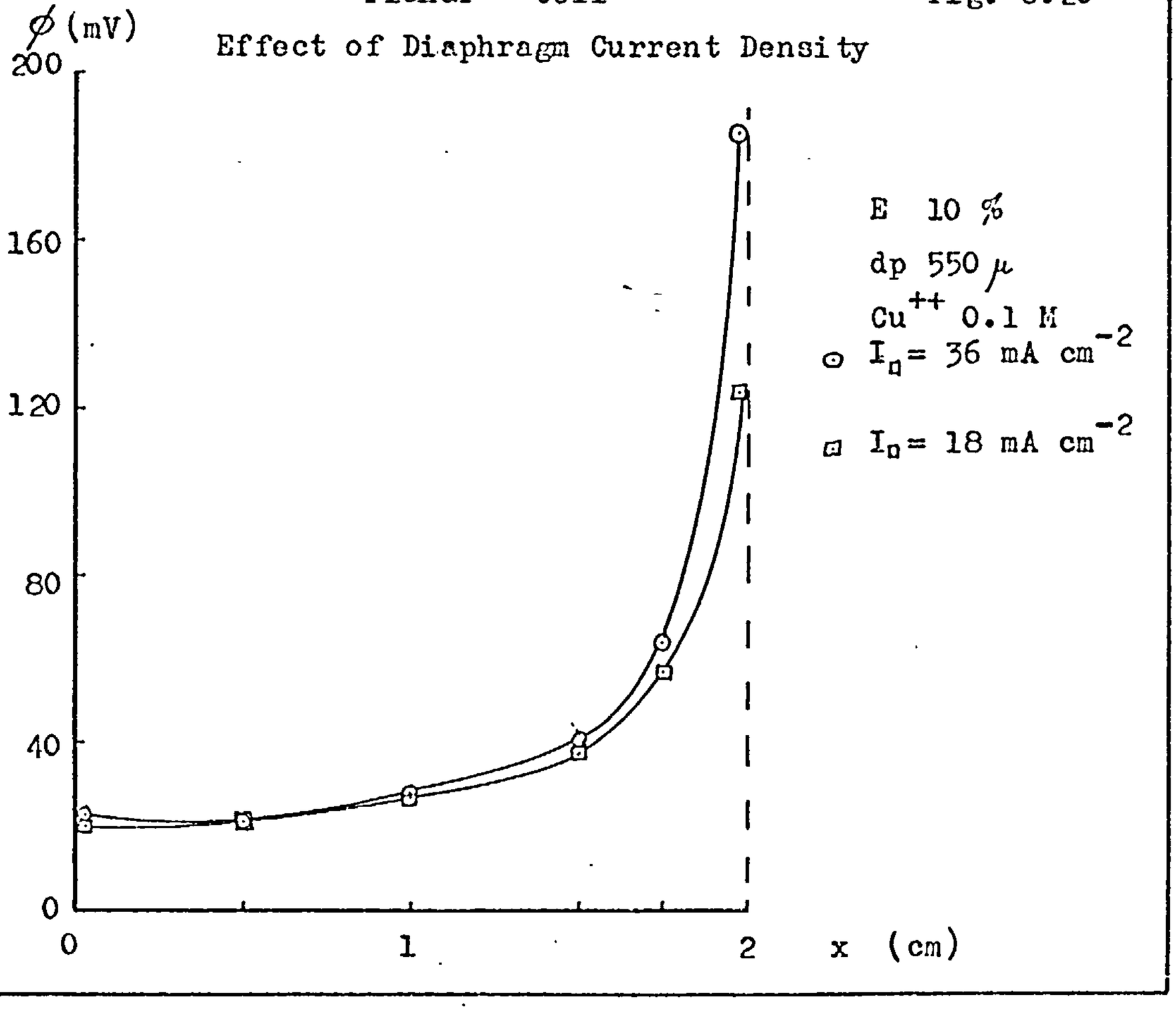

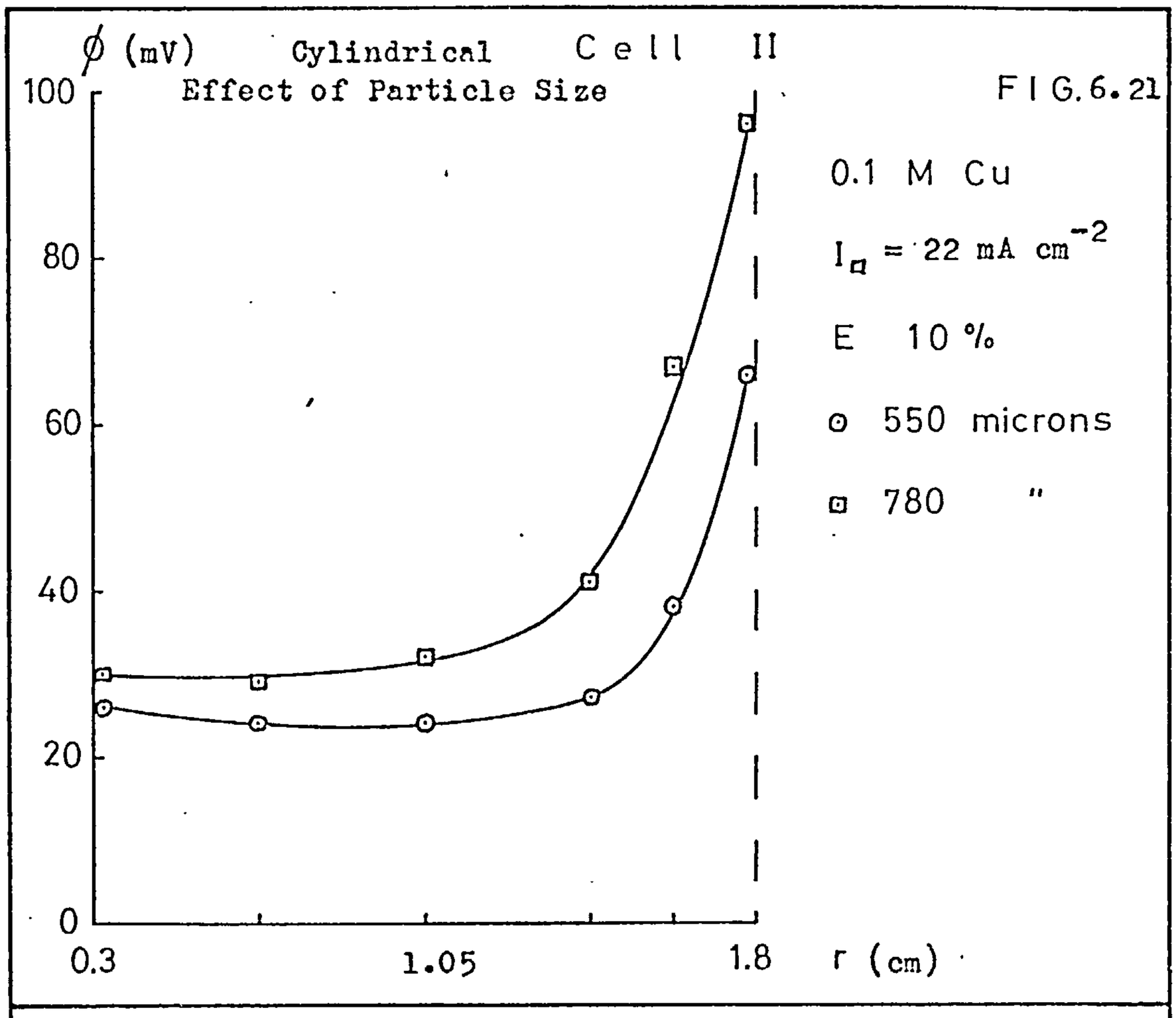

FIG.6.21

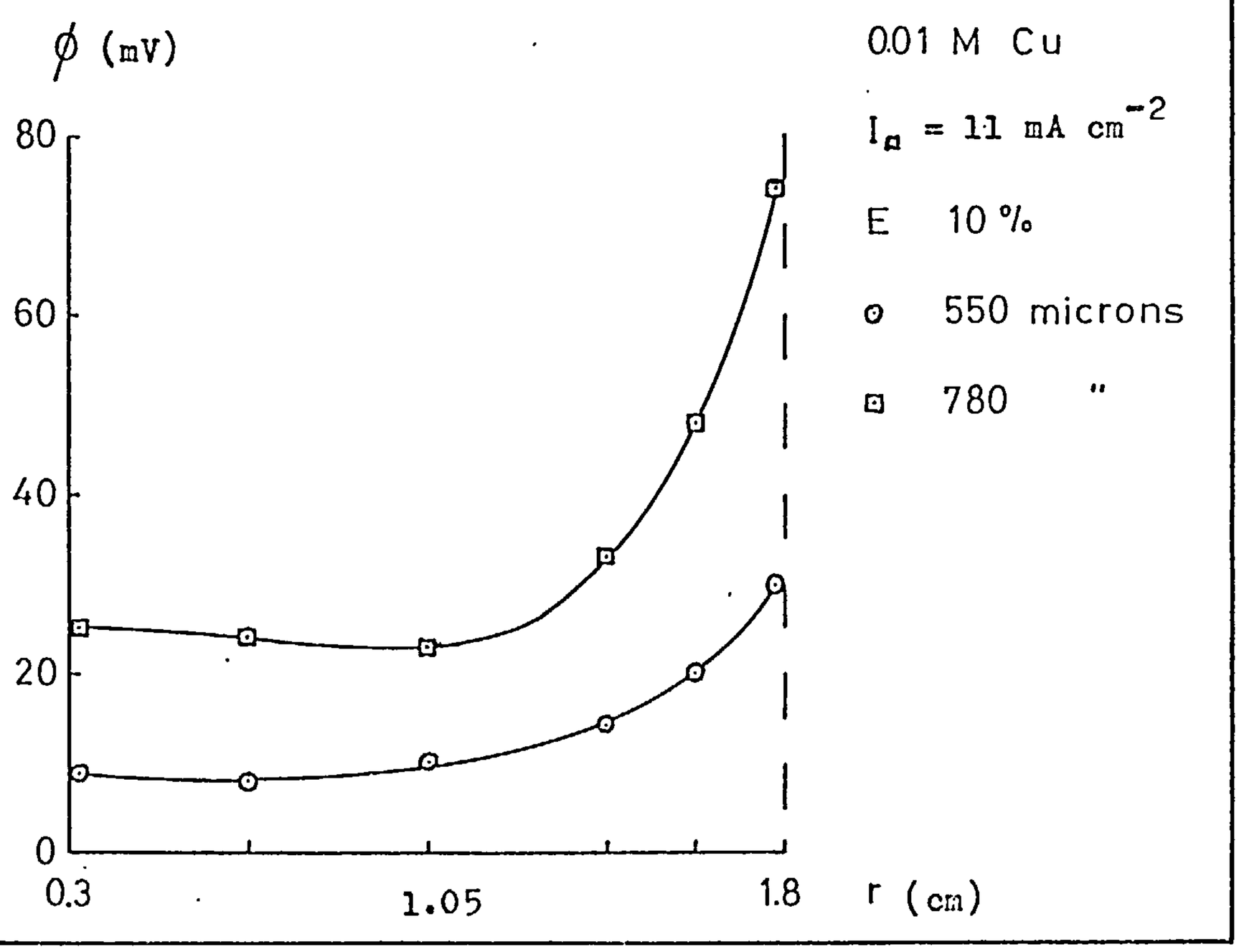

Fig. 6.22

In practical terms the observations suggest that the active thickness of the electrode is some ten particle diameters extending from the diaphragm into the bed. This may not be the "optimum" thickness, however, which in particular cases will be determined by hydrodynamic and residence time considerations in addition to electrical ones.

Up to this point the interpretation of electrode potential distribution in terms of rate of copper ion discharge has been qualitative, but by using the polarisation data of Section 3.7 it should be possible to make it quantitative. This has been attempted and is the subject matter of Section 6.5.

6.4. Distribution of Current in the Fluidised Bed Electrode

In passing through the fluidised bed electrode the cell current divides into two components, one of which flows through the particulate phase, I_m, and the other through the electrolyte phase, I_s. It is supposed that I_m is electronic in nature and I_s ionic. The sum of these components at any plane in the electrode is, of course, equal to the cell current I_c. Thus referring to Figure 6.23 which is a plan of a cylindrical cell, the values of I_m and I_s crossing the plane at r sum to I_c,

$$I_s + I_m = I_c \qquad \ldots\ldots\ldots(1)$$

and in addition the values of I_s and I_m will be given by,

$$I_s = - K_s \; 2\pi \; r \; h \; \frac{d \phi_s}{dr} \qquad \ldots\ldots\ldots(2)$$

Fig. 6.23

Flow of Current in a Concentric Cylindrical Cell.- Plan View.

A Anode

B Diaphragm

C Feeder

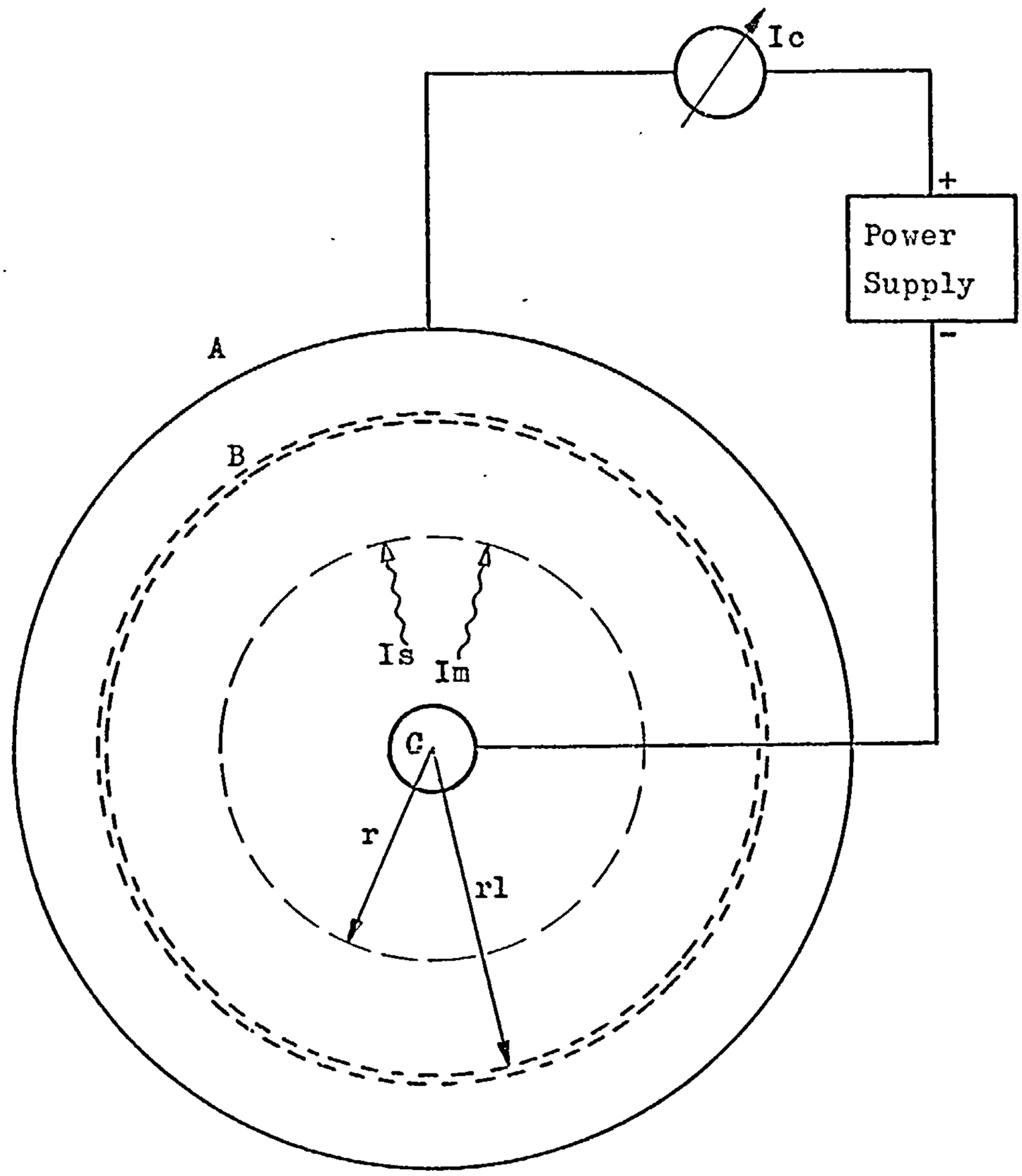

and $$I_m = - K_m \; 2\pi r h \; \frac{d \phi_m}{dr} \qquad \text{.....(3)}$$

Thus, from the slopes of the (ϕ_s - r) and (ϕ_m - r) curves it is possible to determine the variation of I_m and I_s with r. These variations will henceforward be referred to as the current distribution in the electrode. In practice the severe fluctuations encountered in determining ϕ_m values make the readings much less reliable than those of ϕ_s, and so the determination of I_m is better carried out by difference using Equation (1) after determining I_s from Equation (2).

From the electrolyte potential profiles for Cylindrical Cell II (i.e. ϕ_s - r curves) values of d ϕ_s/dr were determined graphically at values of r of 0.3, 0.675, 1.05, 1.425, 1.61 and 1.80 cm respectively. The data were then converted to I_s values using Equation (2) and are presented in the form of plots of I_s/I_c versus r in Figures 6.24, 6.25, 6.26 and 6.27.

In drawing these curves the boundary condition that $I_s = I_c$ at $r = r_1$ has been strictly observed by terminating them at a value of $I_s/I_c = 1$. In addition the slope of the curves was maintained positive so that the improbable situation of the cathode behaving anodically was not implied. This was felt justified in that whenever strict adherence to the data indicated a negative slope the points could readily be interpreted, within experimental error, as a horizontal line.

Values of r $d\phi_s/dr$ determined as described previously are tabulated in Appendix F.

The figures support the conclusions already drawn in Section 6.3.4, in that I_s rises sharply near the diaphragm indicating

Current Distribution
Cylindrical Cell II

Fig. 6.24

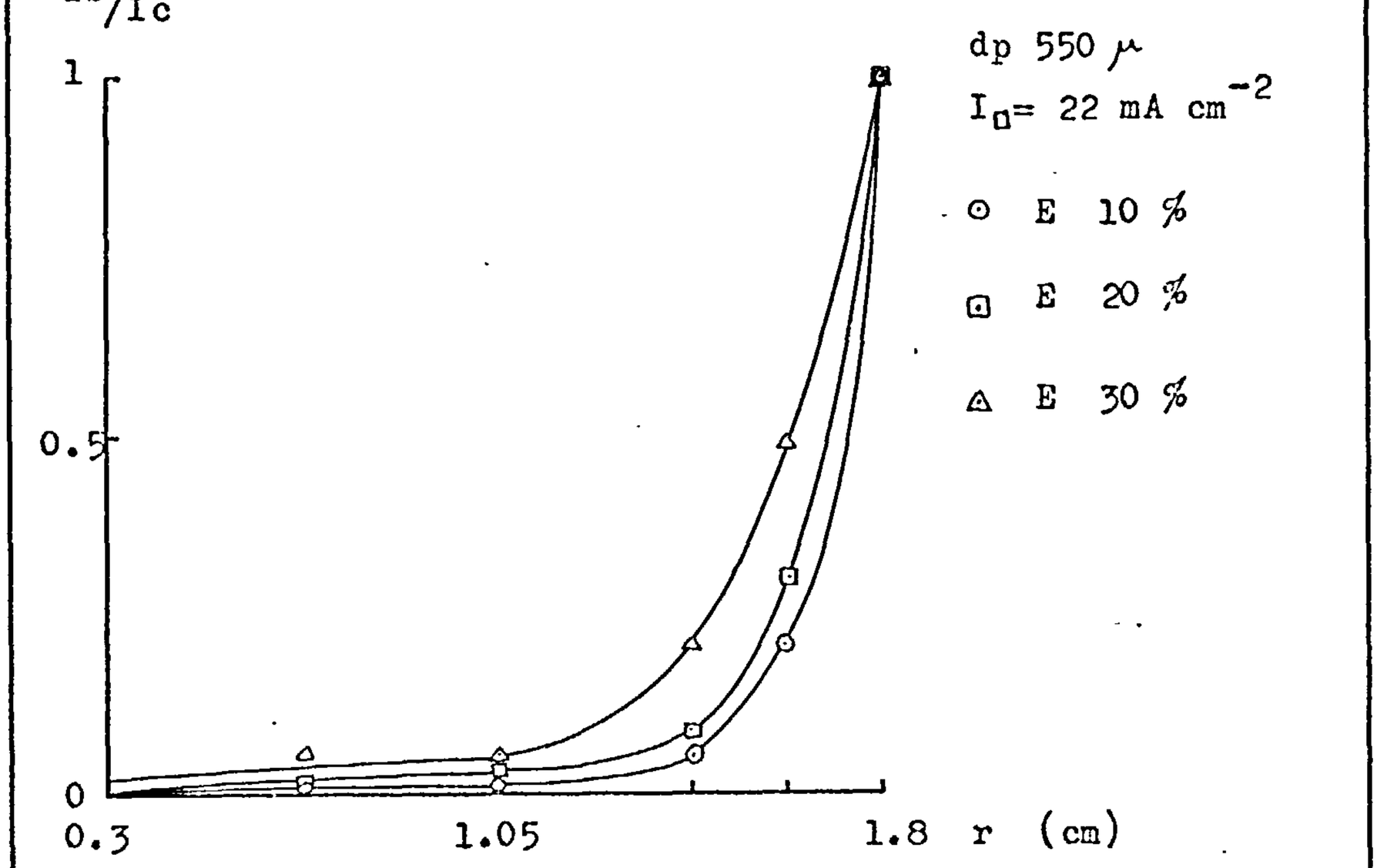

Current Distribution
Cylindrical Cell II

Fig. 6.25

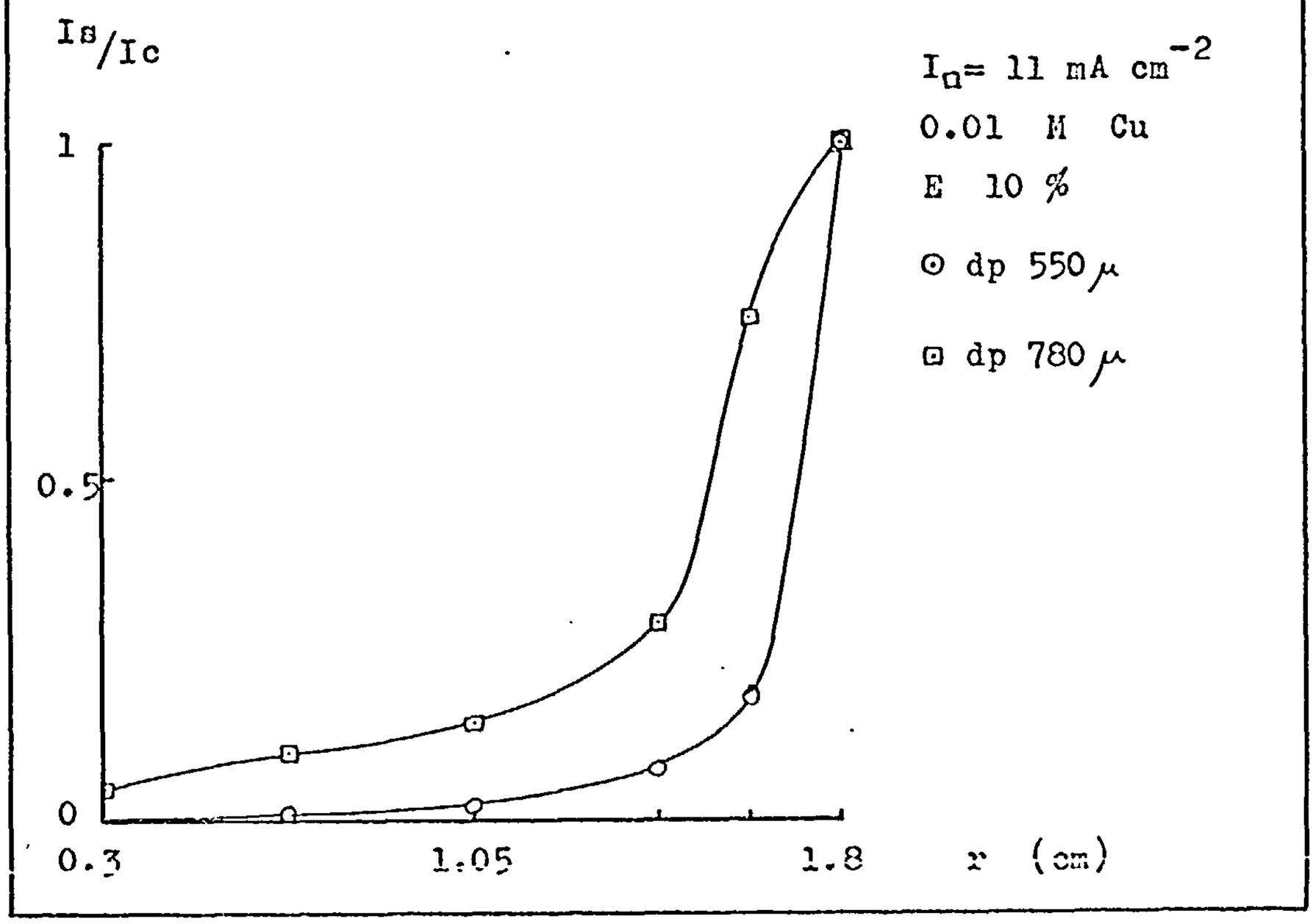

Current Distribution

Cylindrical Cell II

Fig. 6.26

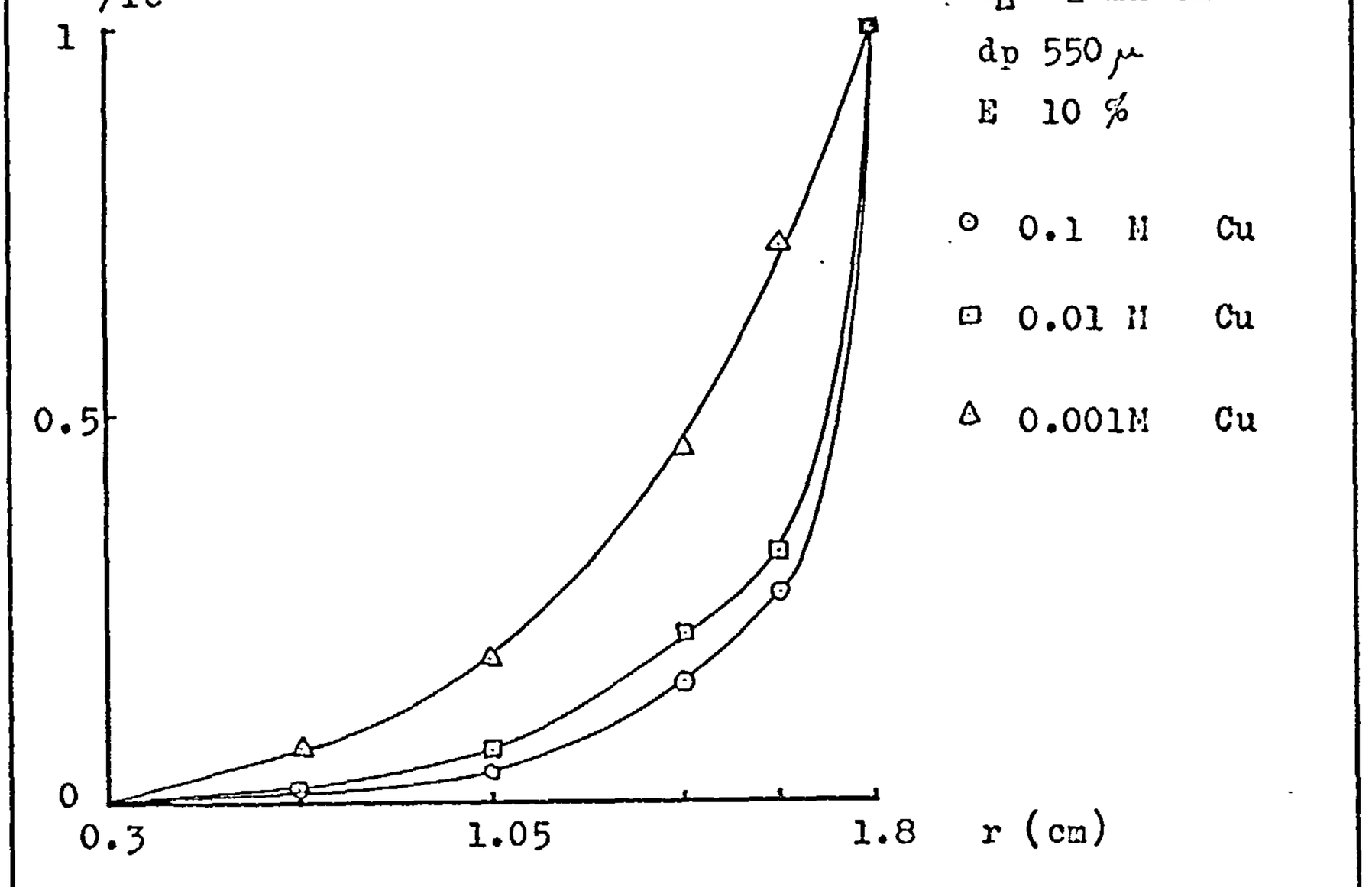

Current Distribution

Cylindrical Cell II

Fig. 6.27

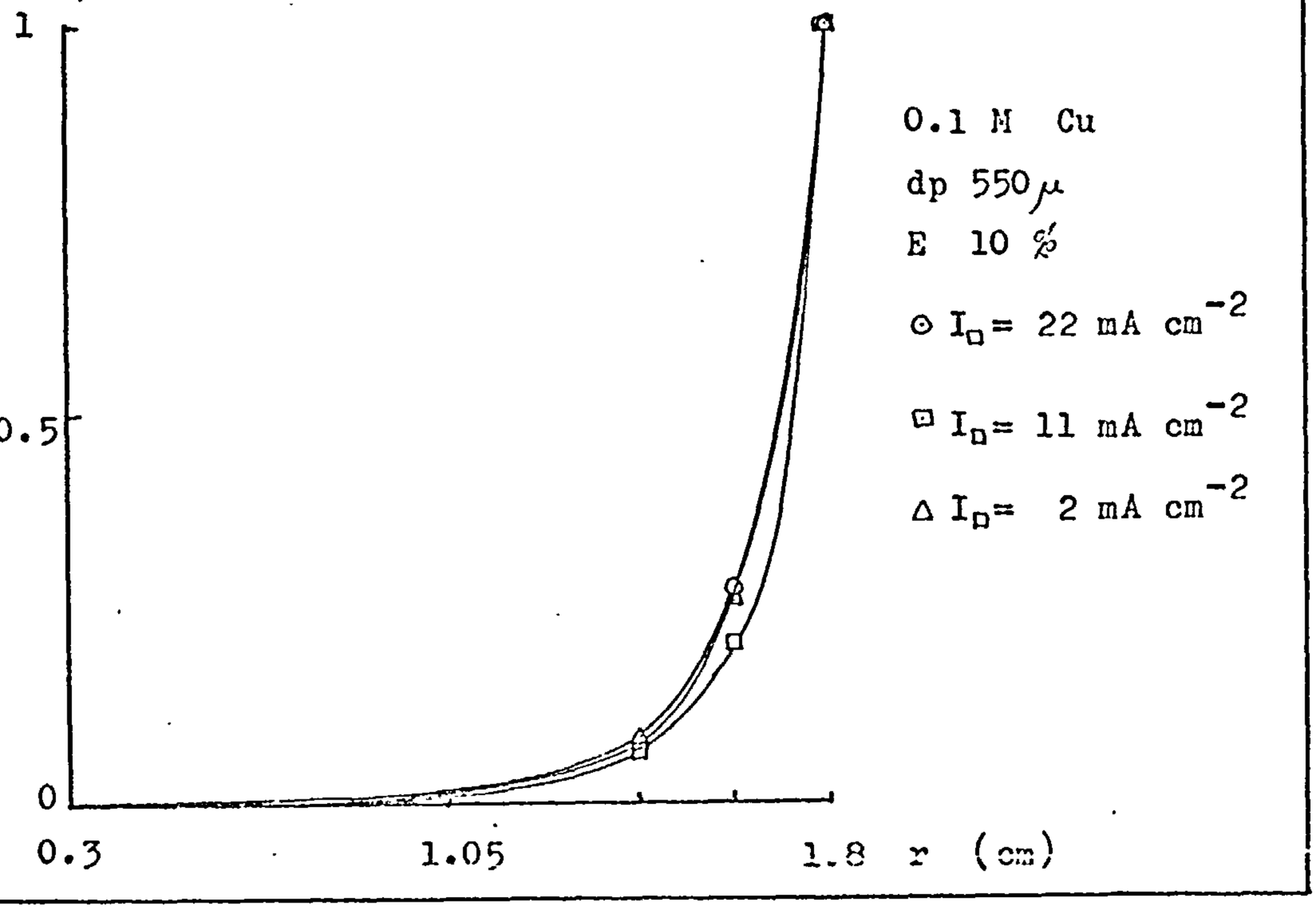

that the deposition process takes place largely in that region. In fact in all cases 50% of the total deposition apparently takes place within seven particle diameters of the diaphragm, and in the majority of cases within four diameters.

Again it will be noticed (Figure 6.26) that a more even distribution occurs at low diaphragm current densities, low copper ion concentration and high expansion.

A method proposed by GOODRIDGE et al[25], different from that used above, can also be employed to determine the distribution of current in the fluidised electrode. Defining σ as the fraction of electrode reaction taking place in a region of the bed lying within a radius r of the feeder, it can be written that,

$$\sigma = \frac{\int_{r_o}^{r} 2\pi r \, dr \, A_p \, F(\phi)}{\int_{r_o}^{r_1} 2\pi r \, dr \, A_p \, F(\phi)}$$

where the relationship between ϕ and r is established by the electrode potential profiles given in Section 6.3.2. Strictly, σ is identical to I_s/I_c but since the means of calculation and therefore source of error, is different, corresponding values may show some discrepancy.

For a planar cell the above equation is written

$$\sigma = \frac{\int_{o}^{x} A_p \, F(\phi) \, dx}{\int_{o}^{x_1} A_p \, F(\phi) \, dx}$$

where σ is now the fraction of electrode reaction taking place in a

region of the bed bounded by the feeder (i.e. x = 0) and the plane x = x. Using the potential profiles obtained for the planar cell with double felt distributor (c.f. Section 6.3.3) values of σ have been determined and are presented in Figures 6.28 and 6.29. Again a consistent picture is presented in which 50% of the deposition process takes place within about seven particle diameters from the diaphragm, but tending to become more evenly distributed at higher expansions and lower cell currents.

6.5. Comparison of the Performance of the Fluidised Bed Electrode with the Polarisation Data

By a simple charge balance, ignoring any side reactions, the total cell current may be equated to the rate of copper deposition in the planar bed according to

$$I_c = \int_o^{x_1} A\, A_p\, i\, dx$$

where A = cross sectional area of the bed perpendicular to the x-axis

A_p = superficial geometric area of the dispersed phase per unit volume of bed

i = current density of the deposition process at the point x

Designating the functional dependency of i on the electrode potential, ϕ, by $F(\phi)$, i.e. letting $F(\phi)$ be the equation of the polarisation curve, the above equation may be re-written in the form

$$I_c = \int_o^{x_1} A\, A_p\, F(\phi)\, dx$$

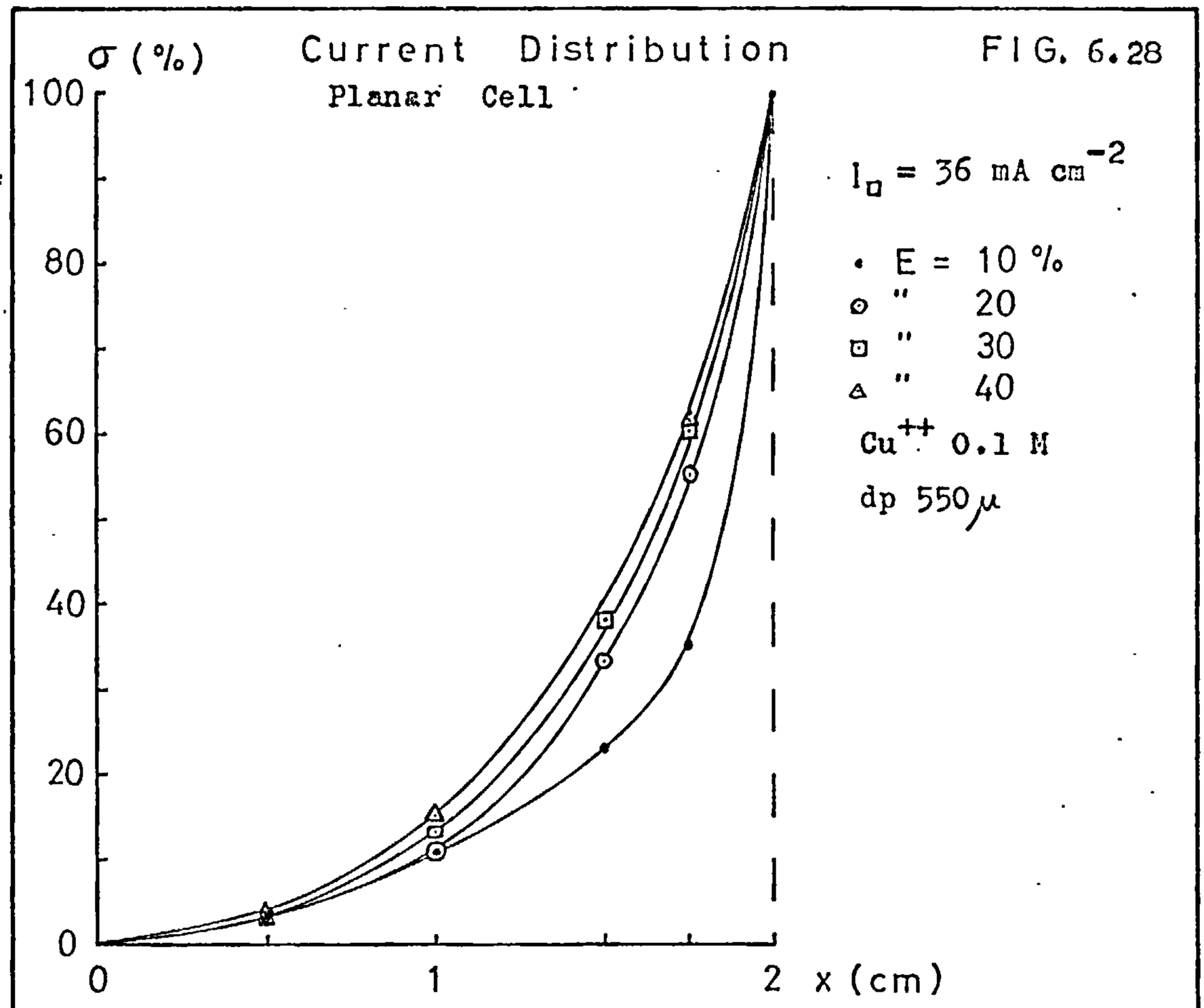

FIG. 6.28

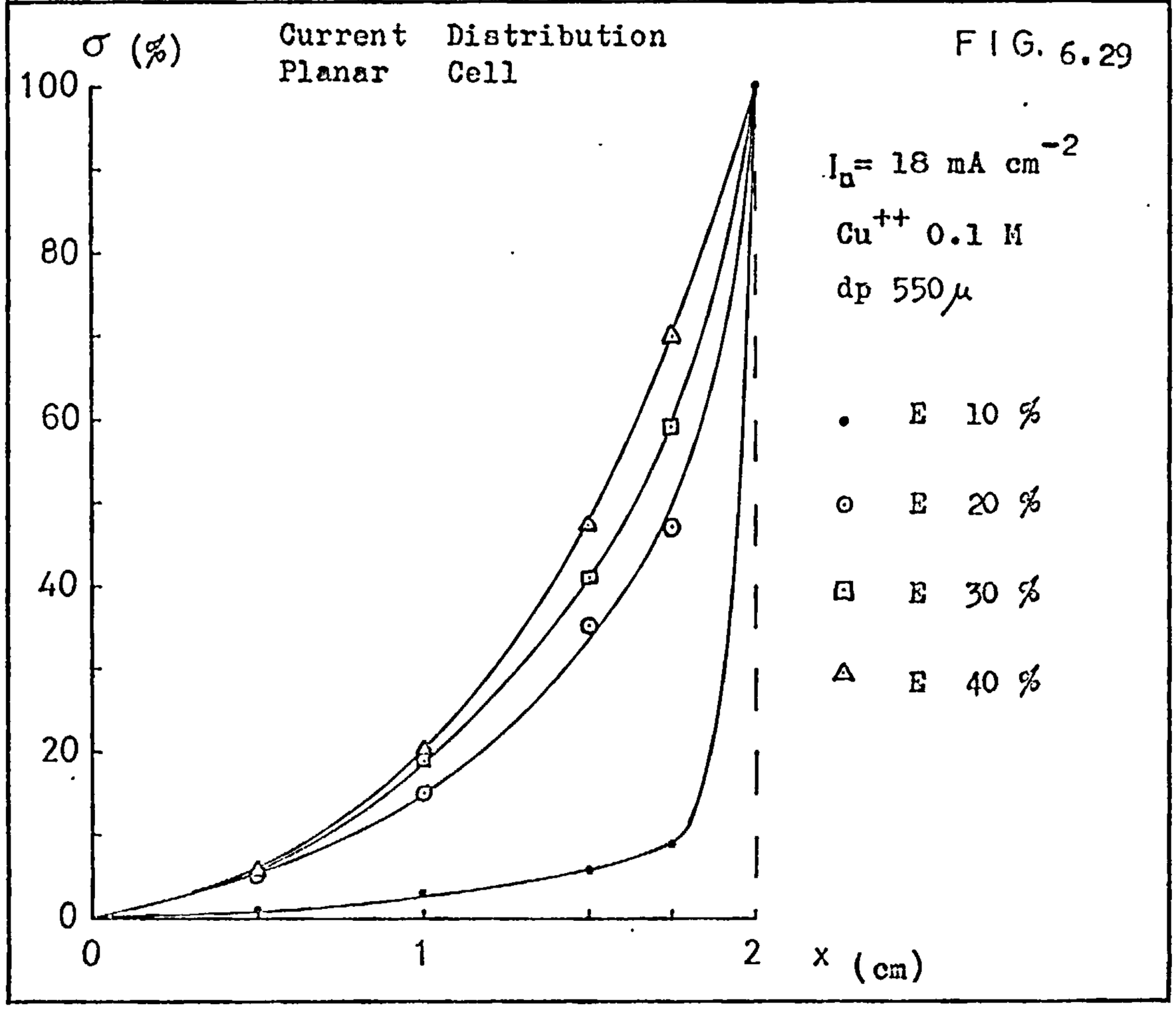

FIG. 6.29

Since the relationship between Ø and x is supplied by the electrode potential profiles which were determined experimentally (c.f. Section 6.3.3), the above equation can be integrated to give a value of I_c. In view of the non-linear nature of the polarisation curves (c.f. Section 3.8.2) and the Ø vs x curves, the integration was carried out numerically. Table 6.5 summarises the values of A_p used, and Table 6.6 the calculated values of I_c. In all cases the cross sectional area of the cell was 60 cm^2 and the limits of integration $0 \longrightarrow 2$ cm.

TABLE 6.5. Values of A_p for Particles of 550

Bed Expansion (%)	A_p (cm^{-1})
10	61.3
20	56.4
30	52.1
40	48.3

TABLE 6.6. Values of Calculated Cell Current and α coefficients.

Planar Cell

E (%)	(I_c) exp. (A)	(I_c) calc. (A)	α
10	2	14	0.143
20	2	108	0.0185
30	2	220	0.0091
40	2	514	0.0039
10	1	6	0.166
20	1	71	0.0141
30	1	106	0.0094
40	1	154	0.0065

The $\propto$ coefficient is defined by

$$\propto = \frac{(I_c)\ \text{experimental}}{(I_c)\ \text{calculated}}$$

and is therefore a measure of the discrepancy between the calculated value of the cell current as indicated by the electrode potential distribution, and its measured value. In every case $\propto$ is not only far removed from unity but falls off sharply with increase in bed expansion. It is relatively unaffected, however, by cell current. Although uncertainty in the polarisation data may be a contributing factor it cannot be wholly accountable for the phenomenon, nor can it explain the effect of bed expansion. Similar findings are reported by ISMAIL[51] who studied the behaviour of particulate electrodes with regard to chlorine evolution. He thought that the low values of $\propto$ (in his case varying from 0.14 to 0.4) reflected a reduction in the effective area of the electrode by a combination of oxide formation and mutual shielding of electrode surfaces in contact or close proximity with one another. In the present context those explanations are questionable, firstly because oxide formation in a cathodic environment is doubtful and secondly, because $\propto$ falls with increase in bed expansion whereas, if shielding was a major factor, one would expect it to rise. An explanation has therefore been sought elsewhere and it is suggested that particle bipolarity and dynamic polarisation may be responsible. These are treated separately below.

Particulate Bipolarity

KING[42] placed a copper sphere, 2 cm in diameter, between copper electrodes, the sphere having no electrical contact with either of them. When a voltage was applied to the cell the sphere became

bipolar, copper being deposited on the side of the sphere facing the anode and dissolved on the side facing the cathode. There was a strip around the centre of the sphere, parallel to the electrodes where no deposition or dissolution seemed to occur. The width of this strip was dependent on the voltage gradient between the electrodes. A similar effect was observed when his experiments were reproduced but using a 2 mm sphere. Similar observations have also been made with a copper rod, 3.2 cm long and 0.4 cm diameter, but in this case the rod was connected through a secondary circuit to the anode (see Figure 6.30). With the secondary circuit open the rod assumed a bipolar mode in which the anodic and cathodic areas each occupied half of its length. Two tests were then carried out with the secondary circuit closed. Again the rod became bipolar but the cathodic area increased at the expense of the anodic as the secondary circuit current was raised. For instance, at 35 mA two-thirds of the rod was cathodic whereas at 70 mA this value rose to seven-eighths. In all these runs the primary circuit was adjusted to give a current density of 17 mA cm^{-2} at the true cathode.

In the fluidised bed electrode, transfer of charge is thought to be brought about by particle collision, and a simple mechanical analog, a development of the previous experiments, was therefore set up to examine the occurrence of bipolarity under these circumstances. In this device the copper rod and cathode made intermittent contact with a third conductor which oscillated between them at the rate of 80 cycles per minute. The arrangement is shown in Figure 6.31. For a cell current density of 17 mA cm^{-2} over the period of 1 hour the rod showed an increase in mass of 3 mg and three quarters of its surface had been cathodic. Higher frequencies of oscillation were not tested owing to

FIG. 6.30

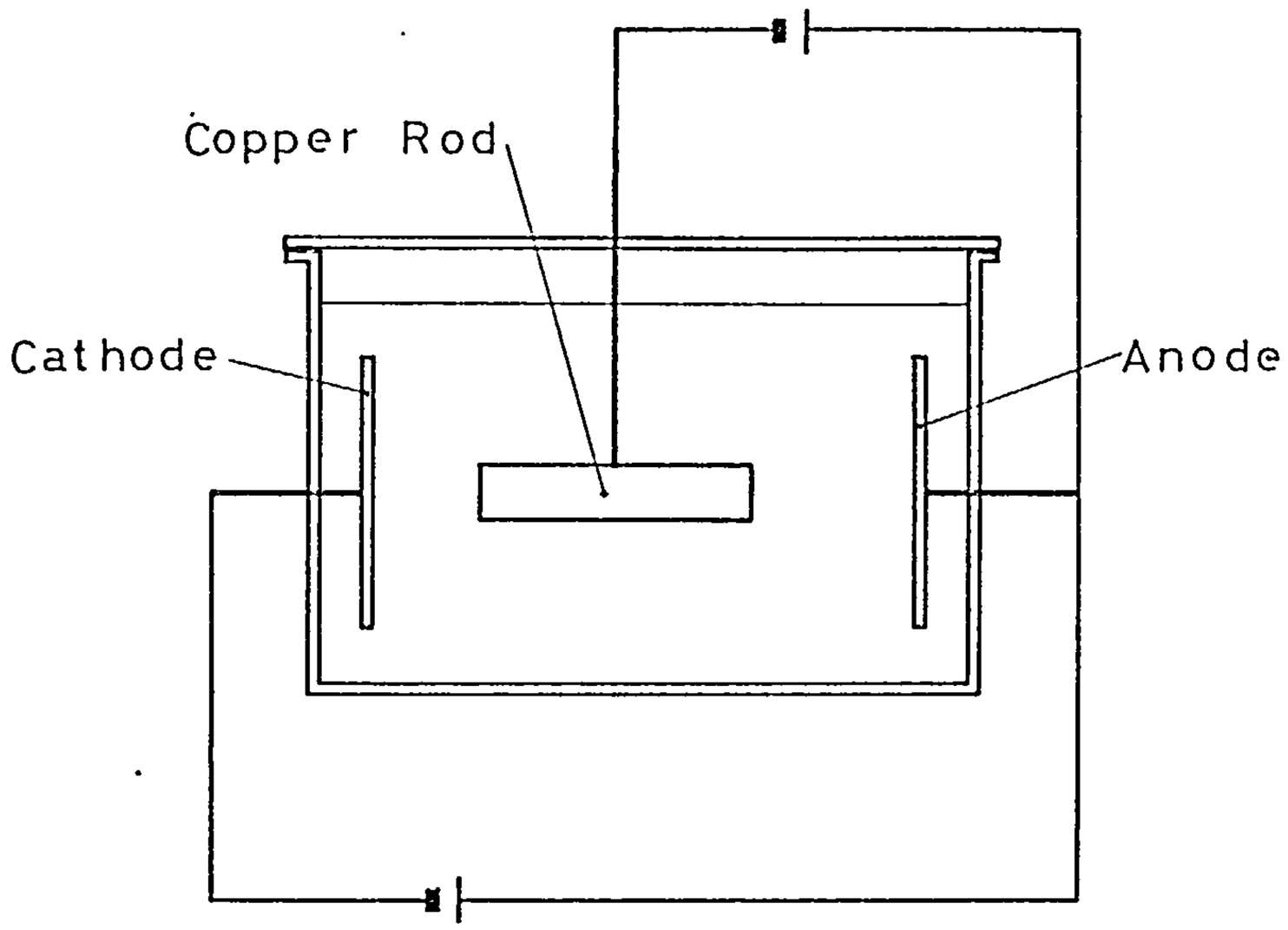

FIG. 6.31

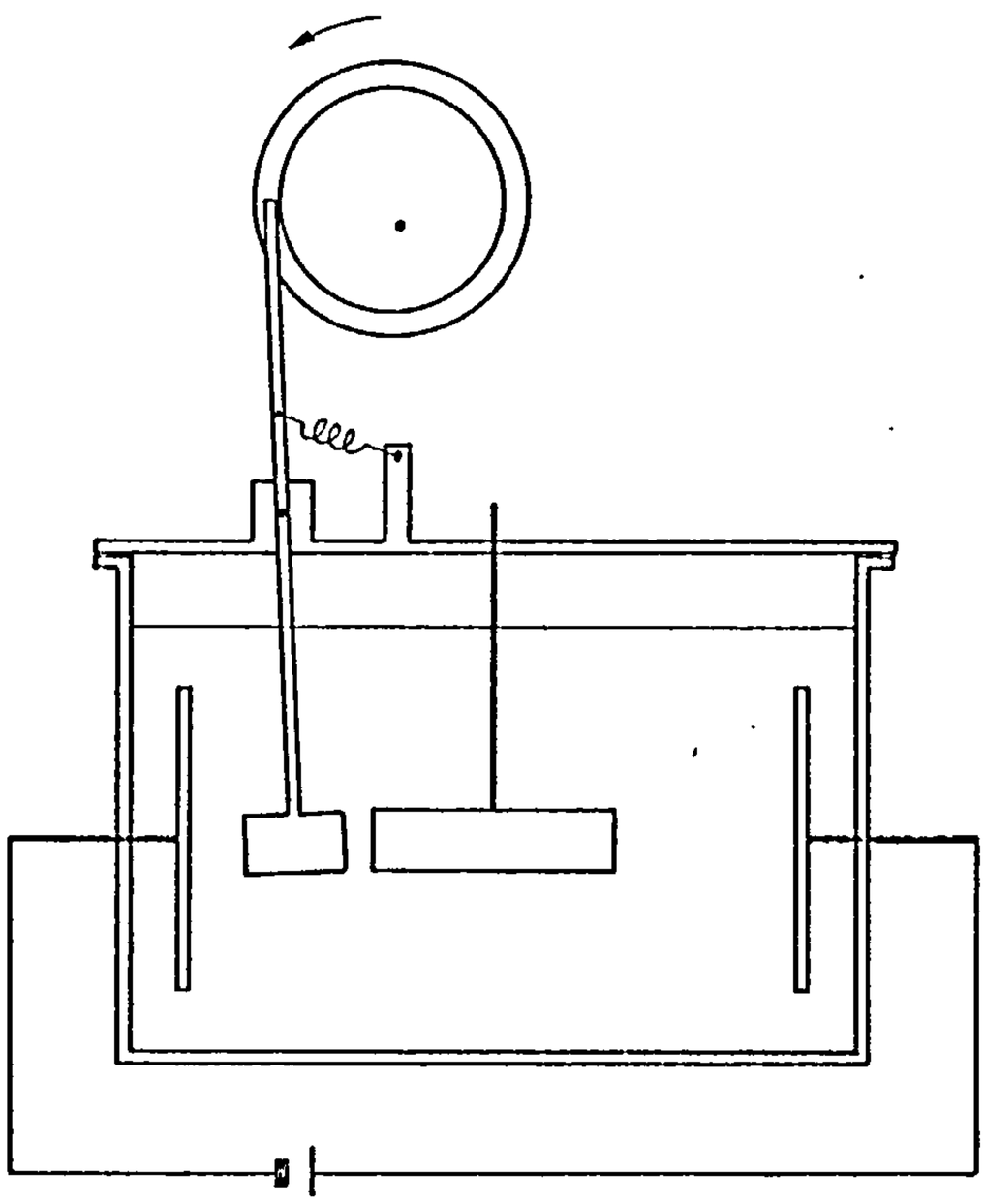

the limitations of the equipment.

Although experiments of this nature can at best be only qualitative, they do serve to indicate that particles and agglomerations of particles existing in a gradient of potential can take up a bipolar characteristic in which only part of the surface area would be polarised for deposition.

In a cathodically charged bed, however, the maximum fraction of area which could be anodically polarised is only one half, and therefore cannot wholly account for the low values of α observed, although it may be a contributing factor.

Dynamic Polarisation

As near as possible the polarisation curves (c.f. Section 3.8.2) determined in the present research programme apply to steady state conditions. An electrode was held at a constant potential for sufficient time for the current to attain a steady value, at which point the potential and current were noted. Quite clearly this condition is never reached by the individual particles of a fluidised electrode even though the overall condition of cell voltage and current may superficially give this impression. It has already been noted that the probes inserted in the bed to detect dispersed phase potentials transmit a rapidly fluctuating signal which may be reasonably assumed to reflect the potential history of the particles surrounding it. Since the potential of the continuous phase is relatively steady, it follows that the fluctuations also occur in the electrode potentials experienced by the particles. It is doubtful if static polarisation data can be used reliably to interpret this situation, since in the one

case hysteresis has been carefully eliminated while in the other an environment is produced which serves to emphasize it.

A picture of the deposition process taking place under these conditions may be obtained by reference to Figure 6.31, which shows a fluctuating electrode potential plotted against time. The rise and fall in potential occurs in approximately 10 μsec[53] which is considerably less than the relaxation time ($\sim$ 1 msec) for metal deposition. The withdrawal and supply of charge at this rate will therefore be mainly utilised in charging and discharging the double layer, and the rate of deposition may well be controlled not by average potential but perhaps by some intermediate value $\beta\ (\phi^1 + \phi_o)$ where β may be a fraction other than one half. On this argument the interpretation of the behaviour of a fluidised electrode in terms of average potentials will be erroneous and will become more so as the amplitude of the fluctuations increases.

This is in line with the observation that with increase in bed expansion $\propto$ falls in value and the fluctuations become more erratic.

Dynamic polarisation may therefore be a key factor in explaining the phenomenon.

6.6. Theoretical Interpretation of the Potential Distribution for Cylindrical Cell II

The experimental potential profiles have been interpreted in the light of the mathematical model for the fluidised bed electrode suggested by GOODRIDGE et al[25]. In particular the results have been used to determine values of the effective conductivity, K_m, of the dispersed phase.

Fig. 6.31'

Fluctuations of Electrode Potential in the Fluidised Bed Electrode.
(cf. Table 6.1)

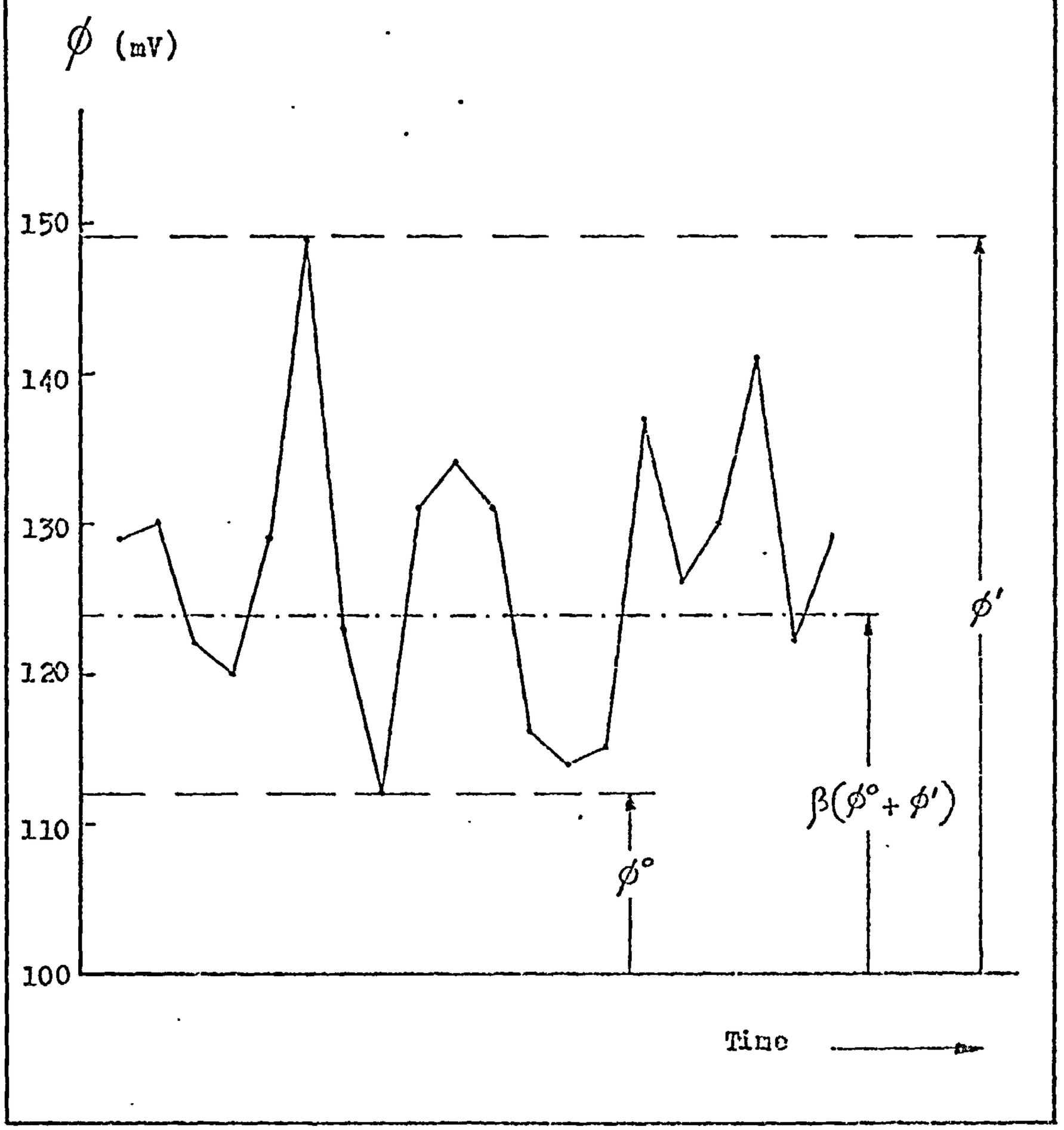

In proposing his model, GOODRIDGE envisaged that it might form the basis of a means of predicting the performance of fluidised bed electrodes, and to this end the accumulation of K_m data may eventually prove useful in cell design..

In a previous section (c.f. 6.4) it has been pointed out that in a cylindrical cell with central feeder, the flow of current across any cylindrical plane of radius r comprises two components, one flowing through the dispersed phase and one through the electrolyte phase, and that the sum of these components is equal to the cell current. This statement is expressed mathematically as follows,

$$I_{Dispersed,\,r} + I_{Electrolyte,\,r} = I_c \qquad \ldots\ldots(1)$$

GOODRIDGE suggests that each of these components is proportionalto the respective potential gradients at r, giving

$$I_{Dispersed,r} = - K_m A_r \left(\frac{d \phi_m}{dr}\right) \qquad \ldots\ldots(2)$$

$$I_{Electrolyte,\,r} = - K_s A_r \left(\frac{d \phi_s}{dr}\right) \qquad \ldots\ldots(3)$$

where K_m and K_s are the effective conductivities of the dispersed and electrolyte phases respectively, and A_r is the area of the cylindrical plane at r. Values of K_s have been determined in Section 6.3.1.

If h is the height of the bed then $A_r = 2\pi r h$, and

$$I_{Dispersed,\,r} = - 2\pi r h K_m \left(\frac{d \phi_m}{dr}\right) \qquad \ldots\ldots(4)$$

$$I_{Electrolyte,r} = - 2\pi r h K_s \left(\frac{d \phi_s}{dr}\right) \qquad \ldots\ldots(5)$$

Furthermore, since the whole of the cell current is concentrated in the electrolyte at the boundary of the electrode, i.e. at the diaphragm,

$$I_c = - 2 \pi r_1 h K_s \left(\frac{d \phi_s}{dr}\right)_{r_1} \qquad \ldots\ldots\ldots(6)$$

where r_1 is the radius of the diaphragm.

Substitution of (4), (5) and (6) in (1) gives

$$K_m r \left(\frac{d \phi_m}{dr}\right) + K_s r \left(\frac{d \phi_s}{dr}\right) = K_s r_1 \left(\frac{d \phi_s}{dr}\right)_{r = r_1}$$

the dependency of $r \left(\frac{d \phi_s}{dr}\right)$ on r for a range of experimental conditions has already been established from the ϕ_s vs. r curves in connection with the determination of the current distribution in the Cylindrical Cell II described in Section 6.4. Designating this known functional relationship by F(r) gives

$$K_m r \frac{d \phi_m}{dr} + K_s F(r) = K_s F(r_1)$$

which may be integrated to give

$$\int_{\phi_{m_1 o}}^{\phi_m} d \phi_m = \frac{K_s}{K_m} F(r_1) \int_{r_o}^{r} \frac{dr}{r} - \frac{K_s}{K_m} \int_{r_o}^{r} \frac{F(r)}{r} dr$$

$$\text{or} \qquad \phi_m = \frac{K_s}{K_m} F(r_1) \ln \frac{r}{r_o} - \frac{K_s}{K_m} \int_{r_o}^{r} \frac{F(r)}{r} dr + \phi_{m_1 o} \qquad \ldots\ldots(7)$$

where subscript o refers to conditions at the feeder surface.

The variation of ϕ_m with r has been evaluated from equation (7) for a

range of values of K_m and compared with the variations observed experimentally. The values of K_m which correspond to the closest agreement between the calculated and observed ϕ_m profiles are assumed to be the "best" values. The criterion of agreement between the profiles was the method of "least squares". It was applied by recording the discrepancy at eighteen equispaced values of r, squaring and summing them. The required integration and "least squares" calculations were carried out numerically with a Digital Equipment PDP8E digital computer. In that a criterion of "fit" has been used in determining the values of K_m the method has advantages over that used by GOODRIDGE et al[25,26] employing an analogue computer.

In all the calculations it was assumed that for any given set of experimental conditions K_m was independent of r. The values of K_m arising from these calculations are tabulated in Tables 6.7 and 6.8. The effect of the experimental variables on K_m is discussed under separate headings below, and is followed by a summary of typical K_m values.

Diaphragm Current Density

Values of K_m corresponding to diaphragm current densities of 11 and 22 mA cm^{-2} and a bed expansion of 10% have been abstracted from Tables 6.7 and 6.8 and are presented in Table 6.9. In the sixth column of this table a set of values described by K_m 2 are given. These represent values of K_m for a diaphragm current density of 2 mA cm^{-2} observed under otherwise the same experimental conditions as the values of K_m in the fifth column. They are used to present K_m in

TABLE 6.7. Charge Transfer Coefficient. Cylindrical Cell II

$d_p = 550\ \mu$

Cu^{++} (M)	I_D (mA cm^{-2})	E (%)	K_m (mho cm^{-1})
0.1 M	22	10	1.59
		20	0.75
		30	0.39
	11	10	1.91
		20	1.09
		30	0.076*
	2	10	1.74
		20	0.71
		30	0.156
0.01	22	10	1.94
		20	0.81
	11	10	2.38
		20	1.27
		30	0.37
	2	10	1.42
		20	0.456
		30	0.103
		40	0.055
0.001	2	10	0.61
		20	0.096
		30	0.0310
		40	0.037

TABLE 6.8. Charge Transfer Coefficient. Cylindrical Cell II

$d_p = 780\mu$

Cu^{++}	$I_{\square}$ (mA cm^{-2})	E (%)	K_m (mho cm^{-1})
0.1 M	22	10	0.148
	11	10	0.118
		20	0.0115
	2	10	0.0725
		30	0.0068
0.01 M	22	10	0.249
		30	0.0292
		40	0.0143
	11	10	0.179
		20	0.041
	2	10	0.176
		20	0.0414
		30	0.0151
		40	0.0125
0.001 M	2	10	0.314

TABLE 6.9. Variation of the Effective Conductivity of the Dispersed Phase with Diaphragm Current Density

$I_\square$ mA cm^{-2}	E %	d_p μm	Cu Molar	K_m ohm^{-1} cm^{-1}	K_m 2 ohm^{-1} cm^{-1}	$[K_m]$
22	10	550	0.1	1.59	1.74	0.91
		550	0.01	1.94	1.42	1.35
		780	0.1	0.148	0.0725	2.04
		780	0.01	0.249	0.176	1.41
				Average		1.43
11	10	550	0.1	1.91	1.74	1.10
		550	0.01	2.38	1.42	1.68
		780	0.1	0.118	0.0725	1.63
		780	0.01	0.179	0.176	1.02
				Average		1.33

the dimensionless form $[K_m]$, which is the ratio K_m/K_m 2. Thus, if $[K_m]$ is greater than unity an increase in K_m is implied for a change of diaphragm current density from 2 mA cm^{-2} to either 11 or 22 mA cm^{-2}. It can be seen that on the whole, this is the case, suggesting that K_m values tend to rise slightly with cell current. The evidence is, however, flimsy considering the scatter in values and needs further experimental verification over a wider range of cell currents.

Bed Expansion

In this respect the pattern of results is uniform, Tables 6.7 and 6.8 showing a sharp fall in K_m with increase in expansion. This is not unexpected, since if particle collision is responsible for the

passage of current through the bed, the greater the degree of separation of the particles the poorer will be its conductivity. GOODRIDGE et al[25] have quantified this argument and have proposed that K_m is proportional to $v/[(1 + E)^{\frac{1}{3}} - 1]$. The present data are plotted in these terms in Figure 6.32 and over a range of bed expansions from 10 to 30% show a linear but not proportional relationship to $v/[(1 + E)^{\frac{1}{3}} - 1]$. Beyond an expansion of 30% the curve veres away to pass through zero.

Particle Size

Somewhat surprisingly a comparison of Table 6.7 with Table 6.8 shows that K_m values for 550 micron particles is some ten times greater than those for the 780 micron particles. At present the difference cannot be explained, but quite obviously needs further investigation in view of the enormous changes in particle size which will occur in a practical situation. In this context it should be remembered that the value of K_m plays a key role in determining the distribution of activity in the bed, and if the present results are confirmed by future work there is the possibility of an operational electrode changing its character of behaviour over the period of the ~~separation~~ deposition process. Thus, low values of K_m tend to induce more activity at the feeder perhaps giving rise to heavier deposits on the feeder and also enhancing the possibility of agglomeration.

Copper Ion Concentration

Figure 6.33 lends evidence to the effect that increase in copper concentration may either reduce or raise the value of K_m. On balance, however, it would appear that it tends to depress K_m, but not

Fig. 6.32

Effect of Bed Expansion on Km.

Cylindrical Cell II

○ I_D = 22 mA cm^{-2} • 0.1 M Cu

□ I_D = 11 mA cm^{-2} X 0.01 M Cu

△ I_D = 2 mA cm^{-2} – 0.001 M Cu

dp 780μ

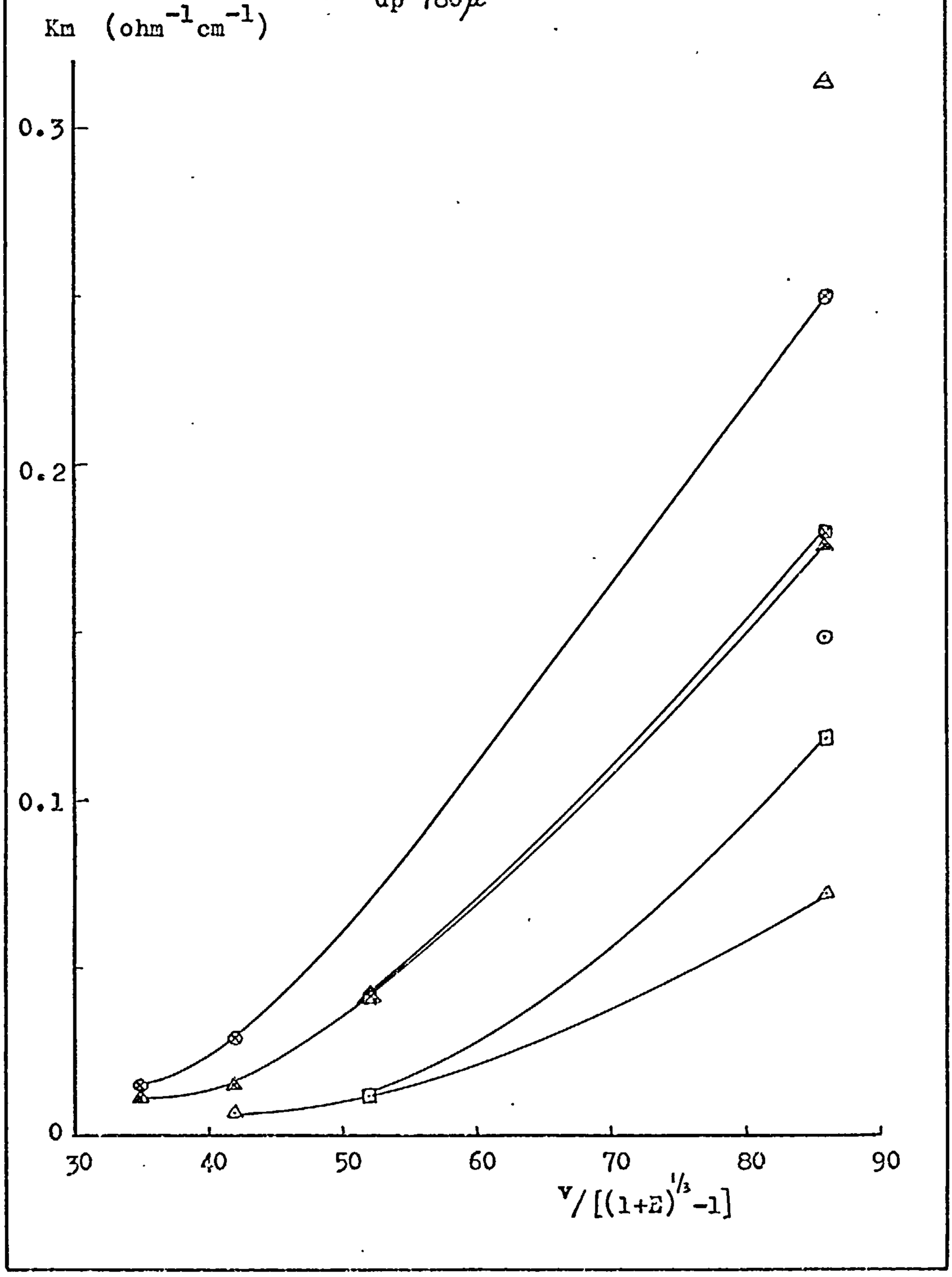

Fig. 6.33

Effect of Copper Ion Concentration on Km.

E 10 %

⊙ I_D= 22 mA cm^{-2} ———— dp 550 μ

⊡ I_D= 11 mA cm^{-2} — — — dp 780 μ

△ I_D= 2 mA cm^{-2}

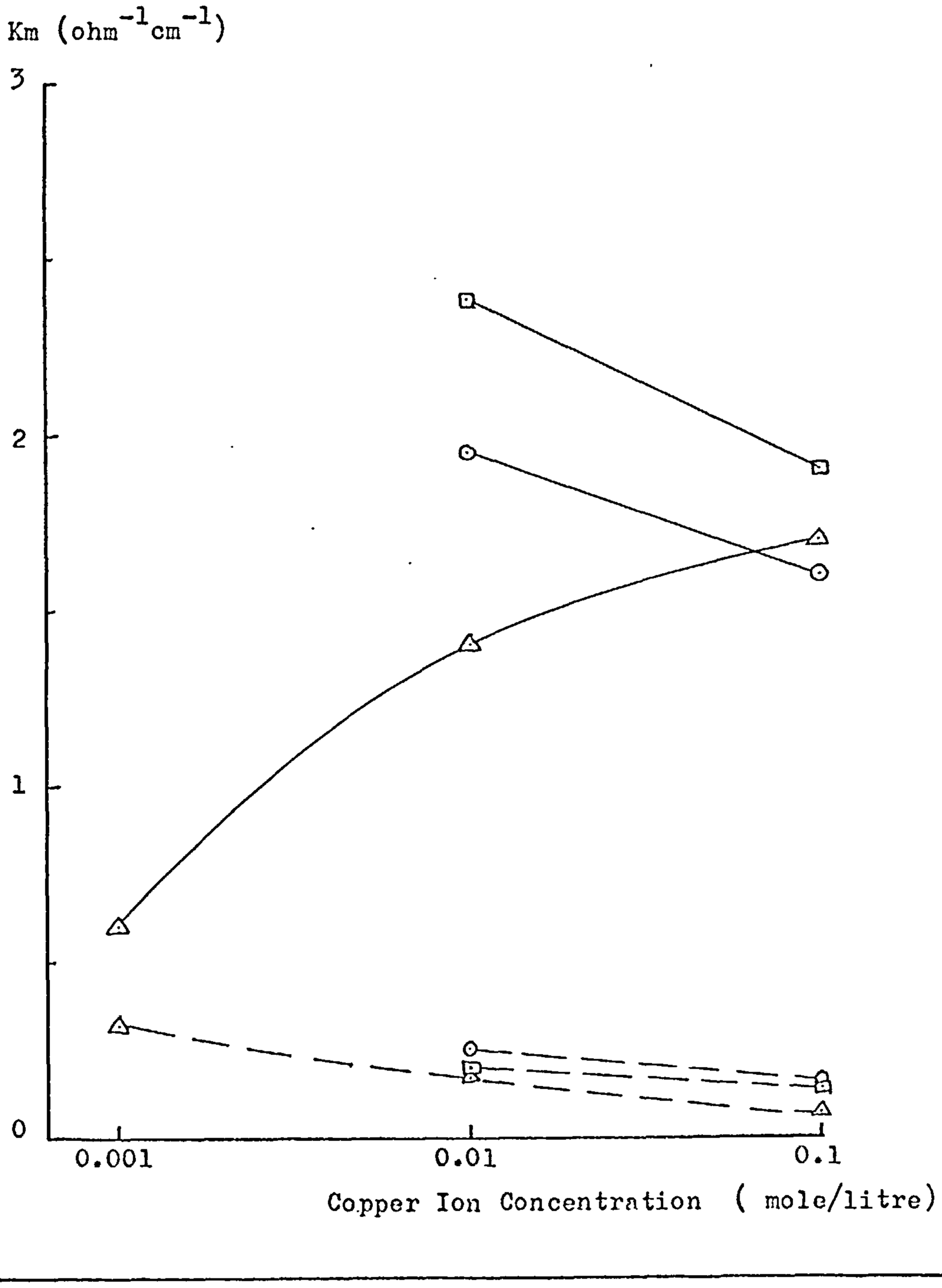

very strongly, and that perhaps at low cell currents the reverse may occur. Again, more work is needed to establish this point.

Typical Values of K_m

If it is accepted that neither copper ion concentration nor diaphragm current density (except very low values) have a particularly marked effect on K_m then typical values may be obtained by averaging the results of Tables 6.7 and 6.8 to give Table 6.10. This table shows clearly the effects of expansion and particle size already described.

The "error" included in the third column is the scatter of the individual values about the mean and does not therefore carry a strict statistical meaning.

TABLE 6.10. Typical Values of K_m

Expansion %	d_p μm	K_m	Comment
10	550	$2.0 \pm 20\%$	
20	550	$1.0 \pm 25\%$	
30	550	$0.4 \pm 5\%$	(1)
10	780	$0.17 \pm 50\%$	

(1) The value of K_m carrying an asterisk in Table 6.7 was not included in the averaging because it was so much lower than comparable values that its accuracy is open to question.

It can be remembered (c.f. Section 2.2) that FLEISCHMANN and OLDFIELD[22] propose an expression for K_m, namely,

$$K_m = \frac{3.6\ \rho^{\frac{1}{3}}\ v_p^{\frac{1}{3}}}{\epsilon^{\frac{1}{3}}\ (\epsilon^{\frac{1}{3}} - 1)\ \gamma^{\frac{1}{3}}\ \rho_s}$$

If the relevant values for a fluidised electrode working with 550 microns particles, 10% bed expansion and 0.1 Molar copper concentration are inserted into the above equation, we have

ρ = 3 gr/cm^3

$v_p \simeq v$ = 1.2 cm/sec

ϵ = 1.1

γ = 1.2×10^{10} dyn/cm^2 (for copper), and

ρ_s = 42 ohm cm

which give a value of $K_m = 1.8 \times 10^{-3}$ which is some one thousand times smaller than the value for the same conditions obtained in this work.

Furthermore, it seems that the term ρ_s, the effective specific ~~sensitivity~~ resistivity of the electrolyte in the above equation does not affect K_m inversely but directly, i.e. K_m increases with an increase in ρ_s.

If values for the same conditions but a 40% bed expansion instead of 10% the value of K_m obtained with the above equation is 0.7×10^{-3} which is more in accordance with the extrapolated value from the present work's results.

It can be concluded, therefore, that the above equation is applicable at high bed expansions i.e. 40% but at low bed expansions it does not agree with the experimental values.

CHAPTER 7. ECONOMIC COMPARISON BETWEEN FLUIDISED BED AND PLATE CELLS

The cost of copper extraction from dilute acid solutions is estimated below with reference to the following systems.

7.1. Recovery Systems

a) Fluidised Bed System

The recovery cell in this system is envisaged to consist of a planar fluidised bed cathode and a plate antimonial lead anode, the cathode and anode compartments being separated by an ion exchange membrane. The particles used would be copper-coated glass and would suffer a change in size from an initial value of 400 microns to a final one of about 600 microns. At this stage they would be removed from the recovery cell and transported to a second cell where they would be fluidised in the anode compartment, the dissolved copper being plated out on a plate copper cathode. Again the compartments would be separated by an ion exchange membrane. In this second cell the copper ion concentration would be maintained at a high enough level to ensure current efficiencies approaching 100% at the plate cathode. The dimensions of the cells would be such that the area of the fluidised bed in both cases would be 1 m^2 and their thickness 2 cm.

It is contemplated that the process would operate on a continuous basis, rather than batch, with particles being withdrawn from the base of the recovery cell and passed to the second cell.

b) Plate Electrode System

In this system only one cell is required, the copper being deposited directly on to a plate cathode. Agitation would be provided

by electrolyte recirculation. It is assumed for the purpose of the present exercise, that good quality plating can be achieved from low concentration solutions, although in practice this may not be so[39].

7.2. Process Conditions

Although in a practical situation the feed would naturally be depleted in terms of copper content as it passed through the cells, the costing has been carried out on the assumption that the conditions prevailing in the cell are determined by the average content. The values selected were 100, 1000 and 6000 p.p.m. Other conditions are tabulated in Table 7.1.

TABLE 7.1. Conditions for Fluidised Bed and Plate Electrode Systems

	Copper Concentration, (p.p.m.)					
	Fluidised Bed			Plate Electrode		
	100	1000	6000	100	1000	6000
Cell Voltage, (Volts)	4.5	4.0	3.5	4.0	3.5	3.0
Diaphragm Current Density ($mA\ cm^{-2}$)	50	75	100	5	5	30
Current Efficiency (%)	60	80	93	15	45	80
Cell Current, (Amps)	1000	1000	1000	4000	1800	1000
Pump Power (hp)	4	4	4	2	1	½
Rectifier Capacity (Amps)	2000	2000	2000	4000	2000	1000
Copper Production (Ton/year)	5.7	7.6	8.8	5.7	7.7	7.6
Approx. H_2SO_4 conc. (Molar)	0.1	0.1	0.1	0.1	0.1	0.1

7.3. Capital Costs

The figures given below refer to copper recovery corresponding to an average copper content of 6000 p.p.m. Since the costing is comparative only, those aspects of the processes which are dissimilar are included.

a) Fluidised Bed System

Cost of Materials for Recovery Cell	£	
PVC sheet	18	
Ion exchange membrane	33	
Porous plate distributor	4	
Copper feeder	17	
Antimonial lead anodes	5	
	77	77
Cost of Materials for second cell	£	
PVC sheet	18	
Ion exchange membrane	33	
Porous plate distributor	4	
Graphite feeder (approx.)	20	
	75	75
Fabrication Costs for both cells	250	250

Fluidised Bed Materials

It is intended in this process that the dissolution of copper from the particles in the second cell is not carried to completion. It is felt, however, that there may be a need for regular re-coating with copper, owing to irregularities in residence time. This period is assumed in the costing to be about 1 year.

Two lots of 36 kg, 400 microns ballotini		
at £0.85 per kg	£60	
One re-coating per year	£200	
	260	260
Rectifier 2000 A, 6V	£1350	1350
TOTAL approx.		£2000

b) Plate Electrode System

Materials and fabrication	£150
Rectifier 1000 A, 6V	£1000
TOTAL approx.	£1150

7.4. Running Costs

a) Fluidised Bed System

Power consumption, 3.5V x 1000A x 8000 hrs = 28,000 kw h

Power costs, £0.01 per kw h £280

The power cost in the second cell is assessed as £30 per ton of copper recovered and is independent of conditions in the recovery cell.

Copper recovery, over 8000 hrs with current efficiency of 93%, 8.8 Tons/annum.

Electrical Power cost per ton of copper recovered, £62/Ton

Running costs for a 4 hp pump £28/Ton

TOTAL Running Costs £90/Ton

b) Plate Electrode System

Power consumption 3V x 1000A x 8000 hrs = 24,000 kw h

Power cost, £0.01 per kw h £240

Copper recovery over 8000 hrs with a current efficiency of 80%, 7.6 Tons/annum.

Electrical power cost per ton of copper, £32/Ton

Running cost for a ½ hp pump £4/Ton

TOTAL Running cost £36/Ton

7.5 Overall Costs

a) Fluidised Bed System

Capital depreciation, 10% per annum £23/Ton

Running Costs £90/Ton

TOTAL £113/Ton

b) Plate Electrode System

Capital depreciation, 10% per annum £15/Ton

Running costs £36/Ton

TOTAL £51/Ton

A summary of the power costs for three concentrations calculated in the above manner is shown in Table 7.2.

TABLE 7.2. Cost of Copper Recovery in Fluidised Bed and Plate Electrode Systems

	Concentration (p.p.m.)	Capital Depreciation (£/Ton)	Running Costs (£/Ton)	Overall Costs (£/Ton)
Fluidised Bed	100	35	132	167
	1000	26	104	130
	6000	23	90	113
Plate Electrode	100	44	245	289
	1000	21	73	94
	6000	15	36	51

7.6. Discussion

The plot of overall costs in Figure 7.1 shows how it increases sharply at low concentrations of copper ion, particularly for plate electrodes due to their low current efficiency. In general it seems that over the whole range of concentration considered fluidised beds have relatively constant costs, whilst plate electrodes costs are much more sensitive to copper ion concentration. From this cursory costing it is suggested that fluidised beds have significant advantages over plate electrodes for copper ion concentrations below about 500 p.p.m.

Cost of Materials

I.C.I. PVC 6' x 4' x ½"	£29
Ion exchange membrane 30" x 12"	£7.50
Copper 14 gauge (2mm) per 100 kg	£80
Lead 6% antimonial per Ton	£240
Lead 1 sheet 4' x 2' x 2 mm	£0.60
Copper beads 1 mm based on Cu price of £450 per Ton, per Ton	£900
Rectifiers Udylite (Oxy Metal)	
1000A 6V	£1000
2000A 6V	£1350
4000A 6V	£2000

Fig. 7.1

Cost of Copper Recovery in Fluidised Bed and Plate Electrode Systems.

Overall Costs.

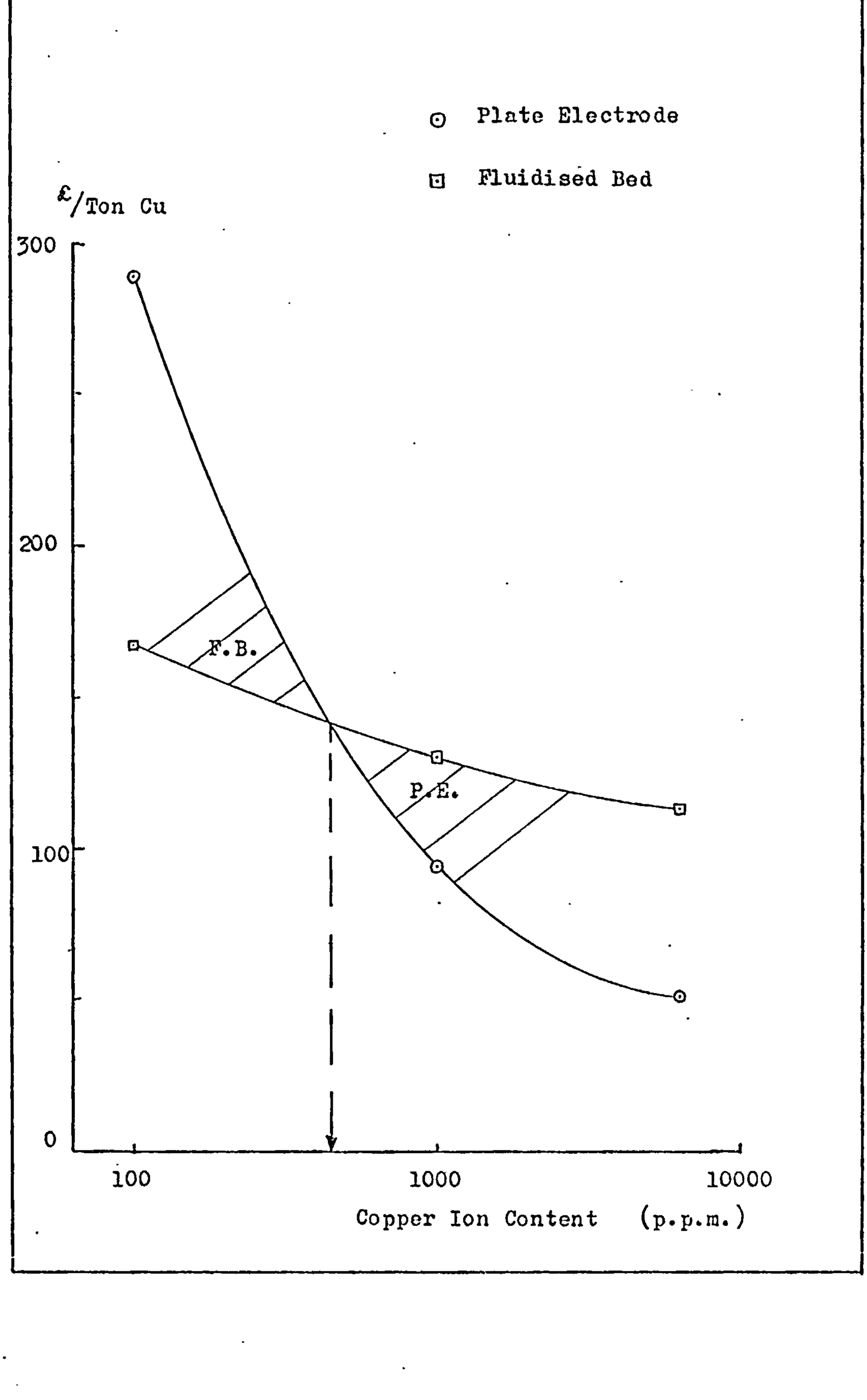

CHAPTER 8. CONCLUSIONS

The polarisation curves for cathodic deposition of copper which were determined prior to the main investigation confirmed the results of previous workers, and in particular reinforced opinion that the rate of deposition is significantly influenced by the previous history of the electrode, both physical and electrochemical.

Deposition of copper on a fluidised bed of conducting particles has been shown to proceed satisfactorily and without difficulty, and gives high current efficiencies (in excess of 60%) even at low concentrations of copper ion (down to 17 p.p.m.). Particle agglomeration was not, in general, a problem and its occurrence was always preceded by maldistribution of electrolyte at the entrance to the bed, the quality of which was assessed visually. This stage of the work led to the conclusion that good electrolyte distribution was associated with high pressure drop across the distributor (comparable to that across the bed) and entry of the electrolyte near to the containing walls of the bed. These twin principles gave rise to the design of distributor described in Section 4.4.2 (c.f. Figure 4.3.e). It should be emphasized, however, that the present work is small scale and that in larger cells and extended runs other factors conducive to agglomeration may become apparent.

Potential profiles in the particulate and continuous phases have revealed that the activity of the bed is non-uniform and that at lower bed expansions (10-30%) there is a tendency for the majority of deposition to occur in the region of the bed nearer to the anode. At higher expansions the region adjacent to the feeder also becomes active,

with the centre of the bed remaining relatively inactive. It would appear, therefore, that increasing the thickness of the bed in the direction of current flow only serves to enlarge the inactive central zone, and that on purely electrochemical grounds there is no advantage to be gained by extending the bed in that direction beyond 1 or 2 cm. There may, however, be good hydrodynamic or constructional reasons for doing so.

The inactive zone is characterised by low cathodic potentials, and is therefore only weakly protected against corrosion. Dissolution of copper may result giving rise to lower overall current efficiencies. This was felt to be the reason for the low values observed at low cell currents. The presence of oxygen is also found to depress current efficiencies probably by intensifying the corrosive nature of the catholyte. For this reason semipermeable membranes were employed in the cell to prevent diffusion or bulk transfer of dissolved oxygen from the anolyte.

Deposition of copper on the feeder is remarkably low. This fact is ascribed to the siting of the feeder in the region further away from the anode where for the majority of runs the electrode activity was low.

Values of cell current have been calculated from the electrode potential profiles and polarisation data, but they are in marked disagreement with the measured values. An explanation in terms of experimental error seemed untenable, and it is proposed that the discrepancy may arise from the incompatibility of interpreting the behaviour of a particulate surface undergoing rapid potential cycling

in terms of static polarisation data. This proposal needs experimental verification and it is suggested that an investigation along these lines be included in any future programme.

Values of the effective conductivity of the particulate phase, determined from the potential profiles in accordance with the mathematical model of GOODRIDGE et al[25] range from 0.3 to 2.0 ohm^{-1} cm^{-1} for the 550μ particles and from 0.012 to 0.25 for the 780μ particles, and reveal that the behaviour of the bed is very sensitive to particle size. In absolute terms the values for the 550μ particles are greater than those reported by GOODRIDGE et al[25] for 500μ copper-coated glass particles used in the cathodic reduction of m-nitrobenzene sulphuric acid. When plotted against $v/[(1 + \ )^{\frac{1}{3}} - 1]$, however, a straight line is obtained which falls below that of GOODRIDGE'S line, the inference being that higher flow rates (probably due to a slight increase in particle size and therefore particle density) may be required for fluidisation under deposition conditions than under desorption-absorption conditions of organic synthesis. It is hoped that this point will be taken up in future work.

A comparative costing between a fluidised and plate electrode process has shown the fluidised bed to be the more attractive of the two for recovery of copper from solutions containing less than 500 p.p.m. of cupric ions. Both processes were assumed to produce plate copper as the final product, which in the case of the fluidised electrode implies an additional re-dissolution step followed by recovery on a plate cathode. If the fluidised bed was operated using solid copper particles as a starting material and the product was left in the particulate state it

is possible that the above value for the cross-over concentration, namely 500 p.p.m., would be increased, depending on the availability of starting solid copper particles.

Although the costing exercise is naturally somewhat tentative in view of the lack of experience on the performance of large scale cells, the present data are sufficiently promising for the programme of work to be continued.

APPENDIX A. METALLURGY OF COPPER

A. Copper Electrowinning Industry.

Copper was the first metal extracted by electrowinning; later it was applied in a more complicated manner to zinc and other metals such as cobalt, chromium, iron and silver.

The advantage of electrowinning or electrodeposition using insoluble anodes is that it yields directly a produce (cathode copper) of the same quality as the cathodes produced by electrolytic refining.

In copper electrowinning, the copper containing minerals are leached, and the copper is dissolved by a solution which becomes the electrolyte. The metal is deposited electrolytically on thin copper sheets, using insoluble anodes. The electrolysis is carried out at about 13 mA cm^{-2}, starting with an electrolyte containing about 5% of copper, until a final copper content of not less than 1.5% is reached, with a mean current efficiency of 80 - 90%. If more copper was deposited the current efficiency would fall too far. The spent electrolyte is then returned for leaching fresh ore in a cyclic process.

B. Cell Reaction.

The reaction at the copper cathode is,

$$Cu^{++} + 2\,e^{-} \longrightarrow Cu$$

and at the insoluble anode,

$$SO_4^{=} + H_2O - 2\,e^{-} \longrightarrow H_2SO_4 + \tfrac{1}{2}\,O_2$$

the net cell reaction is,

$$Cu\ SO_4 + H_2O \longrightarrow Cu + H_2SO_4 + \tfrac{1}{2}\ O_2$$

The electrolysis liberates metallic copper at the cathode and gaseous oxygen at the anode; for every mol of $Cu\ SO_4$ decomposed, a mole of free H_2SO_4 is formed in the electrolyte.

The cell reaction is endothermic,

$Hr = - 55,030$ cal.

In electrolysis, the energy needed for the deposition of copper is supplied by electrical energy. Assuming that the electrical energy and heat energy involved in any given reaction are equal, we have according to Thomson's rule,

$$E = \frac{U}{njF} = \frac{55,030}{2 \times 0.239 \times 96,500} = 1.195 \text{ Volts}$$

This indicates that the voltage drop across the cell must be at least 1.195 V if the reaction is to take place. No current will flow through the cell unless the voltage is greater than 1.195 V, provided that there are no other possible reactions.

C. Impurities.

The most harmful impurities usually found in the electrolyteare:

- ferric ion: it oxidizes copper at the cathode, its reduction to ferrous ion proceeds preferentially at the cathode and current and power efficiencies decrease.
- nitrates, particularly in the presence of small amounts of molybdenum may cause a vigorous oxidation of ferrous ions and can oxidize the cathode too.

- chlorine affects the cathode due to deposits of insoluble cuprous chloride.

D. Sources of Dilute Copper Solutions.

a) Electrowinning.

Spent electrolyte is a very complex solution, containing, apart from copper, sulphate and hydrogen ions, smaller amounts of metals, nitric acid and iron. With the continuous leaching the concentration of nitric acid, iron, etc. in the leaching liquors will build up. To diminish this and control it, portions of electrolyte are discarded either continuously in small amounts or at regular intervals. The amount of acid discarded is either added as sulphuric acid or furnished by the ore's acid-forming constituents.

In cases of ores of too low grade, the resulting leach solutions are too poor in copper, and not suitable for electrolytic precipitation by conventional methods.

b) Electrorefining.

In electrorefining of copper, the same problem of impurity build-up arises, and acid is added, but at more or less regular intervals the electrolyte must be completely renewed.

c) Other sources.

Solutions of low copper concentration are also found in other operations such as electroplating and pickling, e.g. of coils of copper rod before drawing into wire.

E. Methods of copper recovery from dilute solutions.

Copper must be recovered due to economic reasons and besides to comply with contaminated effluent regulations. Various methods are used for the extraction of copper from dilute solutions.

a) The simplest method is copper cementing by scrap or particulate iron[4]. This method, however, produces a foul cement copper which requires further treatment, consumes iron and wastes both the free and combined acid content of the electrolyte.

b) Crystalline Cu SO_4 $5H_2O$ can be obtained by neutralisation of free acid with anode copper. The neutral liquor is then concentrated by boiling followed by crystallisation; the copper remaining in the mother liquor is extracted by cementing with iron.

c) Solvent extraction using special solvents, followed by electrowinning[5,6].

d) Precipitation of Cu $(OH)_2$ by adding caustic soda; the precipitate is thickened and processed to reclaim copper[7].

e) Electrolytic recovery. Most of the processes employ laminar cathodes. The lowest concentration attained with reasonable current efficiency and quality of deposit is about 1 gr Cu/l. A review of the literature is given by KUHN[39].

APPENDIX B. DETERMINATION OF THE AMOUNT OF COPPER DEPOSITED. METHODS OF ANALYSIS

In the experiments with a plane electrode, the amount of copper deposited was determined by difference in weight of the electrode before and after deposition.

The same method cannot be applied to determine the weight of copper deposited on a fluidised bed since it implies drying the bed in an inert atmosphere and this is not practical.

The most suitable method is to determine the concentration of copper in the electrolyte prior to electrolysis and after deposition has taken place. If the volume of electrolyte is known, a mass balance will show the amount of copper deposited.

Titration[28,29], is accurate enough for copper concentrations around 0.1 Molar, but for lower concentrations, i.e. 0.01 and 0.001 Molar, the errors of the burete, sodium thiosulphate concentration and end point determination,pose a limit to the accuracy of titration, and certainly 0.01 and 0.001 Molar lie outside this limit.

The method finally chosen was to determine the copper concentration by absorption spectrophotometry of the diethyldithiocarbamate copper complex[30,31].

Although this method is much more elaborate than titration, its accuracy is 1 microgram of copper.

Reagent Solutions

Alkaline ammonium citrate: a 5:3 mixture of 20% (w/v) aqueous solution of A.R. Citric Acid and 10% (w/v) aqueous ammonia solution.

Carbamate solution: 0.1% (w/v) aqueous solution of A.R. sodium diethyldithiocarbamate. This solution should be stored in an amber container.

Standard copper solution: 0.005% (w/v) copper sulphate.

Procedure

A known volume of standard copper solution (1 to 5 ml) is placed in a separatory funnel. A few drops of 1 N sodium hydroxide are added, followed by 1 N acetic acid; the acid will redissolve the cupric hydroxide precipitated by the addition of sodium hydroxide.

Add 15 ml of the alkaline citrate solution and shake to mix. Add 2 ml of the carbamate solution, and distilled water to a total volume of 22 ml. The carbamate complex is then extracted with 10 ml of carbon tetrachloride. When the layers have separated, run the carbon tetrachloride layer into a 1 cm cell and take the absorbance reading at 435 millimicrons.

Calibration Chart (Figure A)

Samples of standard copper solution (0.5, 1, 1.5 ml etc.) were treated as described in the Procedure and a chart of weight of copper vs. absorbance is recorded. The results are plotted in Figure A and a straight line from the origin is drawn. A check of the calibration chart was made every time that a set of samples was to be analysed.

When the copper concentration in the electrolyte was such that 2 ml contained more than 4×10^{-5} gr Cu (see Calibration Chart) the appropriate dilution with distilled water was carried out so that

Calibration for spectro-

photometry

FIG. A

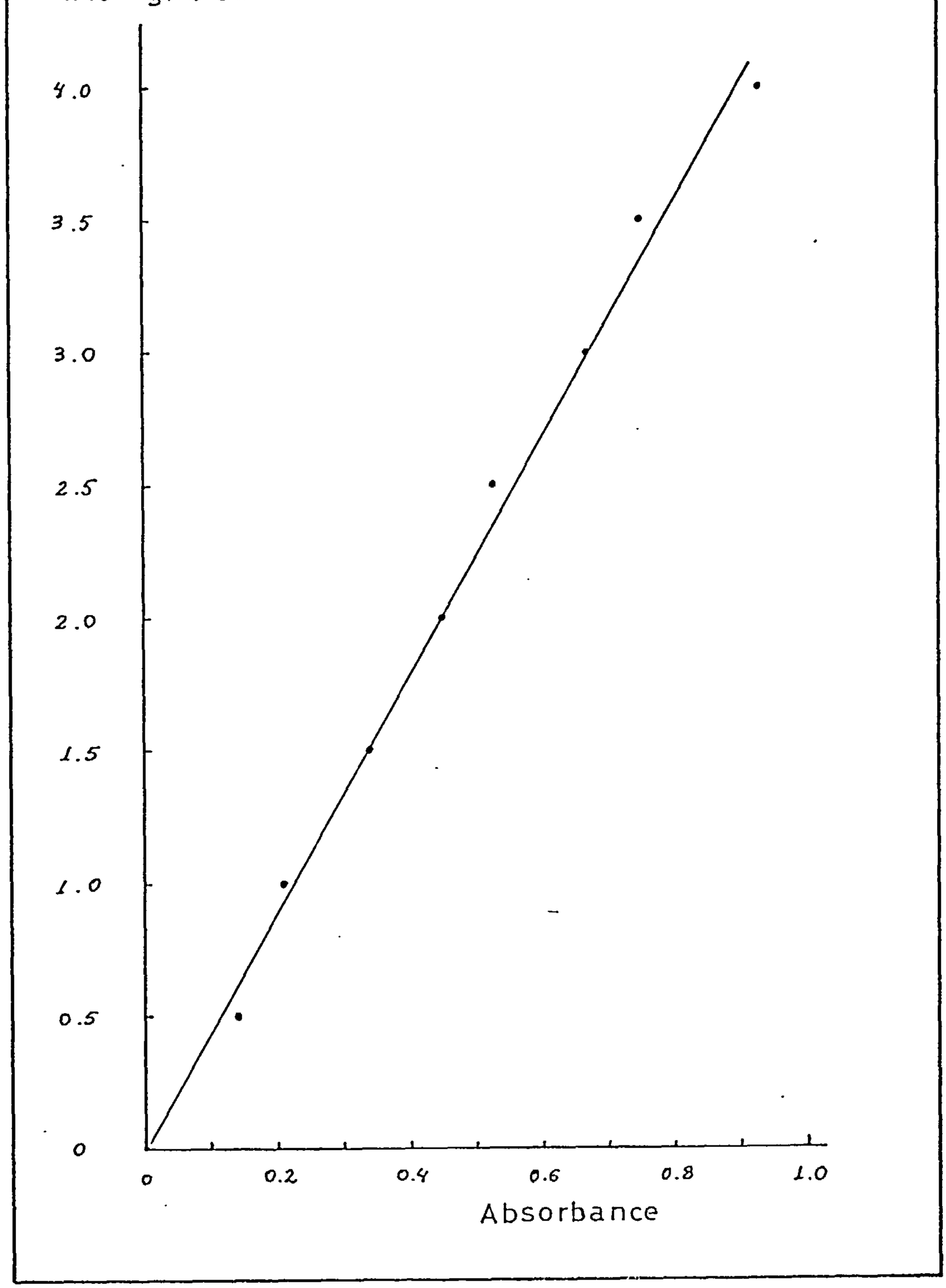

readings of absorbance fell in the region between 0.1 - 0.6 Absorbance. When the copper concentration was unknown, a preliminary test gave an indication of the appropriate dilution.

The glass cells used were 1 cm wide (light path) and optically matched and the spectrophotometer a Unicam SP 500.

APPENDIX C. COPPER COATING OF GLASS BEADS. ELECTROLESS METHOD

Although there are several "electroless" methods of coating, the one used is a modification of the method described by SHOROKHOVA et al[27] as used by BACKHURST[13].

Procedure

a) Clean and degrease the glass beads at 50°C, and wash them afterwards several times with distilled water.

b) Add a 1% (1:1) silver nitrate and ethanol solution and agitate for a few minutes.

c) Dry the beads at 40°C.

d) Put 50 grams of the dry beads in 110 ml of a cupric carbonate solution. This solution is made with 180 grs of glycerol added to 1 litre of 20% sodium hydroxide and finally 180 grams of cupric carbonate are added; it must be kept for 24 hours before use.

e) Add 24 ml of 28% Formaldehyde solution and agitate the mixture until the initial reaction has subsided. The mixture is allowed to stand with occasional agitation until no further reaction is evident.

f) Wash the coated spheres with distilled water followed by 5% sulphuric acid. Dry the beads at 50°C in a nitrogen atmosphere if desired.

This method provided a very satisfactory coating on the 550 microns beads and practically all the beads were coated. However, a small percentage of the 780 microns beads were only partially coated and in the case of beads 1.2 mm in diameter the coating was unsatisfactory. This is due, probably to the coating peeling off the beads due to friction when agitating.

APPENDIX D. PROPERTIES OF COPPER COATED GLASS BEADS AND FLOW RATES REQUIRED FOR FLUIDISATION

A. Particles of 550 microns mean diameter.

The particles were sieved and a batch between 500 and 600 microns was used to determine the following properties:-

Porosity = 0.38

Specific gravity = 3.112 gr/gr H_2O

Ratio area per unit volume a = $\frac{6}{d_p}$ = .109 cm^2/cm^3

This ratio is per unit volume of beads and it does not take into account the porosity of the bed. It is assumed that the particles are perfect spheres, therefore

$$a = \frac{4\pi R^2}{4/3\pi R^3} = \frac{3}{R} = \frac{6}{d_p}$$

B. Particles of 780 microns mean diameter.

This batch was sieved between 710 and 850 microns

Porosity = 0.36

Specific gravity = 3.08 gr/gr H_2O

Area per unit volume = 77 cm^2/cm^3

The apparent anomaly in bigger size particles having a lower porosity is due to the higher difference between the upper and lower sieves, i.e. 140 microns compared with 100 microns in case A.

C. Flow Rates in Cylindrical Cell II.

The flow rates of electrolyte required to fluidise the bed to a certain expansion are shown in Table A. The electrolyte is 0.1 Molar both in copper and sulphuric acid.

TABLE A. Flow Rates in Cylindrical Cell II (l/min.)

Bed Expansion %	d_p 550 microns	d_p 780 microns
10	0.70	0.95
20	0.85	1.17
30	1.03	1.40
40	1.18	1.61

APPENDIX E. EQUIPMENT, INSTRUMENTATION AND MATERIALS

E1 : Magnetic pump

Totton Electrical Products (Southampton). Model 175 B/M/DP

E2 : Centrifugal pump

J. Beresford & Co. Ltd. (Birmingham) Model PV 21

E3 : Power supply

Potentiostat 50V/20A Chemical Electronics Co. Type 50/20A

E4 : Ammeter

Sangano Weston Multiscale Range 100 $\pm$ 1 mA to 5 $\pm$ 0.05 A

E5 : Avometer

Amperes range : 10 $\pm$ 0.1 mA to 100 $\pm$ 1 mA Volts scale 10 $\pm$ 0.1 V

E6 : Linear Sweep Generator

Chemical Electronics Co. Used in conjunction with potentiostat E3.

Adjustable potential range.

E7 : Electronic Digital Voltmeter

Multiscale; the lowest scale is 1.9995 $\pm$ 0.0005 V. Continuous or manual operation. Provided with two RC filters of 0.02 and 0.1 sec.

Dynamco Type DM 2001 Mk 2.

E8 : Recorder

Variable range and recording speeds. Toa Electronics Ltd. (Japan)

Model EPR - 2T

E9 : Flow Meter

0 - 50 Imp. gal/hour. Fischer & Porter Ltd.

E10 : Celloton Ceramic Diaphragm

Maximum pore size 1 micron

Porosity 0.48

Permeability 0.8 ml/h passed through 1 cm^2 at 20°C and a head of 10 cm of water

Electrical Resistance factor, i.e. Resistance of impregnated diaphragm/ Resistance of electrolyte of same dimensions, 3.

Modulus of rupture 2.84 kg/mm^2

Manufacturers Aerox Ltd., Stroud, Glos.

E11 : Felt

Suppliers: Dolman James & Co. Ltd. Morley, Yorks.

E12 : Electrical Integrator

Ether Ltd. (Stevenage) Type 1210

APPENDIX F. POTENTIAL PROFILES

$I_{\square}$ = diaphragm current density, mA cm^{-2}

d_p = particle diameter, microns

E = bed expansion, %

x = normal distance from feeder. Planar Cell, cm.

r = radius for Cylindrical Cells, cm.

ϕ_s = Potential of the continuous phase, mV

ϕ_M = Potential of the dispersed phase, mV

ϕ = Electrode Potential, mV

$r \frac{d \phi_s}{dr}$ = mV factor proportional to the electrolyte current flow

Note

$\phi = \phi_s - \phi_M$ = electrode potential (cathodic) with respect to rest potential (R.P.)

Cu^{++}	R.P. w.r.t. SCE	R.P. w.r.t. H_2 electrode
0.1 M	+ 58 mV	+ 300 mV
0.01 M	+ 25 mV	+ 267
0.001 M	0 mV	+ 242

All experiments were carried out at temperatures ranging from 18 to $21^{o}C$.

F1 Cylindrical Cell I

0.1 M Cu, 0.1 M H_2SO_4, d_p = 550μ $I_{\square}$ = 36 mA cm^{-2}

E	r	ϕ_s	ϕ_M	ϕ
10	0.30	27	4	23
	0.75	31	8	23
	1.20	33	10	23
	1.65	36	12	24
	2.10	87	12	75
20	0.30	29	5	24
	0.75	34	11	23
	1.20	39	14	25
	1.65	46	16	30
	2.10	109	17	92
30	0.30	30	4	26
	0.75	38	12	26
	1.20	48	15	33
	1.65	59	17	42
	2.10	144	19	125

F2 Cylindrical Cell I

: 0.1 M Cu, 0.1 M H_2SO_4, $d_p = 550\mu$, $I_n = 72$ mA cm^{-2}

E	r	ϕ_s	ϕ_M	ϕ
10	0.30	34	8	26
	0.75	37	11	26
	1.20	40	12	28
	1.65	48	14	34
	2.10	110	15	95
20	0.30	36	8	28
	0.75	41	12	29
	1.20	47	16	31
	1.65	61	18	43
	2.10	192	23	169
30	0.30	38	10	28
	0.75	47	16	31
	1.20	59	19	40
	1.65	87	22	65
	2.10	262	26	236

F3 Cylindrical Cell I

0.01 M Cu, 0.1 M H_2SO_4, $d_p = 550\mu$, $I_\square = 36$ mA cm^{-2}

E	r	ϕ_s	ϕ_M	ϕ
10	0.30	19	4	15
	0.75	22	9	13
	1.20	26	12	14
	1.65	37	13	24
	2.10	187	13	174
20	0.30	31	4	27
	0.75	43	21	22
	1.20	57	36	21
	1.65	80	41	39
	2.10	275	45	230

F4 Cylindrical Cell I

0.01 M Cu, 0.1 M H_2SO_4, $d_p = 550\mu$, $I_\square = 72$ mA cm^{-2}

E	r	ϕ_s	ϕ_M	ϕ
10	0.30	24	7	17
	0.75	31	14	17
	1.20	35	19	16
	1.65	49	19	30
	2.10	472	19	453
20	0.30	33	8	25
	0.75	44	28	16
	1.20	52	36	16
	1.65	126	44	82
	2.10	577	44	533
30	0.30	48	8	40
	0.75	72	55	17
	1.20	102	80	22
	1.65	333	95	238
	2.10	685	103	582

F5 Cylindrical Cell II

: 0.1 M Cu, 0.1 M H_2SO_4, $d_p = 550\mu$, $I_{\square} = 22$ mA cm^{-2}

E	r	ϕ_s	ϕ_M	ϕ	$r\, d\phi_s/dr$
10	0.30	27	1.2	26	4
	0.675	31	5.9	24	7
	1.05	34	9.5	24	8
	1.425	39	12.2	27	36
	1.61	51	13.3	38	152
	1.80	80	14.2	66	540
20	0.30	28	1.2	27	5
	0.675	34	12.9	21	12
	1.05	42	22.8	19	23
	1.425	50	29.7	20	64
	1.61	67	33.3	34	222
	1.80	109	36.2	73	540
30	0.30	34	1.3	33	13
	0.675	54	37	18	43
	1.05	78	68	10	38
	1.425	104	89	15	154
	1.61	130	97	33	361
	1.80	172	99	73	740

F6 Cylindrical Cell II

0.1 M Cu, 0.1 M H_2SO_4, $d_p = 550\mu$, $I_\square = 11$ mA cm^{-2}

E	r	ϕ_s	ϕ_M	ϕ	$r\, d\phi_s/dr$
10	0.30	22	0.6	22	0.9
	0.675	24	3.2	21	2.0
	1.05	26	4.8	22	3.2
	1.425	29	6.0	24	20.0
	1.61	34	6.6	27	69
	1.80	42	6.8	34	320
20	0.30	24	0.6	23	3
	0.675	28	6.4	22	7
	1.05	32	10.5	21	9
	1.425	37	12.8	24	37
	1.61	45	14.2	31	89
	1.80	54	14.6	39	342
30	0.30	32	0.6	31	23
	0.675	59	18	41	46
	1.05	83	32	51	65
	1.425	103	42	61	87
	1.61	116	46	70	98
	1.80	122	48	74	110

F7 Cylindrical Cell II

0.1 M Cu, 0.1 M H_2SO_4, $d_p = 550\mu$, $I_{\square} = 2$ mA cm^{-2}

E	r	ϕ_s	ϕ_M	ϕ	$r\, d\phi_s/dr$
10	0.30	20.9	0.1	21	0.21
	0.675	21.3	0.8	21	0.81
	1.05	21.9	1.2	21	3.2
	1.425	23.8	1.6	22	12.5
	1.61	26.1	1.65	25	21.9
	1.80	27.9	1.65	26	74.0
20	0.30	21.5	0.1	21	0.75
	0.675	22.4	1.8	21	1.75
	1.05	23.5	2.8	21	3.3
	1.425	26.0	3.6	22	16.5
	1.61	29.0	4.1	25	30
	1.80	31.8	4.2	28	63
30	0.30	24	0.1	24	2.7
	0.675	28	5.6	22	8.1
	1.05	33	12.0	21	13.1
	1.425	37	15.5	21	19.7
	1.61	42	17.3	25	46.7
	1.80	46	17.6	28	57

F8 Cylindrical Cell II

0.01 M Cu, 0.1 M H_2SO_4, $d_p = 550\mu$, $I_\square = 22$ mA cm^{-2}

E	r	ϕ_s	ϕ_M	ϕ	$r\, d\phi_s/dr$
10	0.30	16	1.3	15	2.4
	0.675	19	6.0	13	5.4
	1.05	23	9.8	13	17
	1.425	34	11.6	22	86
	1.61	54	13.0	41	251
	1.80	106	13.7	92	740
20	0.30	17	1.3	16	4
	0.675	23	12.9	10	13
	1.05	32	23.9	8	28
	1.425	46	28.9	17	83
	1.61	72	31.1	41	241
	1.80	110	33.1	77	640

F9 Cylindrical Cell II

0.01 M Cu, 0.1 M H_2SO_4, $d_p = 550\mu$, $I_\square = 11$ mA cm^{-2}

E	r	ϕ_s	ϕ_M	ϕ	$r\, d\phi_s/dr$
10	0.30	10	0.6	9	0.6
	0.675	11	2.5	8	2.7
	1.05	13	3.9	9	9
	1.425	18	4.8	13	37
	1.61	25	5.3	20	87
	1.80	35	5.5	29	370
20	0.30	10	0.6	9	2.4
	0.675	13	4.4	9	6
	1.05	17	7.2	10	13
	1.425	23	9.3	14	54
	1.61	35	10.2	25	145
	1.80	42	10.5	31	324
30	0.30	16	0.6	15	8
	0.675	26	12.7	13	20
	1.05	38	23.0	15	36
	1.425	53	30.4	23	77
	1.61	65	32.4	34	122
	1.80	77	33.6	43	288

F10 Cylindrical Cell II

0.01 M Cu, 0.1 M H_2SO_4, $d_p = 550\mu$, $I_\square = 2$ mA cm^{-2}

E	r	ϕ_s	ϕ_M	ϕ	$r\, d\phi_s/dr$
10	0.30	6.6	0.10	6.5	0.18
	0.675	7.2	0.75	6.5	1.55
	1.05	8.7	1.20	7.5	5.5
	1.425	11.5	1.60	9.9	17.4
	1.61	14.2	1.70	12.5	26
	1.80	16.6	1.75	14.8	72
20	0.30	7.4	0.1	7.3	1.5
	0.675	9.4	2.0	7.4	4.7
	1.05	12.5	3.8	8.7	10
	1.425	16.3	4.8	11.5	24
	1.61	23.1	5.3	17.8	43
	1.80	25	5.7	19.3	65
30	0.30	12	0.1	12	9
	0.675	25	8.3	17	24
	1.05	40	15.7	24	38
	1.425	51	22.2	29	48
	1.61	60	26.7	33	69
	1.80	66	28.0	38	77
40	0.30	18	0.1	18	20
	0.675	42	19	23	43
	1.05	67	44	23	66
	1.425	90	61	29	68
	1.61	98	67	31	97
	1.80	107	69	38	110

F11 Cylindrical Cell II

0.001 M Cu, 0.1 M H_2SO_4, $d_p = 550\mu$, $I_o = 2$ mA cm^{-2}

E	r	ϕ_s	ϕ_M	ϕ	$r\, d\phi_s/dr$
10	0.30	4.2	0.1	4.1	1.2
	0.675	6.2	1.6	4.6	6
	1.05	10.5	3.0	7.5	15
	1.425	16.8	3.9	12.9	37
	1.61	23.8	4.3	19.5	58
	1.80	27.5	4.5	23.0	81
20	0.30	15.8	0.1	15.7	11
	0.675	30.0	6.2	23.8	25
	1.05	46.5	12.9	33.6	39
	1.425	62.7	17.6	45.1	53
	1.61	69.8	18.8	51.0	60
	1.80	73.1	19.5	53.6	68
30	0.30	80	0.1	80	44
	0.675	135	42	93	98
	1.05	188	78	110	131
	1.425	225	103	122	143
	1.61	246	110	136	161
	1.80	253	111	142	162
40	0.30	137	0.1	137	48
	0.675	200	68	132	121
	1.05	269	126	143	152
	1.425	308	157	151	185
	1.61	333	171	162	209
	1.80	342	176	166	234

F12 Cylindrical Cell II

0.1 M Cu, 0.1 M H_2SO_4, $d_p = 780\mu$, $I_\square = 22$ mA cm^{-2}

E	r	ϕ_s	ϕ_M	ϕ	$r\, d\phi_s/dr$
10	0.30	31	1.2	30	17
	0.675	55	26	29	43
	1.05	84	52	32	80
	1.425	115	74	41	183
	1.61	150	83	67	392
	1.80	190	94	96	641

F13 Cylindrical Cell II

0.1 M Cu, 0.1 M H_2SO_4, $d_p = 780\mu$, $I_\square = 11$ mA cm^{-2}

E	r	ϕ_s	ϕ_M	ϕ	$r\, d\phi_s/dr$
10	0.30	32	0.6	32	32
	0.675	78	45	33	81
	1.05	129	93	36	147
	1.425	185	130	55	305
	1.61	229	160	69	435
	1.80	255	171	84	504
20	0.30	77	0.6	76	126
	0.675	228	171	57	243
	1.05	341	308	33	300
	1.425	434	400	34	314
	1.61	478	429	49	322
	1.80	490	433	57	297

F14 Cylindrical Cell II

0.1 M Cu, 0.1 M H_2SO_4, $d_p = 780\mu$, $I_\square = 2$ mA cm^{-2}

E	r	ϕ_s	ϕ_M	ϕ	r $d\phi_s/dr$
10	0.30	24	0.1	24	12
	0.675	38	20	18	24
	1.05	49	36	13	26
	1.425	60	52	8	77
	1.61	72	60	12	119
	1.80	80	66	14	126
30	0.30	53	0.1	53	69
	0.675	123	105	18	81
	1.05	155	145	10	76
	1.425	180	174	6	90
	1.61	192	185	7	95
	1.80	197	188	9	103

F15 Cylindrical Cell II

0.01 M Cu, 0.1 M H_2SO_4, $d_p = 780\mu$, $I_\square = 22$ mA cm^{-2}

E	r	ϕ_s	ϕ_M	ϕ	r $d\phi_s/dr$
10	0.30	23	1.0	22	9
	0.675	39	32	7	31
	1.05	68	70	0	61
	1.425	76	92	0	134
	1.61	111	105	6	367
	1.80	171	114	57	738
30	0.30	151	1.0	150	210
	0.675	402	324	78	446
	1.05	648	625	23	588
	1.425	868	851	17	698
	1.61	942	945	4	870
	1.80	992	960	32	972
40	0.30	415	1.0	414	324
	0.675	797	607	190	607
	1.05	1096	1003	93	850
	1.425	1385	1281	104	1000
	1.61	1506	1407	99	950
	1.80	1545	1440	105	950

F16 Cylindrical Cell II

0.01 M Cu, 0.1 M H_2SO_4, $d_p = 780\mu$, $I_\square = 1.1$ mA cm^{-2}

E	r	ϕ_s	ϕ_M	ϕ	$r\, d\phi_s/dr$
10	0.30	25	0.6	25	23
	0.675	54	30	26	53
	1.05	84	61	23	74
	1.425	112	79	33	143
	1.61	144	86	58	367
	1.80	170	92	78	489
20	0.30	81	0.6	80	103
	0.675	211	133	78	231
	1.05	349	243	106	370
	1.425	463	330	143	467
	1.61	525	384	141	528
	1.80	567	397	160	590

F17 Cylindrical Cell II

0.01 M Cu, 0.1 M H_2SO_4, $d_p = 780\mu$, $I_\square = 2$ mA cm^{-2}

E	r	ϕ_s	ϕ_M	ϕ	$r\, d\phi_s/dr$
10	0.30	17	0.1	17	4
	0.675	23	9	14	14
	1.05	35	23	12	30
	1.425	46	30	16	57
	1.61	59	33	21	90
	1.80	66	36	30	180
20	0.30	40	0.1	40	29
	0.675	76	39	37	65
	1.05	113	74	39	84
	1.425	137	100	37	90
	1.61	148	110	38	114
	1.80	160	114	46	166
30	0.30	93	0.1	93	53
	0.675	155	88	67	103
	1.05	208	146	62	129
	1.425	244	178	66	137
	1.61	262	188	74	153
	1.80	270	195	75	135
40	0.30	177	0.1	177	36
	0.675	222	136	86	89
	1.05	286	190	96	120
	1.425	304	220	84	131
	1.61	321	241	80	140
	1.80	330	249	81	144

F18 Cylindrical Cell II

0.001 M Cu, 0.1 M H_2SO_4, $d_p = 780\mu$, $I_\square = 2$ mA cm^{-2}

E	r	ϕ_s	ϕ_M	ϕ	$r\, d\phi_s/dr$
10	0.30	2.0	0.1	2.0	1
	0.675	3.8	3.9	0.0	5
	1.05	7.3	7.7	0.0	11
	1.425	13.1	10.8	2.3	30
	1.61	21.0	15.8	5.2	87
	1.80	27.0	17.0	10.0	130

F19 Planar Cell (Double Felt Distributor)

0.1 M Cu, 0.1 M H_2SO_4, $d_p = 550\mu$, $I_\square = 36$ mA cm^{-2}

E	x	ϕ_s	ϕ_M	ϕ
10	0.0	22	0.1	22
	0.5	33	12.8	20
	1.0	51	23	28
	1.5	72	32	40
	1.75	95	35	60
	2.0	221	36	185
20	0.0	44	0.1	44
	0.5	95	34	61
	1.0	185	53	132
	1.5	263	71	192
	1.75	324	76	248
	2.0	446	80	366
30	0.0	81	0	81
	0.5	185	74	111
	1.0	370	144	226
	1.5	524	206	318
	1.75	591	230	361
	2.0	722	238	484
40	0.0	118	0	118
	0.5	322	120	202
	1.0	603	278	325
	1.5	838	440	398
	1.75	976	494	482
	2.0	1118	562	556

F20 Planar Cell (Double Felt Distributor)

0.1 M Cu, 0.1 M H_2SO_4, $d_p = 550\mu$, $I_\square = 18$ mA cm^{-2}

E	x	ϕ_s	ϕ_M	ϕ
10	0.0	20	0	20
	0.5	24	3	21
	1.0	33	6	27
	1.5	45	8	37
	1.75	66	9	57
	2.0	134	9	124
20	0.0	44	0	49
	0.5	81	12	69
	1.0	138	18	120
	1.5	191	27	164
	1.75	231	30	201
	2.0	296	32	264
30	0.0	55	0	55
	0.5	149	49	100
	1.0	259	93	166
	1.5	369	137	232
	1.75	435	161	274
	2.0	504	170	334
40	0.0	87	0	87
	0.5	202	92	110
	1.0	366	174	192
	1.5	523	254	269
	1.75	598	287	311
	2.0	664	310	354

BIBLIOGRAPHY

(1) MANTELL C.L. "Electrochemical Engineering"
McGraw-Hill N.Y. (1960)

(2) MILAZZO G. "Electrochemistry"
Elsevier Pub. Co. (1963)

(3) NEWTON J. and WILSON C.L.
"Metallurgy of Copper" John Wiley & Sons (1942)

(4) BACK A.E.
J. Metals N.Y. 19 May 1967, 27-29

(5) AGERS D.W., HOUSE J.E., SWANSON R.R. and DROBNICK J.L.
"Copper recovery from acidic solutions using liquid ion exchange"
Paper 25th Annual Meeting A.I.M.E. N.Y. Feb-Mar 1966

(6) AGERS D.W. and DEMENT E.R.
"LIX 64 as an extractant for copper, pilot plant data"
Paper Joint Meeting of the Rocky Mountain Minerals Conference and
Fall Meeting of S.M.E. of A.I.M.E. Las Vegas Nevada Sep. 1967

(7) Metals, 2 April 1967, 39

(8) GOODRIDGE F.
Chem. and Proc. Eng. Feb (1968)

(9) MATTSSON E. and R. LINDSTROM
(Compte Rend.) CITCE VI (1954)

(10) MATTSSON E. and BOCKRIS J. O'M.
Trans. Faraday Soc. 55 (1959) 1586

(11) RADOVICI O. and VASS C.
Rev. Roumaine de Chimie 12, 1181-85 (1967)

(12) HURLEN T.
Acta Chem. Scand. 15, 630-44 (1961)

(13) BACKHURST J.R.
Ph.D. Thesis University of Newcastle upon Tyne (1967)

(14) BACKHURST J.R., FLEISCHMANN M., GOODRIDGE F. and PLIMLEY R.E.

(15) BACKHURST J.R., FLEISCHMANN M., COULSON J.M., GOODRIDGE F.
and R.E. PLIMLEY
J. Electrochem. Soc. 116, II, 1600 (1969)

(16) NEWMAN J.S. and TOBIAS C.W.
J. Electrochem. Soc. 109, 1183 (1962)

(17) BACKHURST J.R., GOODRIDGE F., R.E. PLIMLEY and M. FLEISCHMANN
Nature, 221 No. 5175, 55 (1969)

(18) BERENT T., R. MASON and I. FELLS
J. Appl. Chem. Biotechnal. 21, 71 (1971)

(19) HIDDLESTON J.N. and A.F. DOUGLAS
Nature 218, 601 (1968)

(20) HIDDLESTON J.N. and A.F. DOUGLAS
Electrochim. Acta 15 (3), 431 (1970)

(21) FLEISCHMANN M. and J.W. OLDFIELD
J. Electroanal. Chem. 29, 211 (1971)

(22) FLEISCHMANN M. and J.W. OLDFIELD
J. Electroanal. Chem. 29, 231 (1971)

(23) FLEISCHMANN M., J.W. OLDFIELD and D.F. PORTER
J. Electroanal. Chem. 29 241 (1971)

(24) FLEISCHMANN M., J.W. OLDFIELD and L. TENNAKOON
J. Appl. Electrochem. 1, 103 (1971)

(25) GOODRIDGE F., I.D. HOLDEN, H.D. MURRAY and R.E. PLIMLEY
Trans. Inst. Chem. Eng. 49 (2), 128 (1971)

(26) GOODRIDGE F., I.D. HOLDEN, H.D. MURRAY and R.E. PLIMLEY
Trans. Inst. Chem. Eng. 49 (2), 137 (1971)

(27) SHOROKHOVA V.I. and KUZ'MIN L.L.
Int. Chem. Eng. 4 (3), 451 (1964)

(28) PINNER R. "Copper and Copper-alloy Plating"
Copper Development Association Pub. No. 62 (1962)

(29) LANGFORD K.E.
"Analysis of Electroplating and Related Solutions"
R. Draper Ltd. 2nd ed. (1958) 57 ff.

(30) SANDELL
"Colorimetric Metal Analysis"
Interscience Pub. 3rd ed. (1959) 443-450

(31) HADDOCK L.A. and EVERS N.
The Analyst 57, 495 (1932)

(32) KIMBER G.M., D.H. NAPIER and D.H. SMITH
J. Appl. Chem. 17 (Feb), 29 (1967)

(33) SHREIR L.L. and J.W. SMITH
J. Electrochem. Soc. 99, 64 (1952)

(34) SHREIR L.L. and J.W. SMITH
J. Electrochem. Soc. 98, 193 (1951)

(35) GAUVIN W. and C.A. WINKLER
Can. J. Research, 21A, 37 (1943)
" " " 21B, 81 (1943)
" " " 21B,125 (1943)

(36) MARIE C. and THON D.N.
J. Chim. Phys. 29, 11 (1932)

(37) GNUSIN N.P., N.Y. KOVAROVSKII and N.P. FEDOT'EV
Zhurn. Priklad. Khim. 38 (11) 2464-69 (1965)

(38) BUTTS A. (Editor) "Copper"
Reinhold Pub. Co., N. York (1954) 193

(39) KUHN A.T.
Chem. and Ind. 1st May (1971), 473

(40) SURFLEET B.
Electricity Council Report (1970), ECRC/R 251

(41) FLETT D.S.
Chem. and Ind. 13th March (1971), 300

(42) KING C.J.H.
Chem. Eng. Dept. University of Newcastle upon Tyne.
Private Communication

(43) DE LA RUE R. and TOBIAS C.W.
J. Electrochem. Soc. 106 (9) 827-32 (1959)

(44) International Critical Tables
Vol. VI p.p 230-256

(45) COEURET F. and P. LE GOFF
Trans. Inst. Chem. Eng. 45, CE 75 (April 1967)

(46) HANDLEY D.
Thesis Univ. of Leeds (1957), 34 ff.

(47) DORAISAMY A.
Thesis Univ. of Leeds (1958), 25 ff.

(48) Chemical Electronics, Birtley, Co. Durham

(49) LE GOFF P., VERGNES F., COEURET F. and BORDET V.
Ind. Eng. Chem. 61 (10), 8 (1969)

(50) VERGNES F., C. VERREL and P. LE GOFF
Corrosion 17, No.3, 131 (1969)

(51) ISMAIL B.M.
Thesis Univ. Newcastle upon Tyne (1971)

(52) ARMSTRONG D., N.A. HAMPSON and R.J. LATHAM
J. Electroanal. Chem. 23, 361-67 (1969)

(53) S. GERMAIN
Univ. of Newcastle upon Tyne Private Communication

(54) BOCKRIS J.O'M. and A.K.N. REDDY
"Modern Electrochemistry" Vol. II Macdonald London (1970)

(55) BOCKRIS J.O'M. and CONWAY B.E.
J. Chem. Phys. 28, 707 (1958)

(56) WILKINSON J.A.E. and K.P. HAINES
Trans. Inst. Mining and Met. Section C, 81, C157 (1972)